OAK RIDGE
NATIONAL LABORATORY

MANAGED BY UT-BATTELLE FOR THE DEPARTMENT OF ENERGY

Metals Processing Laboratory Users (MPLUS) Facility

Annual Report

FY 2003 (October 1, 2002-September 30, 2003)

UT-BATTELLE

MPLUS
Metals Processing Laboratory Users facility

DOCUMENT AVAILABILITY

Reports produced after January 1, 1996, are generally available free via the U.S. Department of Energy (DOE) Information Bridge.

Web site http://www.osti.gov/bridge

Reports produced before January 1, 1996, may be purchased by members of the public from the following source:

National Technical Information Service
5285 Port Royal Road
Springfield, VA 22161
Telephone 703-605-6000 (1-800-553-6847)
TDD 703-487-4639
Fax 703-605-6900
E-mail info@ntis.fedworld.gov
Web site http://www.ntis.gov/support/ordernowabout.htm

Reports are available to DOE employees, DOE contractors, Energy Technology Data Exchange (ETDE) representatives, and International Nuclear Information System (INIS) representatives from the following source:

Office of Scientific and Technical Information
P.O. Box 62
Oak Ridge, TN 37831
Telephone 865-576-8401
Fax 865-576-5728
E-mail reports@adonis.osti.gov
Web site http://www.osti.gov/contact.html

This report was prepared as an account of work sponsored by an agency of the United States Government. Neither the United States Government nor any agency thereof, nor any of their employees, makes any warranty, express or implied, or assumes any legal liability or responsibility for the accuracy, completeness, or usefulness of any information, apparatus, product, or process disclosed, or represents that its use would not infringe privately owned rights. Reference herein to any specific commercial product, process, or service by trade name, trademark, manufacturer, or otherwise, does not necessarily constitute or imply its endorsement, recommendation, or favoring by the United States Government or any agency thereof. The views and opinions of authors expressed herein do not necessarily state or reflect those of the United States Government or any agency thereof.

ORNL/TM-2004/XXX

Metals Processing Laboratory Users (MPLUS) Facility

ANNUAL REPORT
OCTOBER 1, 2002, THROUGH SEPTEMBER 30, 2003

Compiled by
P. Angelini
M. L. Atchley

Published: November 2004

Research sponsored by the
U.S. Department of Energy
Office of Energy Efficiency and Renewable Energy
Industrial Technologies Program
Industrial Materials for the Future (IMF)
and Industries of the Future (IOF) Activities
1000 Independence Avenue NW
Washington, DC 20585-0121

OAK RIDGE NATIONAL LABORATORY
P.O. Box 2008
Oak Ridge, Tennessee 37831-6285
managed by
UT-Battelle, LLC
for the
U.S. DEPARTMENT OF ENERGY
under contract DE-AC05-00OR22725

CONTENTS

INTRODUCTION 1

HIGHLIGHTS 3

Causes of Damage of Stekel Mill Drums during Hot Rolling of Steel Slab (IPSCO) 7

Cereblak Release Coatings for Aluminum Die Casting (Applied Thin Films). 13

Characterization of Aluminum foam Prepared by Casting Process (Energy Industries of Ohio). 19

Characterization of Dross from a Sidewell Melter Producing 3004 and 3105 Aluminum from Undercoated Scrap (Commonwealth Aluminum) 27

Characterization of Precipitation in In-Line Annealed Aluminum Alloys (University of Kentucky) 33

Coating of Temperature Sensors for Solder Resistance (Pyromation) 37

Determination of the Mechanism Leading to the Formation of Surface Irregularities on Nitrided, Hot-Isostatically-Pressed Nb-50 wt % Ti-20 wt % W Alloy Compacts (MATTEC, LLC) 53

Development of a Process to Hermetically Seal a Thermal Sensor Using a Vitreous Sealing Glass (DELTA M Corporation) 55

Development of Hot Rolling Fabrication Parameters for Aluminum Boron Carbide Metal Matrix Composite Materials (Metamic L.L.C.) 59

Development of Welding Process to Join Aluminum Alloy Sheets Coil to Coil (Commonwealth Industries, Inc.) 62

Effect of Processing/Microstructure on the Corrosion Polarization Response of a Corrosion-Resistant Alloy: Phase II (ALLVAC) 65

Effect of Processing Parameters on Fabrication of Mo Sheet High Powder Metallurgy
(MET Group) 69

The Evaluation of Various Cladding Materials for Down-Hole Drilling Applications using the Pin on Disk Test
(Stoody Company) 73

High-Density-Infrared (HDIR) Densification of Thermal Spray Coatings for Spherical Surface
(F.W. Gartner Thermal Spray Co.). 75

Heat Transfer Modeling of Continuously Cast Aluminum Slab
(Commonwealth Aluminum Concast, Inc.) 81

High-Energy Efficiency Wire Annealing Method
(Ametek) 85

The Measurement of Moisture/Water Content in Recycled Aluminum Scrap and RSI
(IMCO Recycling Inc.) 87

The Mechanism by which Boron and Zirconium Improve the Resistance of Haynes 214 Alloy to Strain Age Cracking
(Haynes International Inc.) 91

The Mechanisms of Oxide Formation Found in Solidified Aluminum 5182 Alloy RSI
(IMCO Recycling Inc.) 95

Melting of Experimental Alloys for Corrosion Studies
(Lehigh University) 97

Metal Filling of Lost Foam Castings
(University of Alabama - Birmingham) 103

Methods to Improve Aluminum Smelter Hardware Materials
(Century Aluminum of West Virginia, Inc.) 105

Methods to Improve Anode Rod Preheat Energy Requirements
(Century Aluminum of West Virginia, Inc.) 111

Microwave Activation of Catalysts
(Equistar Chemical Company) 119

Optimization of IR Imaging of the Lost Foam Metal Casting Process
(Foseco-Morval) 123

Optimized Heat Treatment for Cast A356 Aluminum Wheels
(Amcast Automotive) 125

Optimizing Induction Heating to Obtain Profile Hardening of Gears
(Inductoheat) 129

Process Improvements for Complete Oxidation of Copper Chops
For Ease of Production of Fine, Easily Compactable Cu and Cu
Alloy Powders
(ACuPowder TN LLC) 133

Quantifying and Correlating Lost Foam Pattern Properties with
Metals Fill Casting Performance: Understanding the Process
(Metal Casting Technology, Inc.) 139

Qualifying Production Grade Foam and Coatings with Real Time X-Ray,
Infrared and Capacitive Methods for the Lost Foam Casting Process
(GM Powertrain) 143

Study of Pyrolysis Product Generation and Behavior in the Lost Foam
Casting Process
(Tennessee Technological University) 145

Thermal Conductivity vs. Temperature Measurement of
Nanostructured Insulating Materials
(Lawrence Berkeley National Laboraotry) 149

Thermodynamic Simulation of Porosity Potential in Ductile Irons
(Citation Corporation) 151

Utilizing Graphite Expansion to Compensate Solidification Shrinkage
In High-Strength Gray Cast Iron
(HK Casting, Inc.) 155

Weld Pool Dynamics and Its Effects on Weld Profile and Properties
of High-Strength Steels
(Ford Motor Company) 159

LIST OF PROJECTS 163

STAFF CONTACTS AND GENERAL INFORMATION 167

ACKNOWLEDGMENTS 169

INTRODUCTION

Metals Processing Laboratory Users Facility (MPLUS)

The Metals Processing Laboratory Users Facility (MPLUS) is a Department of Energy (DOE), Energy Efficiency and Renewable Energy, Industrial Technologies Program, user facility designated to assist researchers in key industries, universities, and federal laboratories in improving energy efficiency, improving environmental aspects, and increasing competitiveness. The goal of MPLUS is to provide access to the specialized technical expertise and equipment needed to solve metals processing issues that limit the development and implementation of emerging metals processing technologies. The scope of work can also extend to other types of materials.

MPLUS has four primary user centers (Fig. 1):

1. **Processing** – casting, powder metallurgy, deformation processing (including extrusion, forging, rolling), melting, thermomechanical processing, and high-density infrared processing
2. **Joining** - welding, monitoring and control, solidification, brazing, and bonding
3. **Characterization** – corrosion, mechanical properties, fracture mechanics, micro-structure, nondestructive examination, computer-controlled dilatometry, and emissivity
4. **Materials/Process Modeling** – mathematical design and analyses, high-performance computing, process modeling, solidification/deformation, microstructure evolution, thermodynamic and kinetic, and materials databases

A fully integrated approach provides researchers with unique opportunities to address technologically related issues to solve metals processing problems and probe new technologies. Access is also available to 16 additional Oak Ridge National Laboratory (ORNL) user facilities ranging from state-of-the-art materials characterization capabilities, and high-performance computing to manufacturing technologies.

MPLUS can be accessed through a standardized user-submitted proposal and a user agreement. Nonproprietary (open) or proprietary proposals can be submitted. For open research and development, access to capabilities is provided free of charge, while for proprietary efforts, the user pays the entire project costs based on DOE guidelines for ORNL costs.

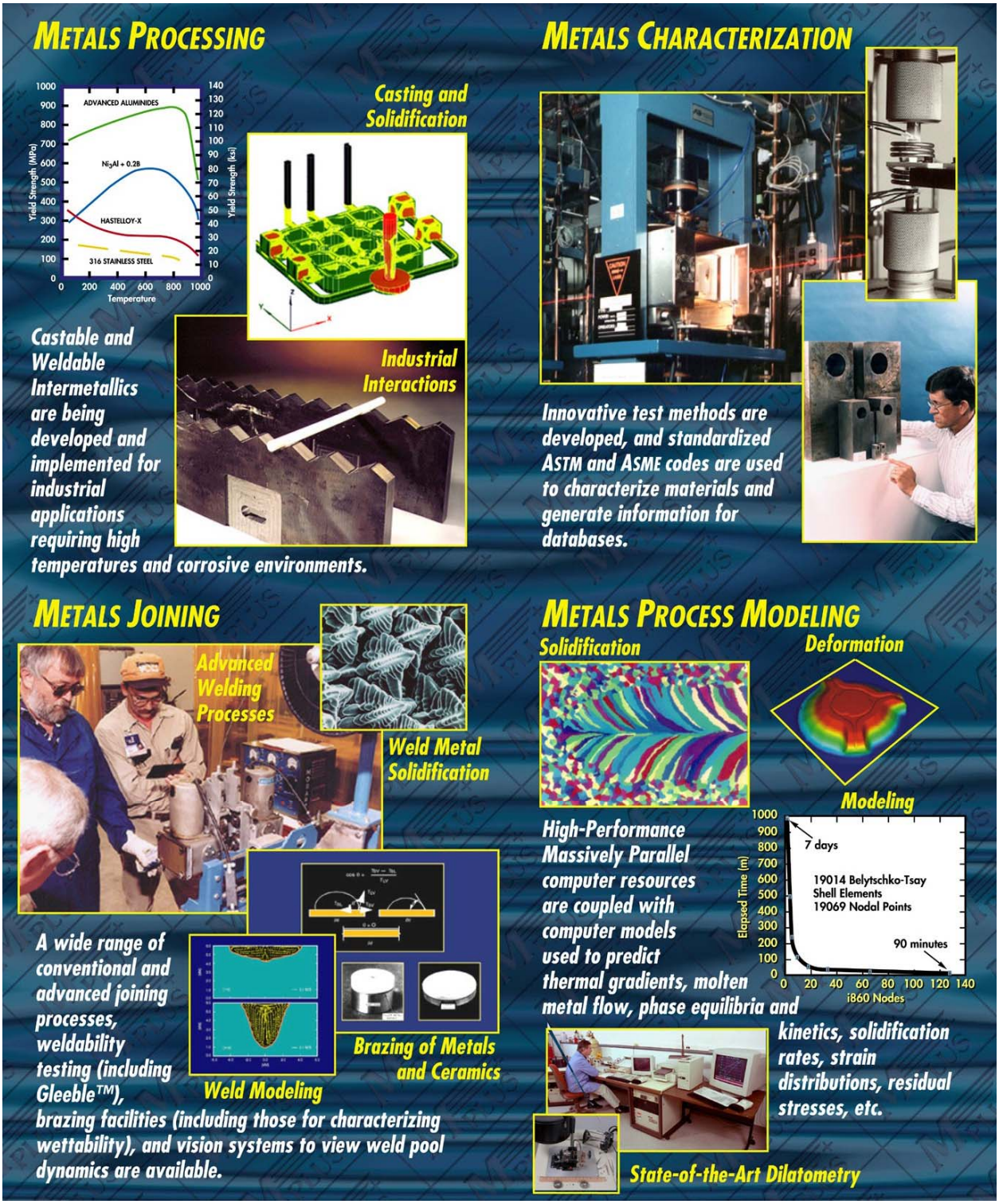

Fig. 1. The MPLUS user facilities at Oak Ridge National Laboratory.

HIGHLIGHTS

The Materials Processing Laboratory Users (MPLUS) activity is an officially designated U. S. DOE, Office of Energy Efficiency and Renewable Energy, Industrial Technologies Program, Industrial Materials for the Future user facility at the Oak Ridge National Laboratory. The goal of MPLUS is to work with industries, universities, and other organizations in helping to meet the mission of Industries of the Future efforts. The MPLUS efforts are typically high risk feasibility research and development (R&D) activities that can help the development and implementation of new and emerging technologies. MPLUS projects can lead to improved understanding or show feasibility of materials technologies and processing methods in specific applications in various industries of the future areas. In this way the initial MPLUS results often identify significant materials issues and a path forward to improved energy, environmental, and economic benefits. There were 35 MPLUS user projects in FY 2003 and examples of energy benefits are presented below.

1. The MPLUS project with .
2. The MPLUS project with .
3. The MPLUS project with .
4. The MPLUS project with .
5. The MPLUS project with .
6. The MPLUS project with .
7. The MPLUS project with .
8. The MPLUS project with .
9. The MPLUS project with .
10. The MPLUS project with .
11. The MPLUS project with .

MPLUS No.: MC-03-008

Title: Causes of Damage of Steckel Mill Drums during Hot Rolling of Steel Slab

User Organization: IPSCO Steel – Alabama Inc.
Axis, AL 36505

User Contacts: Steven S. Hansen, 251-662-4450
shansen@ipsco.com

Kevin Marsden, 412-390-2715
kmarsden@whemco.com

ORNL R&D Staff: Vinod K. Sikka, 865-574-5112
sikkavk@ornl.gov

Yogesh Bhambri, 865-576-6032
bhambriy@ornl.gov

Jackie Mayotte, 865-574-8956
mayottejr@ornl.gov

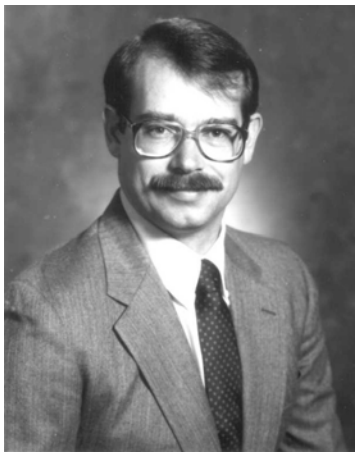

Steven Hansen from IPSCO Steel – Alabama Inc.

Relevance to ITP: Steel production industry is one of the high-energy-using industries with the product.

Steel is one of the most widely used materials. Its production uses large amounts of energy, and the final product has low-profit margins. Both of these factors require that steel production by optimized to a point that minimal down time and rejection rates are encountered. The steel production technology is a highly matured industry; however, there are still some issues with certain production hardware that can result in frequent replacement of hardware and some penalty in the quality of the final product. At IPSCO, the coiler drums, used for coiling the plate, undergo: (1) extensive surface cracking, and indication of thermal fatigue; and (2) oxidation of the coiler surface, which becomes embedded onto the plate surface. This project investigated the microstructure of the samples taken from a surface-cracked coiler, identified possible causes for cracking, and made progress toward possible surface weld treatments to improve the oxidation resistance. One of the weld treatments consisted of welding the coiler surface (made of stainless steel) with aluminum wire. This resulted in aluminum, rich areas near the surface with improved resistance to oxidation at plate-coiling temperatures.

The outcome of this MPLUS project is being pursued by IPSCO for production trial test on a coiler drum.

Objective: The objectives of this project were three-fold: (1) identify the causes for surface damage of coiler drums through ThermoCalc™ microstructural analysis;

(2) explore the possibility of weld overlay with aluminum and thermal cycling of the aluminum-clad specimens for their resistance to oxidation, debonding, and cracking; and (3) develop recommendations jointly with IPSCO for improving the coiler drum performance.

Results: The samples of surface-cracked coiler drum are shown in Fig. 1. The microhardness traverse across the surface-cracked samples is shown in Fig. 2. The micrographs of cast stainless steel HP alloy (HP-11) with aluminum clad produced at ORNL are shown in Fig. 4. The microhardness traverse for the aluminum-clad sample is shown in Fig. 5.

The cracking in Fig. 1 is believed to be caused by thermal fatigue. The thermal fatigue resistance, R, for an alloy is given by

$$R' = k\,(ys)(1-v)/\alpha E \quad , \qquad (1)$$

where k = thermal conductivity, ys = yield strength, v = Poisson's ratio, α = thermal expansion coefficient, and E = modulus,

From the above Eq. (1), thermal stress resistance can be improved by increasing thermal conductivity or by decreasing thermal expansion coefficient of the material. Cast stainless steel has high thermal-expansion coefficient & low thermal conductivity, which makes it more prone to thermal stress effects.

Figure 1: Samples of surface-cracked coiler drum at IPSCO Steel – Alabama Inc. in Axis, Alabama.

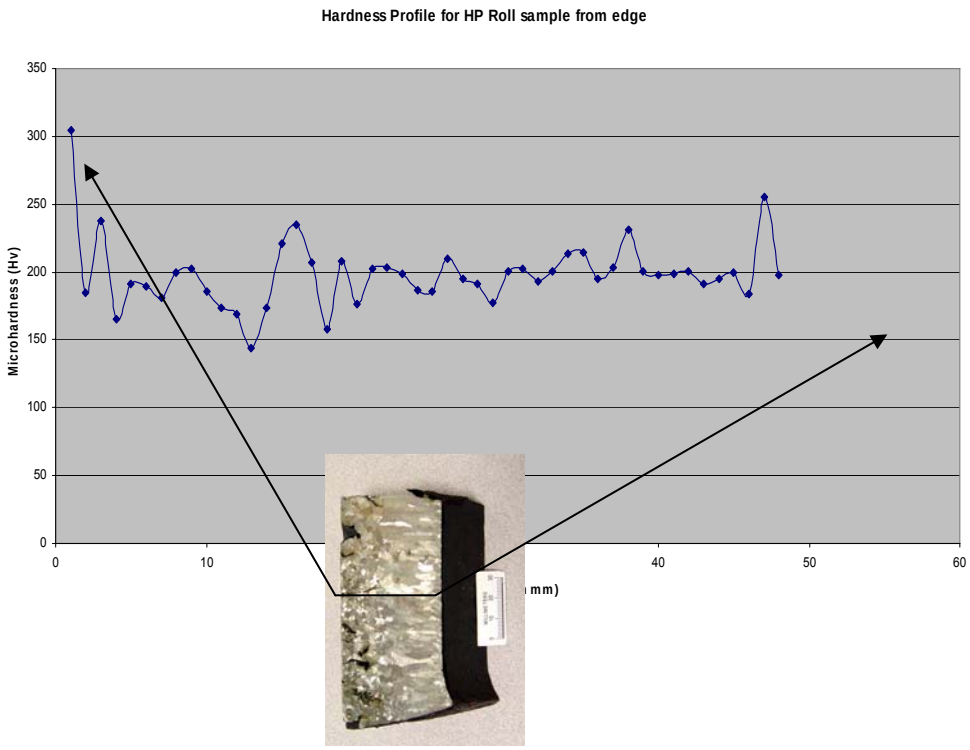

Figure 2: Microhardness traverse across the surface-cracked sample.

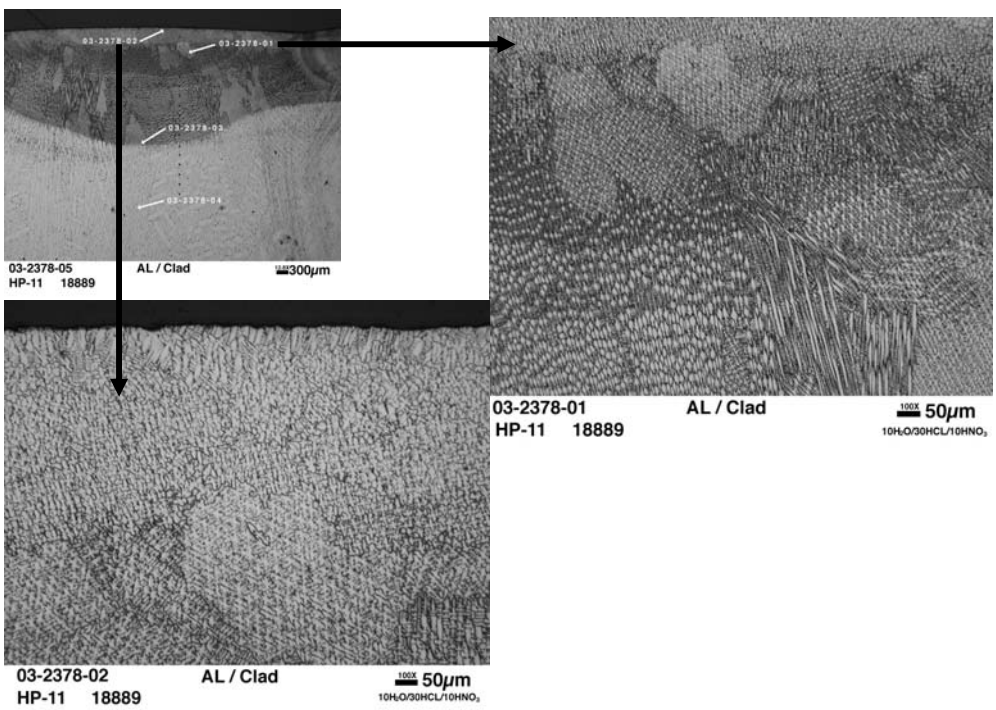

Figure 3: Micrographs of cast stainless steel HP alloy (HP-11) with aluminum clad produced at the Oak Ridge National Laboratory in Oak Ridge, Tennessee.

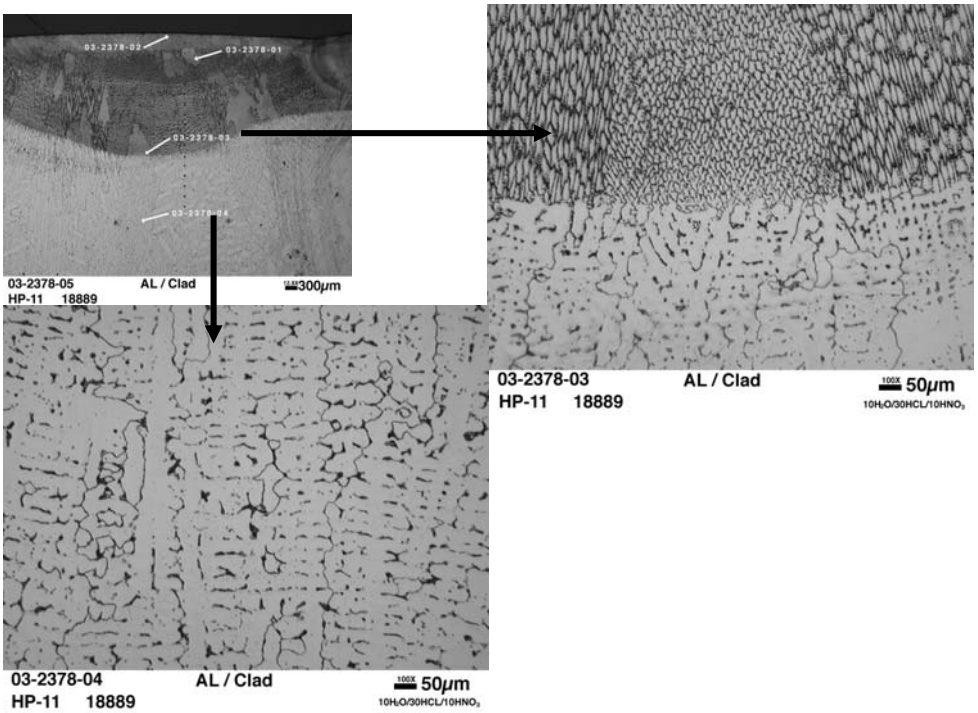

Figure 4: Micrographs of aluminum-enriched aluminum-clad weld sample (HP-11).

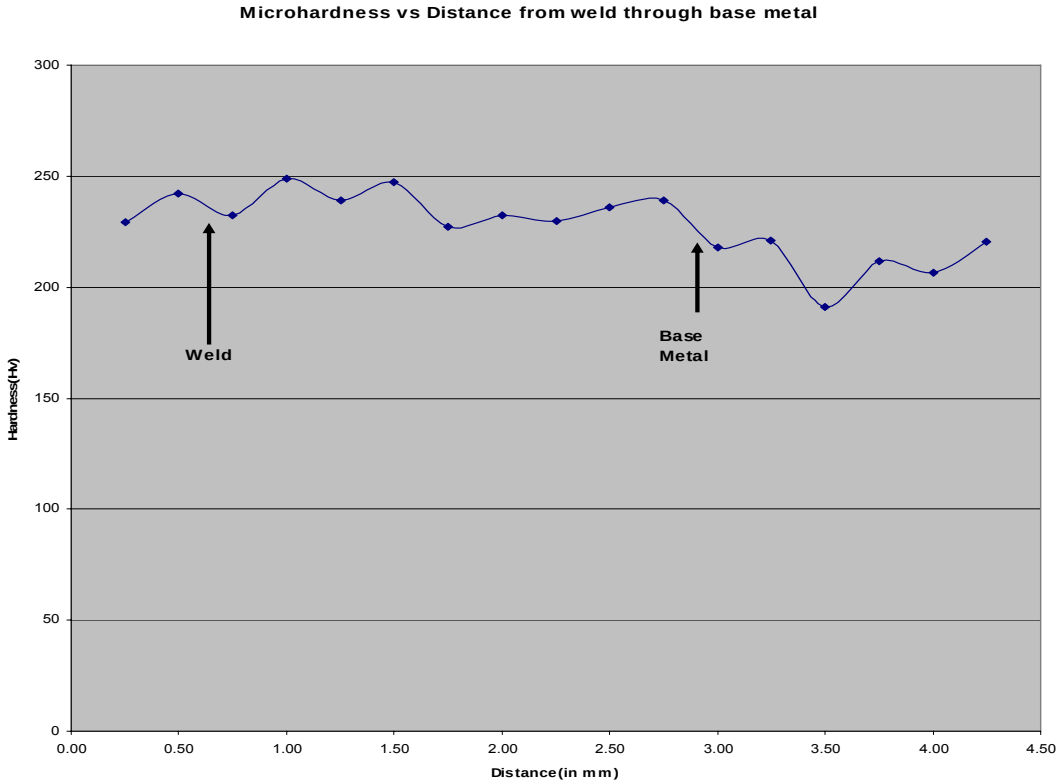

Figure 5: Microhardness traverse profile of the aluminum-clad sample.

The aluminum enrichment by weld overlay showed the following:

1. Aluminum enrichment of HP grade is possible with good quality interface with the substrate.

2. Microstructure of the aluminum-enriched region is finer than the cast substrate.

3. Welding process can be controlled to achieve the desired aluminum-enriched depth.

4. Hardness of the aluminum-enriched surface and substrate is quite uniform and in the acceptable level (not too hard).

The weld overlaid samples were thermally cycled ten times from 2000°F to water quench. The following observations were made from the microstructural analysis of these specimens:

1. No debonding of the aluminum-enriched area was noted on either side of 1 or 2 of sample.

2. No significant difference in hardness profile was noted from ten thermal cycles as opposed to the as-welded sample.

3. Some difference in the nature of the surface oxide was noted between the aluminum-enriched samples vs. the surface of the HP sample. The noted differences were: (a) aluminum-enriched sides (1 and 2) showed a more continuous oxide as opposed to without aluminum enrichment, (b) aluminum-enriched sides showed a layer of internal oxidation below the surface oxide, and (c) surface oxide on the aluminum-enriched sides were thinner than the oxide thickness of the HP alloy.

4. Effect of internal oxidation on performance of the aluminum-enriched region is not clear.

All of the data from this MPLUS was communicated to IPSCO n a timely basis. They are currently pursuing a weld-overlay possibility with the help of Stoody Company.

Reports/Publications/Awards:

Yogesh Bhambri, Vinod Sikka, and Steven Hansen, “Analysis of Cracked HP Alloy Roll Sample & Role of Al Enrichment,” Report No. 1, August 15, 2003.

Yogesh Bhambri, Vinod Sikka, Jackie Mayotte, and Steven Hansen, “HP Alloy Roll Sample with Higher Al Enrichment (Report 2),” September 30, 2003.

Yogesh Bhambri, Vinod Sikka, Jackie Mayotte, and Steven Hansen, “HP-Al Enriched Sample after 10 Thermal Cycles (Report 3),” October 10, 2003.

MPLUS No.: MC-03-005

Title: Cerablak Release Coatings

User Organization: Applied Thin Films

User Contacts: Sankar Sambasivan, 847-467-5282
sankar@atfinet.com

Kimberly Steiner, 847-431-8026
ksteiner@atfinet.com

ORNL R&D Staff: Gail M. Ludtka, 865-576-4652
ludtkagm@ornl.gov

Kimberly Steiner from Applied Thin Films

Relevance to ITP: These coatings have the potential to substantially lower maintenance and part costs for both the aluminum and metal casting industries.

Objective: To determine whether Cerablak coatings form an effective, easy to apply, environmentally friendly mold release agent for molten aluminum processing.

Results (in progress): An experimental apparatus (called the "Dipper"), shown in Fig. 1, was used as an accelerated test to evaluate the soldering resistance of various coatings for die casting applications. This apparatus simulates conditions during die-casting, but under accelerated conditions. One sample measuring 0.75-in. diam was successively dipped in molten aluminum, die lubricant, and then exposed to an air spray. Baseline H13 steel samples, without any coating, are being tested by this Dunk test, and then compared to samples with the ATFI coatings. After testing is completed, these coatings will be further characterized.

Dwell time in different positions:

- Position 1: 15s (Rotation speed 60rpm); Position 2: 80s
- Position 3: 3s; Position 4: 1s

Total Cycles: 200

XRD and EDAX Analysis of ATFI 36-8-1 Coating before Dunk Test

Major Phase(s) – Fe substrate, $AlPO_4$ coating, (PDF cards 6-696, 51-1674, respectively)

Figure 2 shows the energy spectrum acquired from the sample ATFI 36-8-1 on the JEOL 8200. The spectrum shows peaks indicating that Al, Si, P, Cr, and Fe are present in the near surface of the sample (1 to 2 μm^3; 15-KeV electron beam). The nominal composition of H13 substrate is 0.4 C-0.35 Mn-1.0 Si-5.15 Cr-1.4 Mo-1 V-Bal Fe.

The Si peak was felt to be too weak to originate from any silicate based coating, which eliminated a possible XRD phase match. The Al and P are not from the substrate. No aluminum phosphides fit the XRD data. The EDAX detector used could not detect oxygen. Based on the EDAX and XRD data, the coating was identified as $AlPO_4$ (see Fig. 3). It was assumed (and seemed likely) that the Fe, Si, and Cr originated only from the substrate. The other coatings (ATFI 36-8-2, -3, and -4) displayed very similar but less intense than that of the ATFI 36-8-1 sample. These lower intensities are likely due to the thinner coating layers on the other samples. Consequently, these were not analyzed further. Figure 4 shows the secondary electron images of where the spectrum was collected. The coating topography appears rough at high magnification, which agrees with physical inspection.

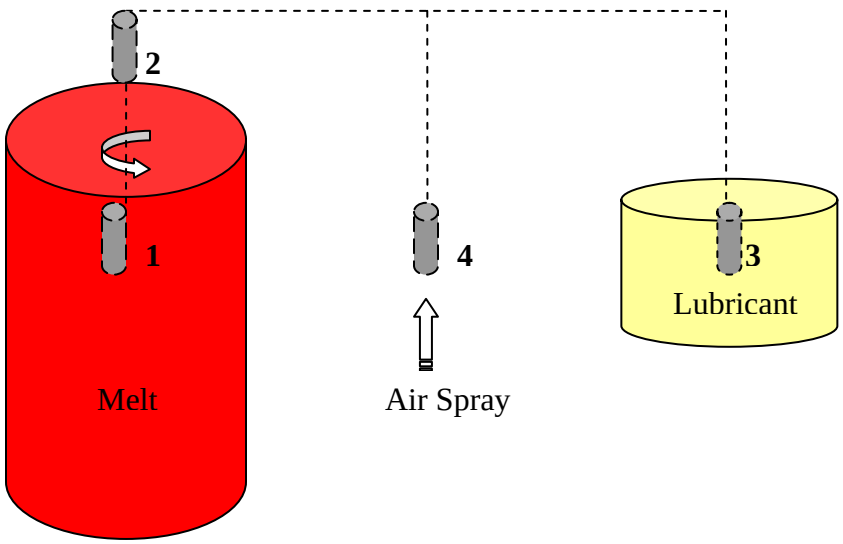

Figure 1: Schematic view of the “dipper” after improvement.

Results after Dunk Test

Figure 5 shows the surfaces of the samples after 200 cycles testing. It can be seen from these two photos that the sample with ATFI coatings has the better surface quality than the sample without coating. Some of the coating still can be seen on the sample with ATFI coating. For further observation, the sample was sectioned for the optical microscopy.

Figure 6 shows the microstructures of baseline H13 steel sample with no coating after 200 cycles. Figure 6(a) shows there is some oxide on the surface of the sample, and Fig. 6(b) shows the soldering of the aluminum and steel base and there is also some oxide on the surface.

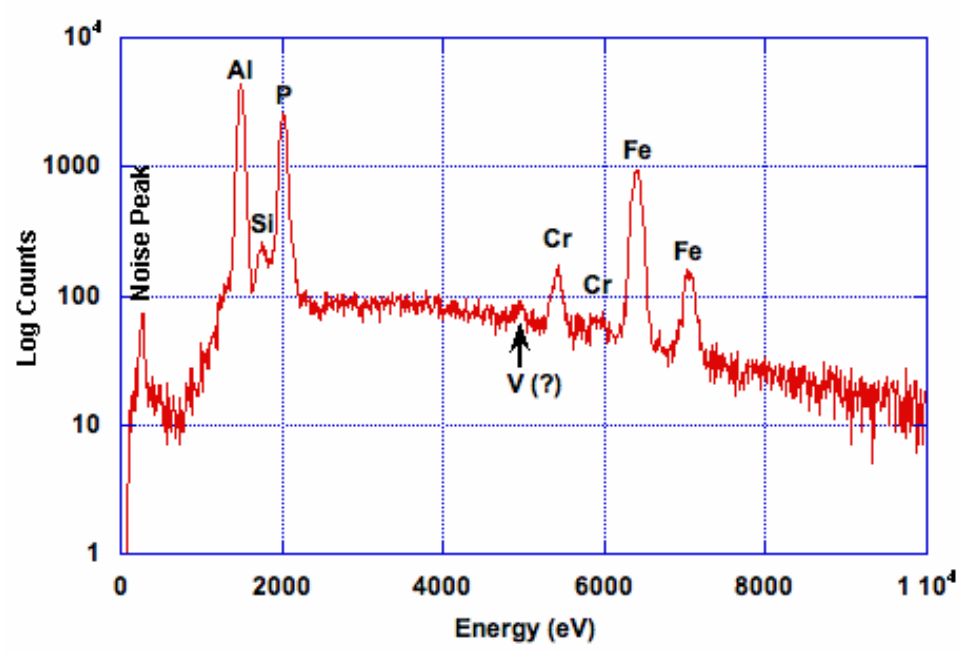

Figure 2: EDAX energy spectrum from JEOL 8200 showing the presence of large amounts of aluminum and phosphorous in the top layers of the sample. Vanadium peak is quite weak and therefore suspect.

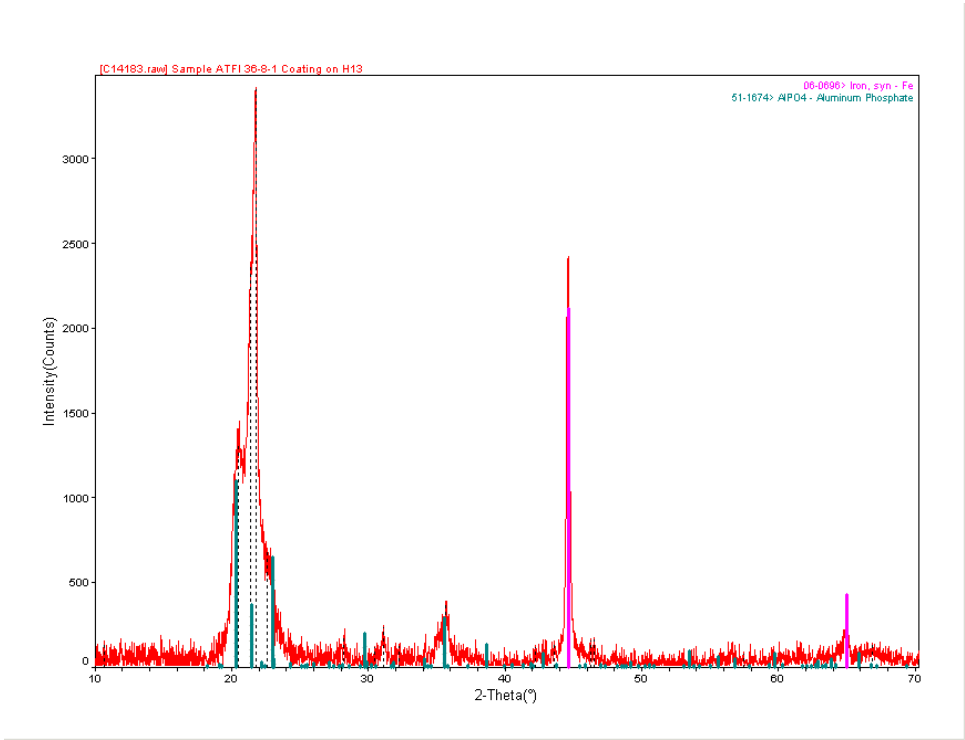

Figure 3: GIXD shows iron substrate and $AlPO_4$ coating.

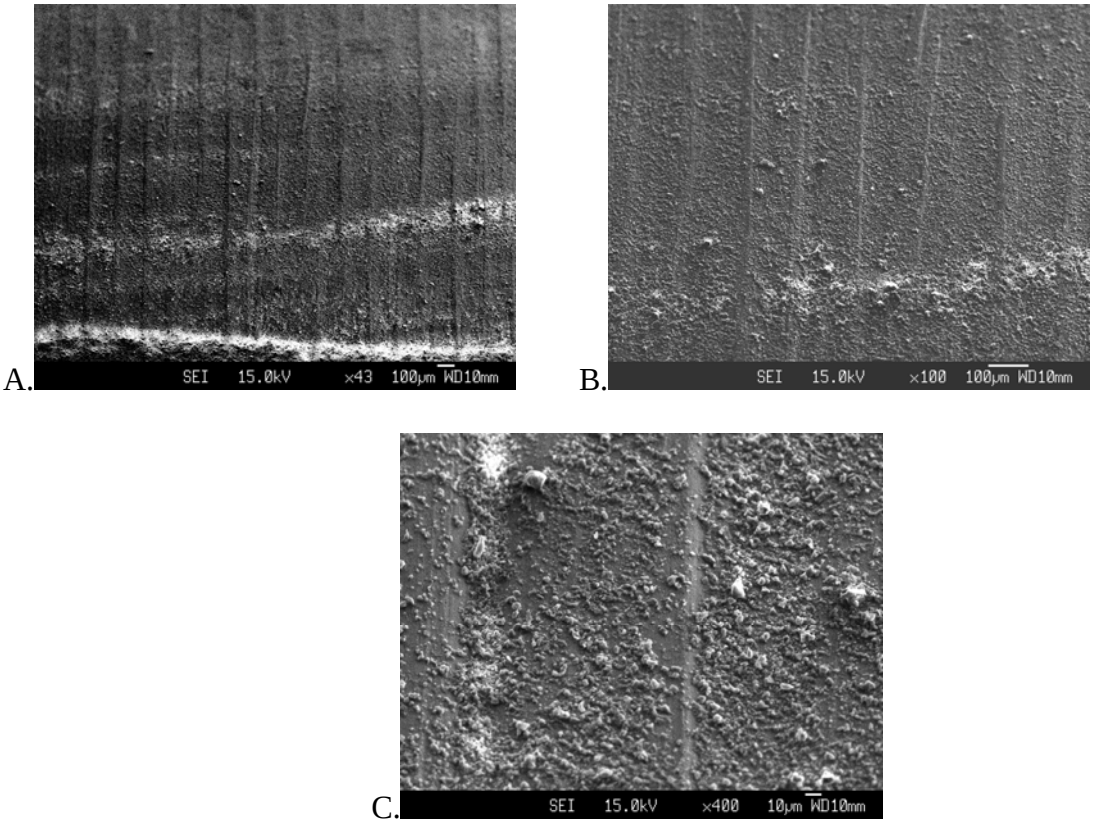

Figure 4: Secondary electron images of the coating from sample ATFI 36-8-1. The coating was on a cylinder of H13 steel. The axis of the cylinder runs left to right above.

(a) (b)

Figure 5: Photos after 200 cycles: (a) baseline H13 steel with no coating, and (b) ATFI 36-8-4.

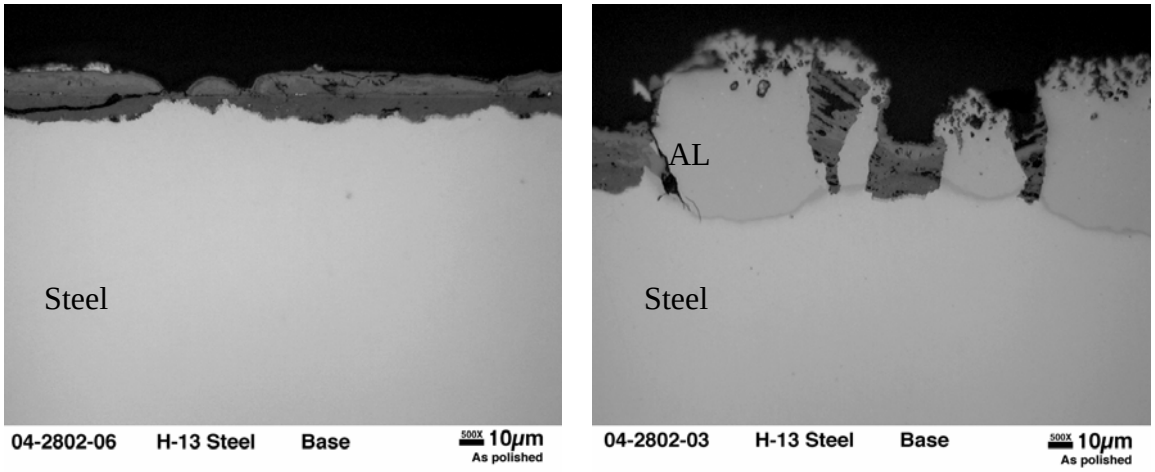

(a) (b)

Figure 6: Microstructures of baseline H13 steel with no coating after 200 cycles.

Figure 7 shows the microstructures of sample ATFI 36-8-4 after 200 cycles. There are some discontinuous phases on the surface. It could be the $AlPO_4$ coating that was shown from XRD results. Under the surface, there also are some newly formed phases. These may be the same oxide in Fig. 6. Compared with Fig. 6(a), the thickness of the oxide is thinner. No soldering of Al and the steel substrate were observed in this sample. It can be concluded that this coating hampers the growth of the oxide and the reaction between the molten Al and steel substrate. Further SEM analyses will be needed to identify the phases on the surface.

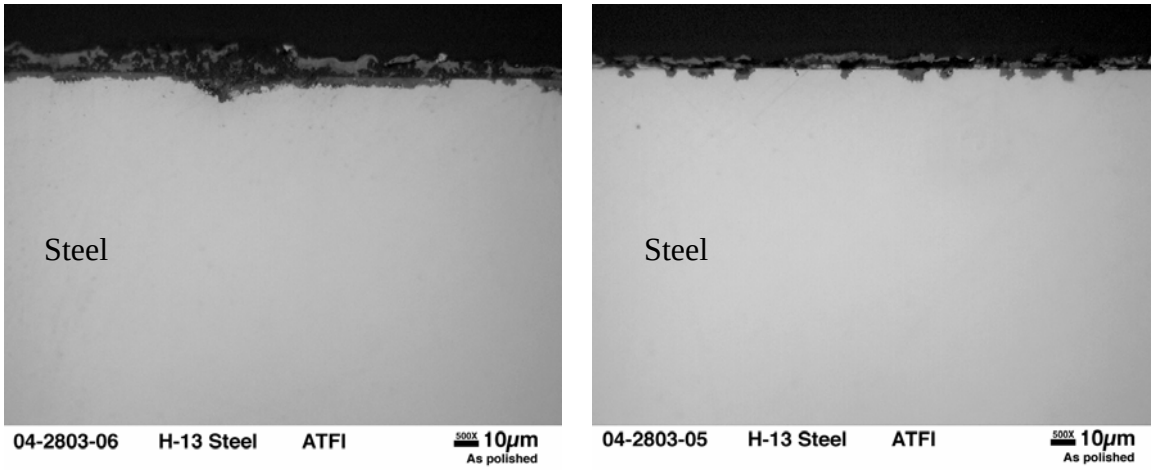

(a) (b)

Figure 7: Microstructure of Sample ATFI 36-8-4 after 200 cycles.

Reports/Publications/Awards: None

MPLUS No.: MC-03-026

Title: Characterization of Aluminum Foam Prepared By Casting Process

User Organization: Energy Industries of Ohio
Independence, OH 44131

User Contacts: Robert M. Purgert, 216-643-2952
purgert@msn.com

ORNL R&D Staff: Vinod K. Sikka, 865-574-5112
sikkavk@ornl.gov

Yogest Bhambri, 865-576-6031
bhambriy@ornl.gov

Bob Purgert from Energy Industries of Ohio with Vinod K. Sikka (ORNL)

Relevance to ITP: Porous materials are of interest for many industrial applications because they can deliver special properties of low density, unique physical properties such as thermal conductivity, and sound properties. Porous materials can also be used to selectively separate materials. Energy Industries of Ohio (EIO) has recently developed foams that use hollow cenospheres from coal ash for creating the porous structures. The cenosphere agglomerates are used to create the porous structure which, when infiltrated with molten aluminum, provides the bonding and structural strength. The microstructure and strength of the fly ash-based foam can be controlled through: (1) selection of agglomerate size of the foam, (2) temperature of infiltration of aluminum, and (3) the selection of an aluminum alloy versus pure aluminum as infiltration media.

Objective: The objective of this proposal was to characterize the microstructure and mechanical properties of aluminum-based foams containing varying amounts of coal fly ash. Part of the project was also devoted to incorporating fly ash in aluminum alloy die castings for reducing the density and cost of the castings.

Results: Foam samples produced with three different fly-ash aggregate sizes are shown in Figs. 1 through 3. Three foams had densities of 0.4, 0.5, and 0.55 g/cm^{3}s, respectively. Each of the foams was cut into 1- $\times$ 1- $\times$ 1-in.-thick samples that were subjected to compression testing at a stroke speed of 0.02 in./min up to ultimate strength and at 0.2 in./min up to crushing limit. Typical stress-strain plot for one of the foams is shown in Fig. 4. Mechanical properties data on all of the foams tested are summarized in Table 1. Yield strength data of various foams tested in this MPLUS are compared with two commercial foams in Fig. 5 which shows that the aluminum foam containing fly ash has better yield strength properties than Al-SiC foams. These foams are only slightly poorer than all of the aluminum foams.

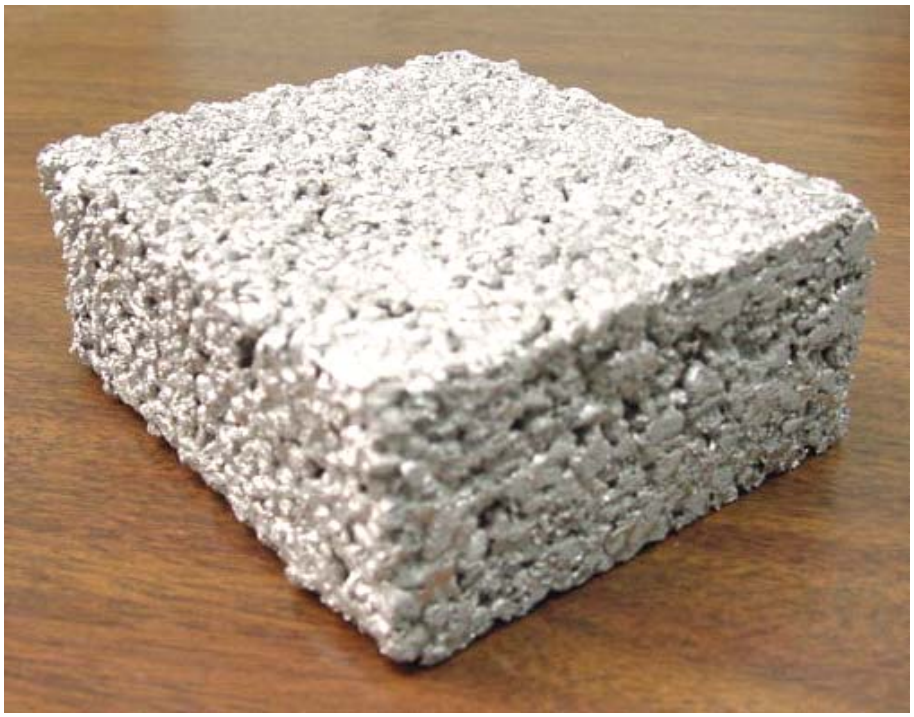

Figure 1: ALFA foams 2.8 to 6.8 mm aggregate with a density of 0.4 gm/cc.

Figure 2: ALFA foams 2.8 to 4.0 mm aggregate with a density of 0.50 gm/cc.

Figure 3: ALFA foams 1.0 to 2.8 mm aggregate with a density of 0.55 gm/cc.

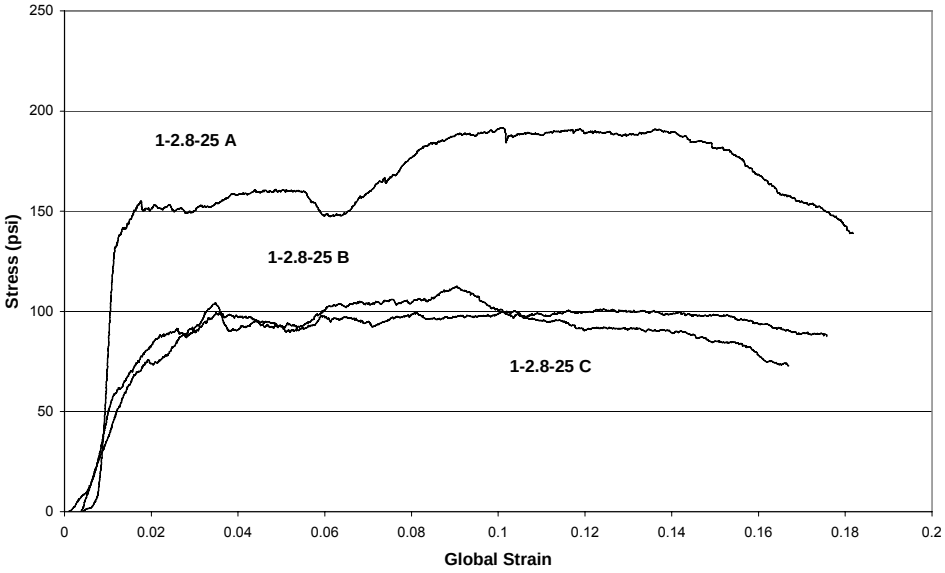

Figure 4: Stress-strain curves from 1-2.8-25 ALFA foam taken from three different locations.

Table 1: ALFA foam composite data

Foam ID	Stiffness (psi)	Compressive Strength (psi) 0.2% YS	Ultimate Strength (psi)	Crush Strength (psi)
1-2.8-25A	34,293	152.4	191.7	78.84
1-2.8-25B	9,798	95.4	112.6	56.23
1-2.8-25C	5,626	99.59	104.3	113.16
1-2.8-27A	29,267	154.7	185.6	77.95
1-2.8-27B	6,380	57.65	87.13	68.37
3-7-33A	34,306	71.31	126.3	125.99
3-7-33B	9,869	86.45	91.65	32.01
3-7-34A	11,142	128.8	134.4	30.51
3-7-34B	10,944	53.32	75.38	20.79
5-7-40A	8,759	73.36	83.75	49.72
5-7-40B	7,007	67.91	97.49	80.80
5-7-41A	13,863	93.79	101.9	65.32
5-7-41B	6,947	90.57	101.4	77.89

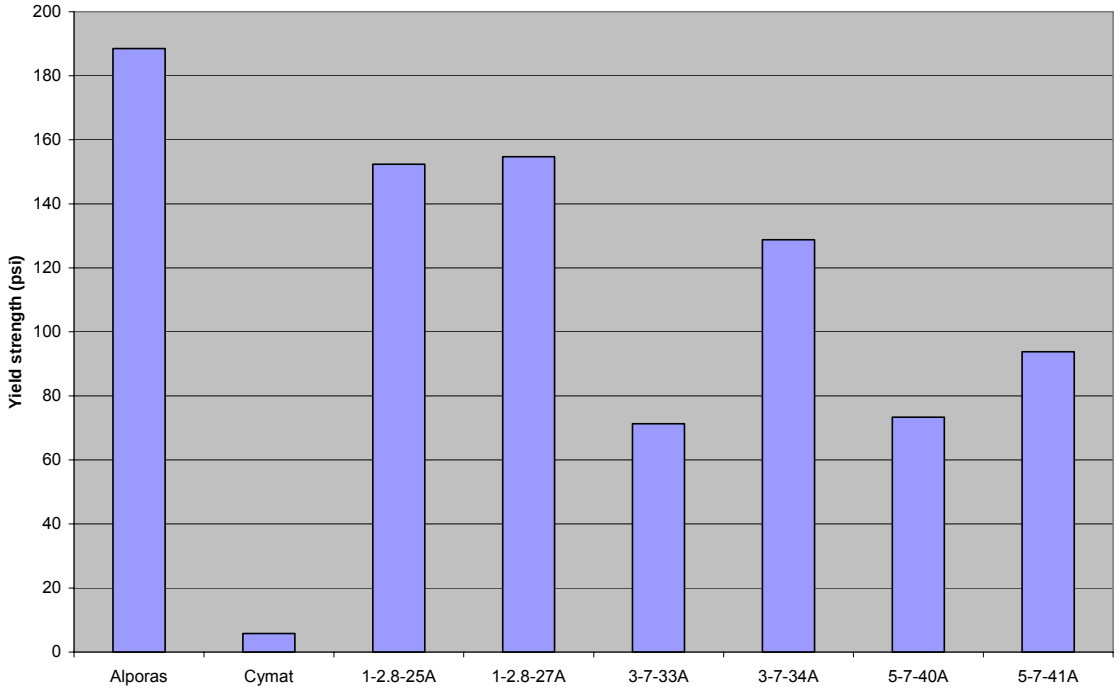

Figure 5: Bar chart illustrating comparison of ALFA yield strengths of ALFA foams with commercially available foams.

The optical microstructures of various aluminum foams containing fly ash are shown in Fig. 6. The phase analysis of these foams (from micrographs in Fig. 6) is summarized in Table 2. Figure 6 and Table 2 show that the aluminum content of the foams tested during this MPLUS varied from 6.9 to 26.7% and pore density varied from 19 to 34.5%. The correlation of ultimate tensile strength and crushing strength with aluminum content and pore content are shown in Figs. 7 and 8. These figures show that the ultimate tensile strength of the foams increases with increasing aluminum content and crushing strength decreases with increasing porosity.

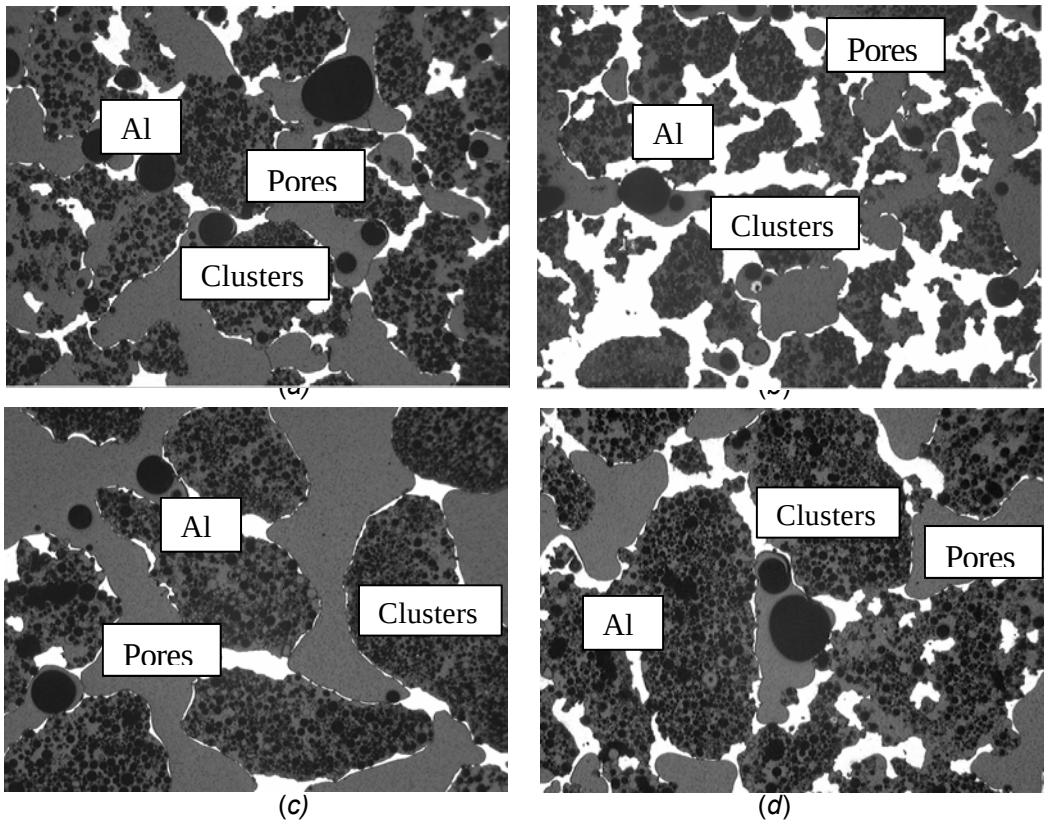

Figure 6: Microstructure of different ALFA foam types showing its constituent phases: (*a*) 1-2.8-25-B, (*b*) 1-2.8-27-A, (*c*) 3-7-34-B, and (*d*) 5-7-40-B.

Table 2: Summary of microstructure phase analysis of different foam types

Foam type	Clusters (%)	Pores (%)	Aluminum (%)
1-2.8-27 A	54.3	19.0	26.7
1-2.8-25 B	60.1	32.0	7.8
3-7-34 B	55.6	34.5	6.9
5-7-40 B	67.6	19.8	11.6

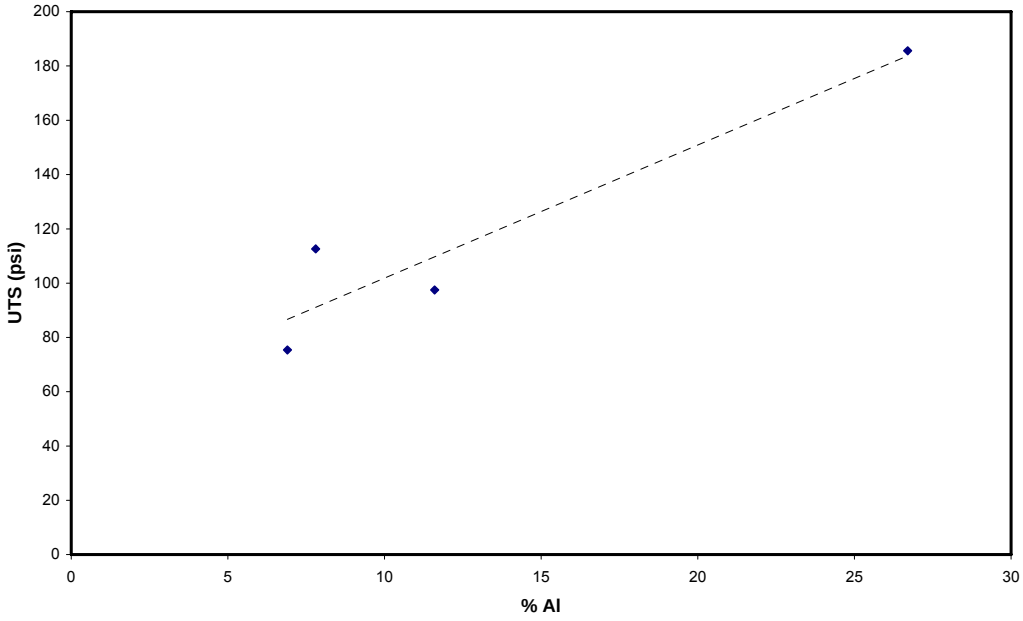

Figure 7: Plot showing increase in ultimate tensile strength with increase in aluminum concentration.

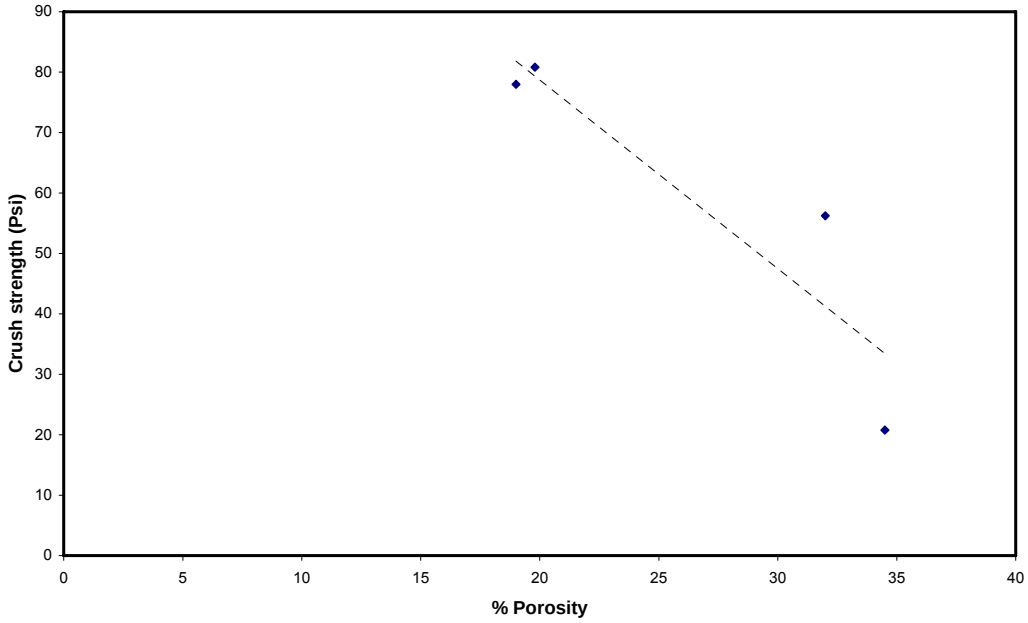

Figure 8: Plot showing decrease in crush strength with increase porosity.

Data presented in Figs. 1 through 8 and Tables 1 and 2 will be used by EIO to further optimize the foam properties and also to properly select the foam for the identified applications.

Reports/Publications/Awards:

Vinod K. Sikka and Yogesh Bhambri, "Characterization of Aluminum Foam Prepared by Casting Process," Final MPLUS report, June 2004.

Y. Bhambri, J. Snider, V. Sikka, L. Boyd, and R. Purgert, "ALFA Foams - Production Process, Characterization and Applications," submitted for publication in proceedings of the Pittsburgh Coal Conference, September 15, 2005.

MPLUS No.: MC-03-019

Title: Characterization of Dross from a Sidewell Melter Producing 3004 and 3105 Aluminum From Undecoated Scrap

User Organization: Commonwealth Aluminum
Lewisport, KY 42351

User Contacts: Joe Tessandori, 270-295-5431
joe.tessandori@cacky.com

ORNL R&D Staff: Karren More, 865-574-7788
moreka@ornl.gov

Larry Walker, 865-574-5339
walkerlr@ornl.gov

Tom Geer, 865-574-4487
geerts@ornl.gov

Joe Tessandori and Gary Funk of Commonwealth Aluminum with Larry Walker (seated) from ORNL

Relevance to ITP: Aluminum must be melted to produce most Al products. However, during the melting process, nearly 4% of the molten Al is lost to oxidation, primarily due to dross formation. Dross is a mixture of aluminum oxides and aluminum metal, which normally forms on the surface of the melt and is skimmed off. Some aluminum metal can be recovered from the dross, but this is an added cost. By understanding the factors that affect the amount and type of dross that forms on different Al alloys, measures can be taken to alter melt practices to reduce the amount of Al lost to oxidation.

Objective: The objectives of this project were to develop an understanding of the microstructural and compositional characteristics of the different drosses formed from using un-decoated scrap as the primary furnace charge as compared to the dross that forms when using cleaner, decoated scrap or clean mill scrap and primary ingot. This information is to be used to help efforts by Commonwealth Aluminum to minimize losses due to dross formation on molten aluminum.

Results: Four different dross samples (~5 in. high × 5 in. diam) were taken (by dipping/scooping using a ladle) from the sidewell during the melting of alloy 3004 from undecoated scrap that was transferred into the heating chamber. Each of the following four dross samples represented a different type of undecoated scrap used for the furnace charge:

1. In-plant shred and delaquered Class 1 briquette (with salts)
2. Painted undelaquered coil
3. Class 1 undelaquered briquette

4. Whole painted coil

A fifth dross sample (control/baseline) was prepared from in-plant shred and delaquered class 1 briquette for comparison with the dross formed by using undecoated scrap.

Each of the five dross samples was cut in half and polished in cross section in its entirety. Images for each complete dross cross section are shown in Figures 1 through 5 for comparison purposes. Figures 1 through 5 also show the smaller, representative areas of dross selected for microstructural analysis for each sample (blue squares). Note that dross sample #5 (control) had the least amount of oxidation product near the surface of the dross sample whereas dross samples #2 and #3 are composed entirely of friable dross particles.

Fig. 1: Dross #1 – in-plant shred and delaquered Class 1 briquette (with salts).

Fig. 2: Dross #2 – painted undelaquered coil.

Fig. 3: Dross #3 – Class 1 undelaquered briquette.

Fig. 4: Dross 34 – foil scrap bales and 3004 briquette melted into 3004.

Fig. 5: Dross #5 – whole painted coil.

Dross sample #1 was difficult to analyze due to the amount of salts within the dross, however, the dross looked fairly "typical" in that it was primarily composed of $MgAl_2O_4$ and much larger regions of amorphous a-Al_2O_3. A scanning electron microscopy (SEM) image of the dross is shown in Figure 6. The different phases comprising the oxidized layer are labeled on the image. Regions of high titanium were associated with the thin strip-like phase, identified by arrows in Figure 6 and by the titanium elemental map shown in Figure 7. These elongated regions also showed high aluminum, magnesium, and oxygen and are possibly remnants of painted shred or coil, which have oxidized to form a titanium-rich $MgAl_2O_4$ phase.

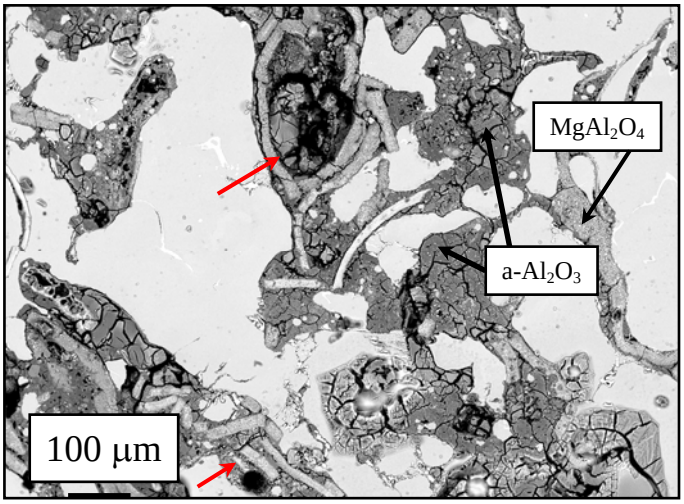

Fig. 6: Scanning electron image of dross sample #1 showing the different phases comprising the oxidized layer and regions of high titanium. identified by the red arrows.

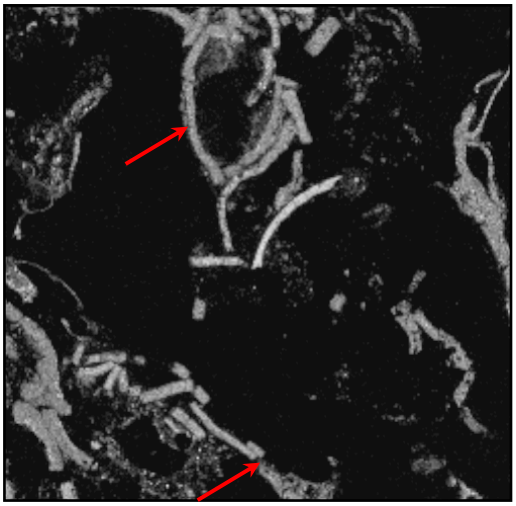

Fig. 7: Elemental map of dross sample #1 shows regions of high titanium are associated with the thin strip-like phase Identified by the red arrows.

Dross samples #2 and #3, both of which were skimmed from a melt produced from a charge with undelaquered coil or briquette, were very similar in that each dross sample was very friable and crumbly. The samples barely held together during cutting and sample preparation. The two dross samples were also filled with salts making analysis quite difficult. The SEM images from dross #2 and #3 are shown in Figures 8 and 9, respectively. Both dross samples were composed primarily of large areas of $MgAl_2O_4$ (shown by red arrows in Figures 8 and 9) as well as much smaller spinel particulates distributed throughout the trapped aluminum metal. In each of these two samples, there is clearly more dross formed during melting of the undelaquered charge and the oxide particles (mostly $MgAl_2O_4$ compared to a-Al_2O_3) within the dross layer are more densely packed.

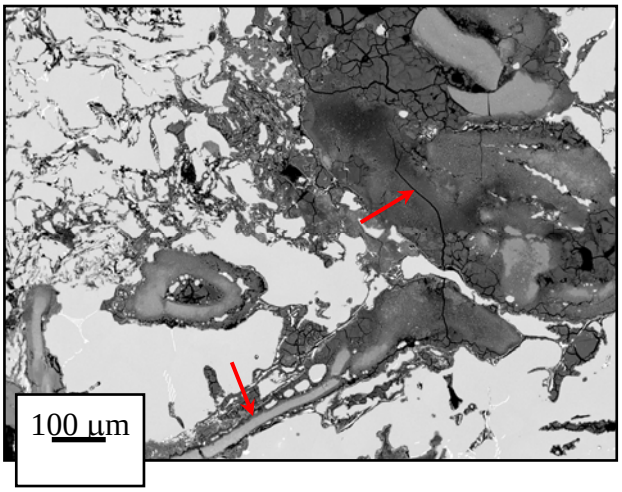

Fig. 8: Scanning electron image of dross sample #2 composed primarily of large areas of $MgAl_2O_4$ as shown by the red arrows.

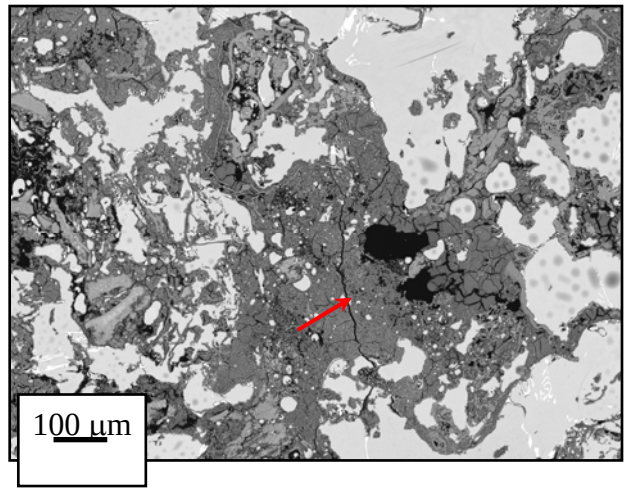

Fig. 9: Scanning electron image of dross sample #3 showing a large area of $MgAl_2O_4$ (red arrow).

Dross sample #4, which was skimmed from the surface of a melt prepared from whole painted coil, had finely distributed oxide particles comprised nearly entirely of $MgAl_2O_4$ spinel, as shown in Figure 10. The painted coil charge used for this melt was delaquered, unlike sample #3, where the charge was composed of undelaquered painted coil. The primary difference between the two dross samples appears to be related to the size and distribution of the oxide particles (very large regions in sample #3 vs fine distribution in sample #4) rather than the oxide phase that forms (mostly spinel in both samples). It was also observed in both samples #3 and #4 that any “remnant” coil or shred (elongated features shown by arrows in Figures 6, 8, and 10) were titanium-enriched (presumably from paint) as shown for dross sample #4 in Figure 11.

The results from the microstructural characterization comparing the dross resulting from charging the melt furnace using undelaquered and delaquered scrap showed that the primary difference between the dross samples was in the size and distribution of the oxide particles. In most cases, the primary phase that formed was $MgAl_2O_4$, except for sample #1 which contained mostly a-Al_2O_3. By using undelaquered shred or painted

coil, much larger regions of spinel formed compared to when delaquered scrap was used. In the dross layers skimmed from melts where painted scrap was used, a significant amount of titanium was identified within $MgAl_2O_4$ "remnants" of shred and coil.

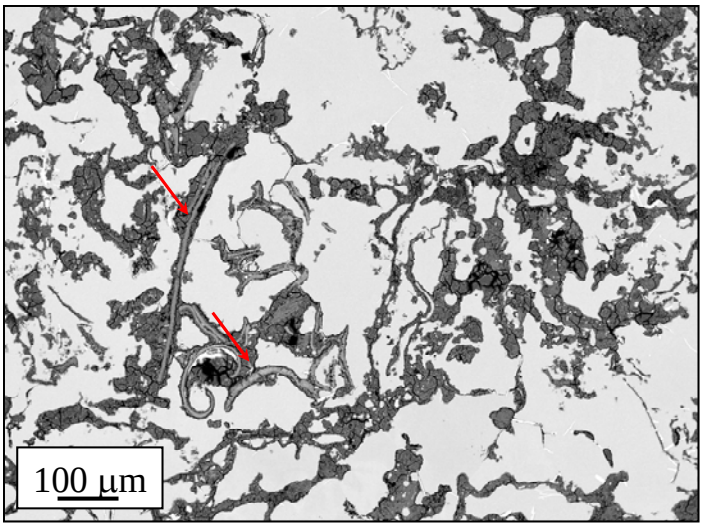

Fig. 10: Dross sample #4 is comprised nearly entirely of $MgAl_2O_4$ (red arrows).

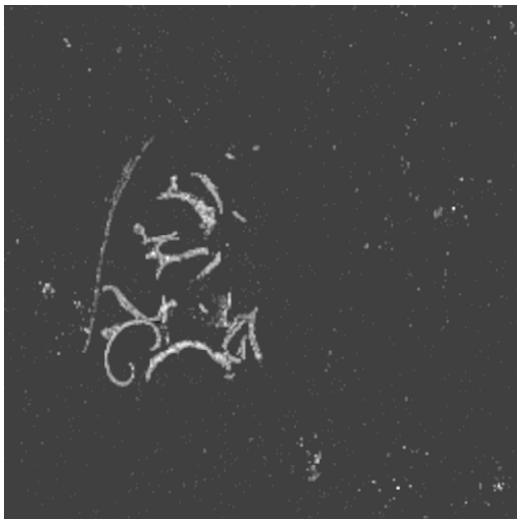

Fig. 11: Dross sample #4.

All of the data from this MPLUS was communicated by telephone and oral discussions to Commonwealth Aluminum in a timely basis. Joe Tessandori and co-worker, Gary Funk, visited ORNL on June 1, 2004 to review the results of the work and to tour the characterization facilities.

Reports/Publications/Awards:

None

MPLUS No.: MC-03-020

Title: Characterization of Precipitation in In-Line Annealed Aluminum Alloys

User Organization: University of Kentucky
Lexington, KY 40506

User Contact: T. Zhai, 859-257-4958
tzhai@engr.uky.edu

ORNL R&D Staff: E.A. Kenik, 865-574-5066
kenikea@ornl.gov

Tony Zhai from
University of Kentucky

Relevance to ITP: Continuous casting of aluminum alloys could provide at least 25% energy savings and significant reduction of subsequent processing costs involved in production of sheet alloy form. Differences in the mechanical properties of continuous cast/in-line annealed materials as compared to conventionally processed AA5000 series aluminum alloys in part reflect their different precipitate microstructures.

Objective: Investigate the precipitate structure of AA5754 and AA5083 aluminum continuous cast and subsequently either in-line or batched annealed. Transmission electron microscopy and x-ray microanalysis were employed to characterize the precipitate structure and composition.

Results: Conventional electropolishing techniques were used to prepare thinned TEM specimens. Specific observations included,

1. Both the in-line and batch annealed AA5754 contained intermetallic precipitates contained Al, Fe and Mn (likely the Al_6(Fe, Mn) phase), as well as oxide inclusions. There was a bimodal distribution of the intermetallic phase (Figs. 1 and 2). The coarse (>100 nm diameter) population of this phase was larger and at low number density in the batch annealed material; whereas the fine (<100 nm) intermetallic precipitates in the batch annealed material were ~3x smaller (10-20 nm diameter) than for the in-line annealed material. There was extensive dislocation pinning by these smaller precipitates (Fig. 2b). The differences in the precipitate microstructure reflect differences in the thermal histories of the in-line annealed material versus the hot-rolled and subsequently batch annealed material. The oxide inclusions contained either Al, S, and Ca or Si, Mo, and Fe and were presumably slag that was incorporated during the continuous casting process.

2. One of the AA5083 materials (N) was the as-cast hot band material, whereas the other material (H) was the same material that was homogenized at 510ºC. Both materials were subsequently cold rolled 70% and then annealed at 400ºC for 3 h. While both materials exhibited precipitates containing Al, Mg, Mn and Cr (presumed to be the $Al_{10}(Mg,Mn,Cr)_3$ phase), the size and number density of these precipitates

were higher in the H condition. This difference in the resulting precipitate microstructure impacted the recrystallization of the cold-worked material during the 400ºC anneal. Dislocation pinning in the H material apparently resulted in the observed elongated dislocation cell structure and high dislocation densities; whereas the N material exhibited only a dislocation network without the formation of any cell structure.

These microstructural comparisons will aid research at University of Kentucky aimed at understanding of the relative mechanical properties of continuous cast versus batch cast aluminum alloys and on the impact of in-line versus batch annealing.

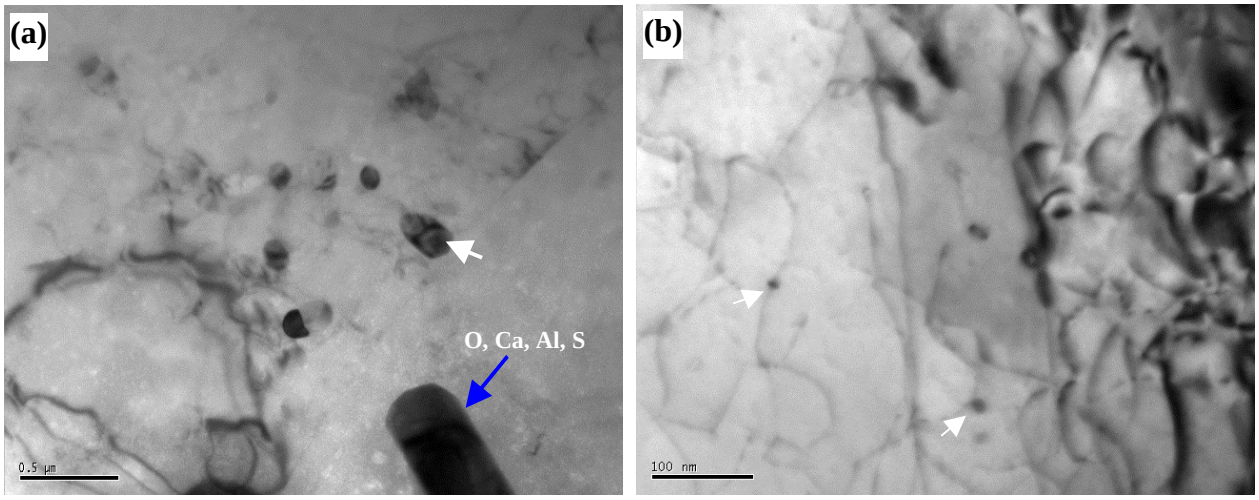

Figure 1: Bimodal distribution of the Al6(Fe,Mn) phase for in-line annealed AA5754.

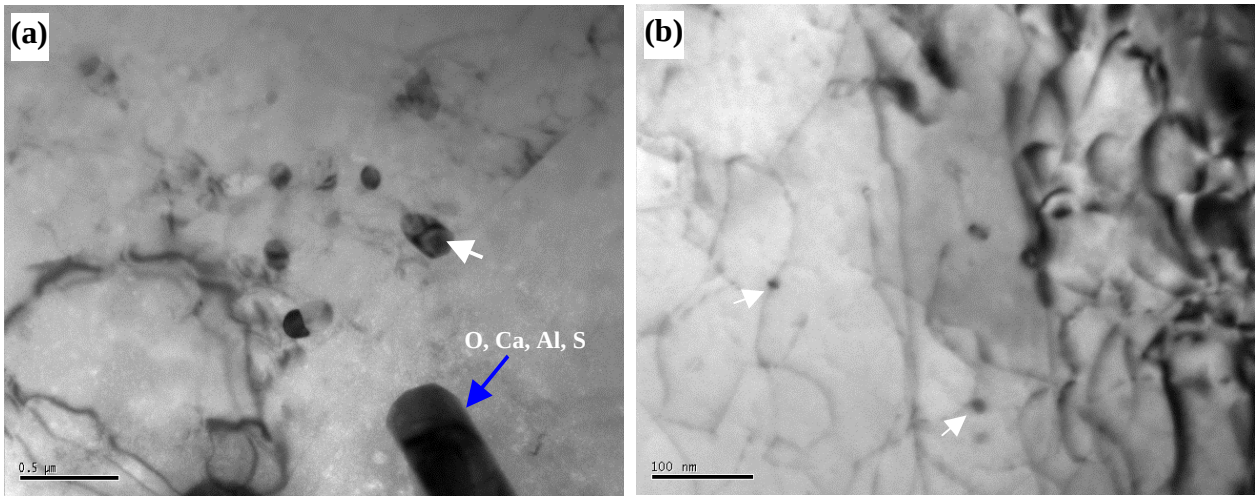

Figure 2: Bimodal distribution of the Al_6(Fe,Mn) phase (white arrows) for batch-annealed AA5754. Note oxide in (a) and pinning of dislocations by fine precipitates in (b).

Reports/Publications/Awards:

E. A. Kenik, T. Zhai, and X. Y. Wen, “Characterization of Precipitation in In-Line Annealed Aluminum Alloys,” Final MPLUS report, 2004.

MPLUS No.: MC-03-018

Title: Coating of Temperature Sensors for Solder Resistance

User Organization: Pyromation, Inc.
Fort Wayne, IN 46825

User Contacts: Richard F. Wilson, 231-386 -5094
pw1dw2@aol.com

Mark Everhart, 260-484-2580
marke@pyromation.com

ORNL R&D Staff: Craig A. Blue, 865-574-4351
blueca@ornl.gov

Puja Kadolkar, 865-574-9956
kadolkarp@ornl.gov

Relevance to ITP: Coatings for solder resistances are clearly spelled out as a major area of interest to the die casting, aluminum, extrusion, and forging industries. In addition, coatings in general are cross cutting in that they are needed by all industries of the future in some form.

Objective: The objective of this project is to study the performance of various coatings applied to 1010 steel thermocouple sheaths when dipped in molten aluminum. The coatings were fused using laser and rapid infrared heating technique and were intended to prevent the tube material from direct contact with molten metal, thereby increasing the life of the thermocouple and reducing the costs incurred in its replacement.

Results: Twelve different coatings were tested for solder resistance. Figure 1 show the solder test rig located at Pyromation, Inc. The test rig consists of a kiln with a control panel and a pneumatic cylinder. The kiln is set at 1400°F, whereas temperature of the molten aluminum is controlled between 1300 and 1380°F. Aluminum alloy A380 was used for the dip tests. Figure 1 show two probes attached to the pneumatic cylinder. The timer controls the cylinder time cycles; approximately 1 min in the molten aluminum and 4 min out. This was done to provide a thermal shock to the probes. There is a thermocouple in each probe to monitor temperature and a counter for counting the number of cycles (times in and out of the aluminum).

Figure 1: Solder test rig at Pyromation, Inc. in Ft. Wayne, Indiana.

The following gives details of a bare thermocouple (uncoated) sheath and eight different coatings and their results obtained while they were being tested with molten aluminum. The tables include the time in molten aluminum and the temperature the probe came up to, and time out of the process, with the temperature the probe came down to. The thermocouple sheath or tube is 1010 steel with 0.25-in.-OD by 0.035-in.-wall. Except for TiB2 that is laser coated, all other coatings were fused using infrared heating.

1) Bare thermocouple sheath (uncoated)

1010 Steel tube, NO COATING.			
11/19/2002, 1:16 PM,			
In time	**Probe temp. °F**	**Out time**	**Probe temp. °F**
44 s	1264	4:00 min	540
	1264		545

11/19/2002, 3:15 PM, 24 Cycles			
In time	**Probe temp. °F**	**Out time**	**Probe temp. °F**
44 s	1320	4:00 min	590
	1321		589

11/20/2002, 10:35 AM, 58 Cycles			
In time	**Probe temp. °F**	**Out time**	**Probe temp. °F**
44 s	1339	4:00 min	620
	1339		584
It is apparent the sheath is being attacked			

11/20/2002, 2:14 PM, 106 Cycles			
In time	**Probe temp. °F**	**Out time**	**Probe temp. °F**
44 s	1353	4:00 min	624
	1354		581
Removed, multiple holes/pits in sheath. T/C still works. ~ 8 h			

05/14/2002 – 8:05 AM – Set point 1400°F – 3180 Cycles			
In Time	**Probe Temp**	**Out Time**	**Probe Temp**
42 s	1355	1.52 min	995
	1356		1000
	1356		998
	1355		998
Readings taken with dross build up on probe. When probe was scrapped clean the hole was found.			

Failure of sheath occurred somewhere between 2615 and 3180 cycles (565), due to the size of the hole it would appear to have happened early, although the hole/element was sealed from the molten aluminum by a layer of dross which would have taken a while to build up. When the probe is cleaned, aluminum immediately sticks to the sheath, but after a while the dross builds up under the aluminum.

Molten aluminum, level line

Top of sheath (No immersion)

Approximately 1in. from tip.

Another hole starting 180° from first hole.

3) Probe #2 – PYRO PROBE coated with TiB_2 (TiB_2 2)

06/27/2002 – 7:45 AM – Set Point 1400°F			
In Time	**Probe Temp**	**Out Time**	**Probe Temp**
48 sec.	1391	4.00 Min.	390
	1391		418
Up to 1390 43 sec.	1390		407

06/27/2002 – 2:40 PM – Set Point 1400°F – 87 Cycles			
In Time	**Probe Temp**	**Out Time**	**Probe Temp**
48 sec.	1384	4.00 Min.	441
	1386		530
Up to 1380 35 sec.	1386		537

06/28/2002 – 7:55 AM – Set Point 1400°F – 381 Cycles			
In Time	**Probe Temp**	**Out Time**	**Probe Temp**
48 sec.	1378	4.00 Min.	376
	1377		390
Up to 1350 28 sec.	1378		450

06/28/2002 – 1:10 PM – Set Point 1400°F – 441 Cycles			
In Time	**Probe Temp**	**Out Time**	**Probe Temp**
48 sec.	1382	4.00 Min.	403
	1383		441
Up to 1350 27 sec	1382		463
Shut down for the weekend			

07/01/2002 – 10:00 AM – Set Point 1400°F – 441 Cycles			
In Time	**Probe Temp**	**Out Time**	**Probe Temp**
48 sec.	1375	4.00 Min.	461
	1374		456
Up to 1350 26 sec	1374		480

07/01/2002 – 1:30 PM – Set Point 1400°F – 487 Cycles			
In Time	**Probe Temp**	**Out Time**	**Probe Temp**
48 sec.	1368	4.00 Min.	416
	1369		417
Up to 1350 29 sec	1369		447

07/02/2002 – 8:00 AM – Set Point 1400°F – 718 Cycles			
In Time	**Probe Temp**	**Out Time**	**Probe Temp**
48 sec.	1367	4.00 Min.	373
	1367		389
Up to 1350 33 sec	1367		383

07/02/2002 – 11:00 AM – Set Point 1400°F – 753 Cycles			
In Time	**Probe Temp**	**Out Time**	**Probe Temp**
Hole in tip, T/C still working			

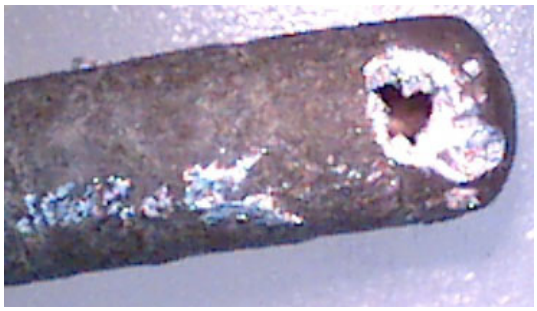

4) ORNL Cerium Coatings

Cerium Coating, 2-air, 440°C/5 Min.			
11/14/2002, 1:15 PM			
In time	Probe temp. °F	Out time	Probe temp. °F
44 Sec.	1376	4:00 Min.	613
	1370		617

11/14/2002, 2:55 PM, 24 Cycles			
In time	Probe tem. °F	Out time	Probe temp. °F
44 Sec.	1315	4:00 Min.	686
	1316		645

11/15/2002, 7.55 AM, 214 Cycles			
In time	Probe tem. °F	Out time	Probe temp. °F
Large hole in sheath. Open T/C. Approx. 16 Hours			

5) ORNL Ce X 4 Coating

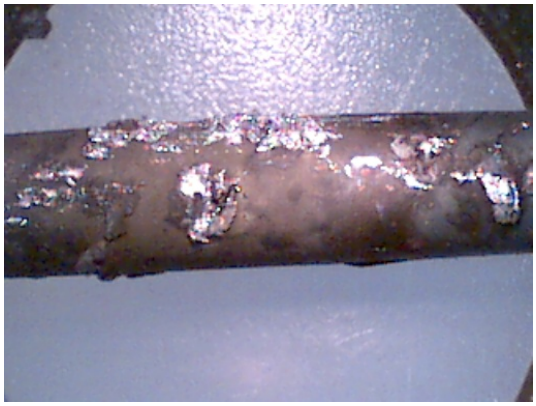

345 cycles

Process Molten Aluminum
1 cycle = 45 s In (1375°F) 4:00 min Out (800°F)

At 250 cycles coating had dulled, there was no scaling, wetting or pitting.
Top pictures taken at 345 cycles, 15 to 20% wetting, and some pitting.
Bottom photos taken at 439 cycles, 50 tp 60% wetting and pits, one large hole.

439 cycles

6) ORNL Ce X 6 Coating

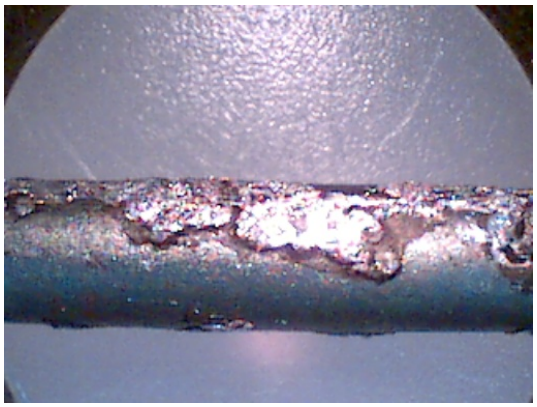

606 cycles

Process Molten Aluminum
1 cycle = 45 s In (1375°F) 4:00 min Out (800°F)

At 300 cycles the finish had started to dull and was non-wetting.
At 400 cycles some flaking had started and 10 to 15% surface area was wetting.
Above photos taken at 606 cycles, wetted areas starting to pit.
Bottom photo's taken at 629 cycles, 85 to 90% wetting, pits have progressed to large holes.

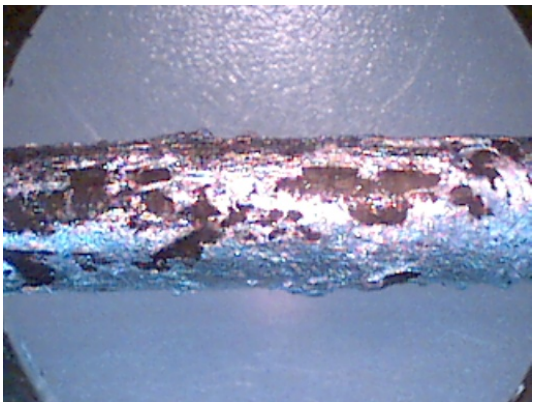

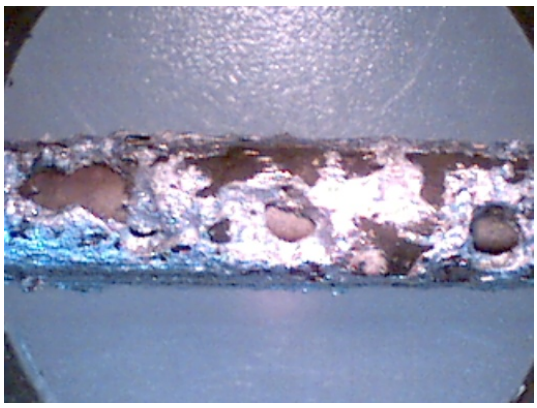

629 cycles

7) ORNL Fluorine Coatings

Flourine Coating, 2-air, 440°C/5 Min.			
11/15/2002, 8:14 AM			
In time	Probe temp. °F	Out time	Probe temp. °F
44 Sec.	1331	4:00 Min.	557
	1332		565

11/15/2002, 3:08 PM, 87 Cycles			
In time	Probe temp. °F	Out time	Probe temp. °F
44 Sec.	1317	4:00 Min.	575
	1317		610

11/18/2002, 8:15 AM, 89 Cycles			
In time	Probe temp. °F	Out time	Probe temp. °F
44 Sec.	1398	4:00 Min.	543
	1393		648

11/18/2002, 3:00 PM, 174 Cycles			
In time	Probe temp. °F	Out time	Probe temp. °F
44 Sec.	1330	4:00 Min.	512
	1327		478
Detected small hole/pit in sheath.			

11/19/2002, 10:15 AM, 206 Cycles			
In time	Probe temp. °F	Out time	Probe temp. °F
44 Sec.	1341	4:00 Min.	573
	1339		495

11/19/2002, 1:00 PM, 241 Cycles			
In time	Probe temp. °F	Out time	Probe temp. °F
44 Sec.	1255	4:00 Min.	450
	1256		550
Removed, multiple holes/pits in sheath. T/C still works. Approx. 18 h			

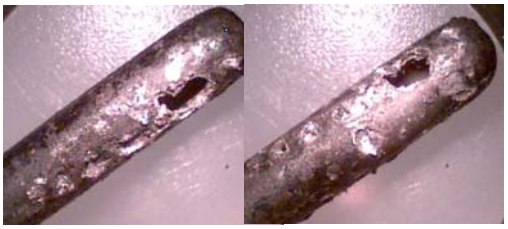

8) ORNL F x 4 Coating

Process Molten Aluminum

1 cycle = 45 s In (1375°F) 4:00 min Out (800°F)

Sheath failed at 311 cycles.
To that point the sheath had looked great, no wetting, no scaling, no pitting.

Appears that a layer of the coating has peeled off all the way around the tube about 1 in. from the tip. That is where what looks to be rust has developed (the transition area between the two layers)?
The other "F" coated tube also did this but on very small areas.

9) ORNL F x 6 Coating

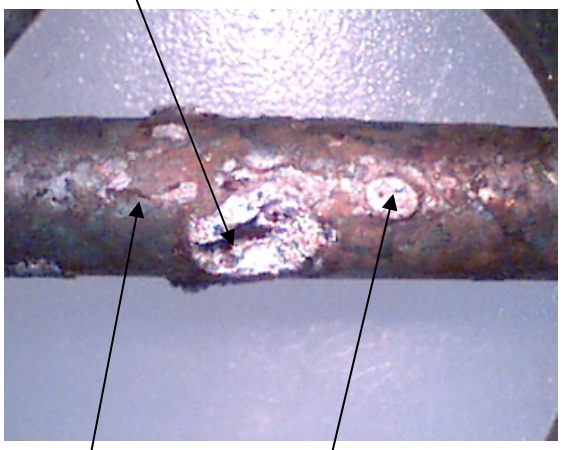

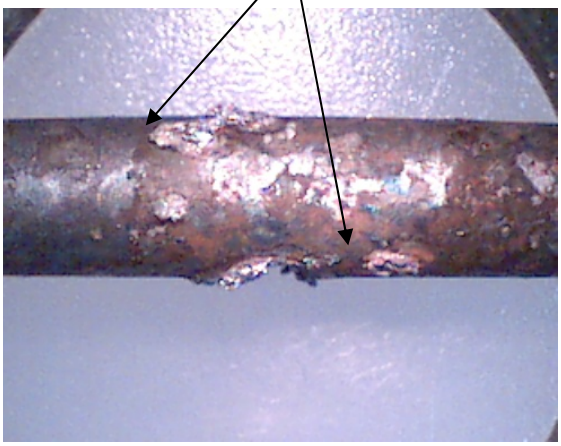

Process molten aluminum

1 cycle = 45 s In (1375°F) 4:00 min out (800°F)

At 467 cycles sheath was in good shape, sheath was no longer shinny, there was no wetting and no pits.

Pulled sensor at 706 cycles, large hole in sheath, some scaling and pitting, but still about 95% non-wetting.

10) ORNL C3 X 6 Coating

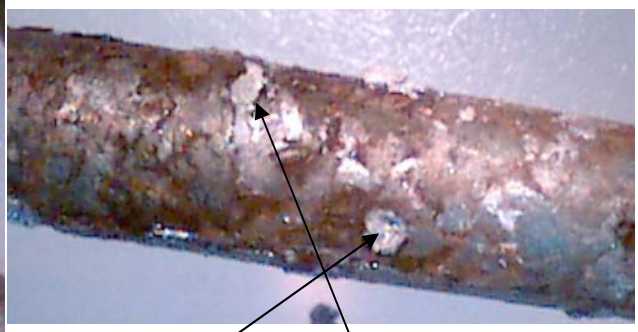

Scales

Dross line

Pits

Pictures taken at 699 cycles

Aluminum deposits stuck to sheath / coating

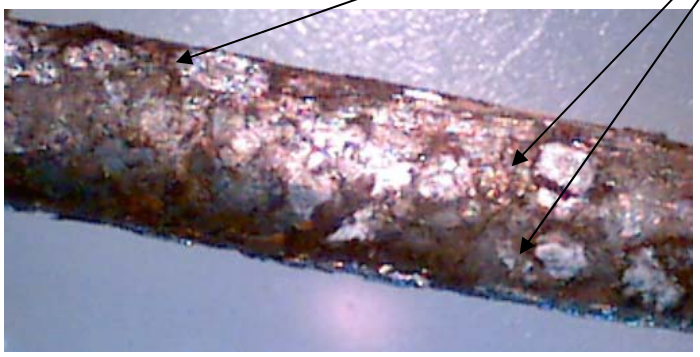

Process molten aluminum
1 cycle = 45 Sec. In (1375°F) 4:00 min Out (800°F)

At 400 cycles the coating was still non-wetting, but the finish had started to dull.

At 699 cycles, there was a lot of scaling; a couple of pits, and 10 to 15% of the surface had aluminum deposits.

Pictures taken at 788 cycles.

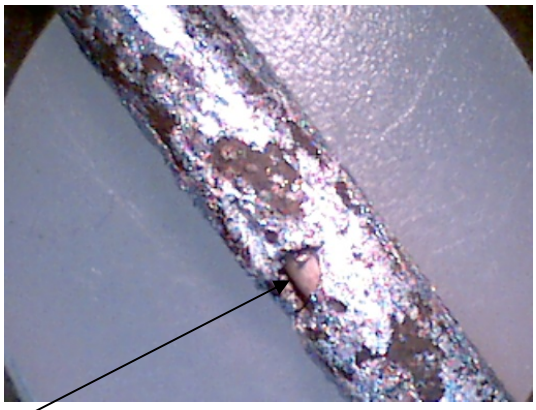

Holes

11) M1, M2 and M3 are Ni-10P coated with Cr_2C_3

Probe M1 & M2 - 1 Cycle = 45 s In molten Aluminum (1400°F), 4:00 min out (700-800°F)
Probe M3 - 1 Cycle = 4:00 min In molten Aluminum (1400°F), 4:00 min out (700-800°F)

AFTER 81 CYCLES

PROBE M1

AFTER 95 CYCLES

Ceramic Insulator

AFTER 74 CYCLES

PROBE M2

AFTER 103 CYCLES

Open End

Ceramic Insulator

PROBE M3

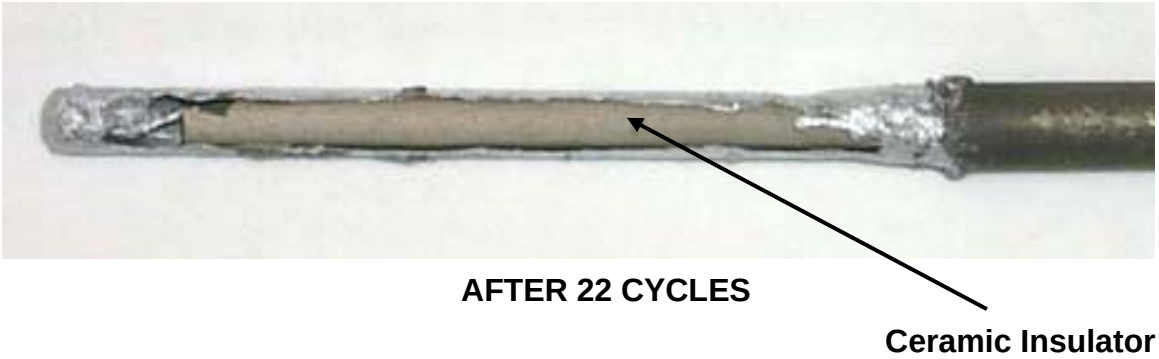

Table 5: ORNL C3 zirconia coatings

Zirconia	
Probe	**Number of cycles**
Zr-1[a]	853
Zr-2	291
Zr-3	851
Zr-4	467
Zr-5[b]	623

[a]Zr-1 represents one layer of coating; [b]Zr-5 represents five layers of coating.

Table 6: ORNL C3 cerium coatings

Cerium	
Probe	**Number of cycles**
Cr-1[a]	191
Cr-2	620
Cr-3	429
Cr-4	475
Cr-5[b]	757

[a]Cr-1 represents one layer of coating; [b]Cr-5 represents five layers of coating.

SUMMARY OF RESULTS

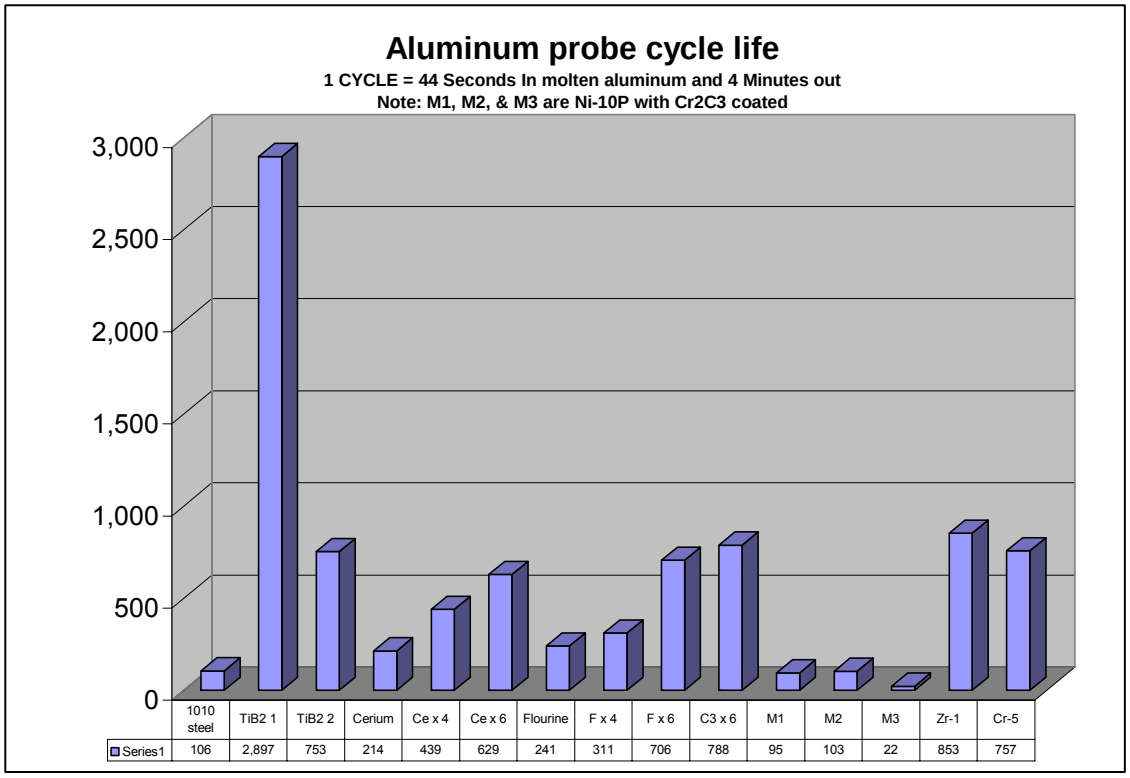

CONCLUSIONS

The results of the molten aluminum dipping test showed improved performance with most of the coatings. Out the 12 coatings that were tested, laser coated TiB_2 sheaths were found to be of typical interest. Investigators of this project believe that change in the OD of the sheaths from 1/4” to ½” can make the thermocouple probes more rugged and can further help to increase its life by providing more material to be consumed by aluminum before failing.

REPORTS/PUBLICATIONS/AWARDS:

Craig A. Blue, Puja B. Kadolkar, Richard F. Wilson, and Mark Everhart, “Coating of Temperature Sensors for Solder Resistance,” Final MPLUS report, June 2004.

MPLUS No.: MC-03-002

Title: Determination of the Mechanism Leading to the Formation of Surface Irregularities on Nitrided, Hot-Isostatically-Pressed Nb-50 wt % Ti-20 wt % W Alloy Compacts

Bill Snyder from MATTEC with Vinod Sikka, ORNL

User Organization: MATTEC, LLC
Knoxville, TN 37922

User Contacts: William B. Snyder, Jr., 865-966-1194
mattec@mindspring.com

ORNL R&D Staff: Vinod K. Sikka, 865-574-5112
sikkavk@ornl.gov

G. (Murali) Muralidharan, 865-574-4281
muralidharag@ornl.gov

Relevance to ITP: This project dealt with assisting in solving a processing problem for a niobium-based alloy which has application for various components in the molten aluminum baths and aluminum die casting. The niobium-based alloy is quite expensive and, thus, any issues with its proper processing should be kept to a minimum. This MPLUS identified the issue of blistering of the alloy billets that occurred after hot-isostatic pressing. Reducing the processing issues to a minimum saves substantial amounts of energy in two ways: (1) by producing a reproducible material that performs reproducibly in molten aluminum applications with extended life, and (2) by not having to remanufacture the material and, thus, saving the energy that is consumed during various steps of the manufacturing processes.

Objective: The objective of this project was to identify the causes for blistering observed in the hot-isostatically-pressed billets of Nb-50 wt % Ti-20 wt % W alloy. This is one of the intermediate steps in manufacturing the alloy. This alloy is used in molten aluminum bath and in die casting applications.

Results: In order to identify the causes for blistering, the following tests were carried out:

Dye Penetrant Inspection: Dye penetrant inspection of welds made on the can that contained the pressed billets, prior to going into hot-isostatic pressing was carried out. This inspection revealed no cracks or discontinuities in the weld. Inspection of the billets showed that they were fully dense.

Machining and Heat Treatment: A cylinder from the HIPped billet was machined and heat treated at 1800ºC for 4 h. This treatment resulted in excessive blistering.

X-Ray Diffraction: X-ray diffraction of the starting powder showed it to be phase pure.

Encapsulation: In order to check if blistering happened under vacuum, a machined cylinder was encapsulated in a molybdenum can and heated at 1800ºC under 10^{-6} torr vacuum. This cylinder also blistered, indicating that it occurred in neutral atmosphere, was not affected by the nitriding treatment of this alloy prior to use.

Elemental Scans: Elemental scans of the sample by microprobe analysis showed some inhomogeneity of elements. The pure tungsten regions noted indicated that tungsten might have been rejected from the matrix by preferential nitradation of titanium in the alloy during the nitriding process.

The above tests provided very valuable data. However, no conclusions could be drawn based on these data. It was realized that the powder used for this run of the niobium-based alloy was made from the machine turnings. The turnings were hydrided, ground, and dehydrided. More careful analysis showed the presence of iron on particles, which could have been picked up during the machining operation. The heat-treatment temperature of 1800ºC is substantially above the melting point of iron and the vapor pressure of iron at this temperature is approximately 1 atm. Upon melting of iron, volume expansion occurs and it could be this expansion that caused blistering on the surface of the niobium alloy.

Based on these results, it is concluded that great care needs to be taken in the selection of the starting powder. The iron contamination is critical and should be controlled carefully.

Reports/Publications/Awards:

W. B. Snyder, “Observation of Surface Blisters in Hot-Isostatically-Pressed Tribocor® 532N,” Final MPLUS report, 2003.

MPLUS No.: MC-03-023

Title: Development of a Process to Hermetically Seal a Thermal Sensor using a Vitreous Sealing Glass

User Organization: DELTA M Corporation
Oak Ridge, TN 37830

User Contacts: Reg McCulloch, 865-483-1569
rmcculloch@deltamcorp.com

ORNL R&D Staff: Craig A. Blue, 865-574-4351
blueca@ornl.gov

Puja B. Kadolkar, 865-574-9956
pbk@ornl.gov

Relevance to ITP: All industries within the Office of Industrial Technologies (OIT) have to measure gas or liquid flow in one form or another. Typically, this is accomplished by measuring velocity per unit time. This newly developed sensor would be able to measure mass per unit time which is much more desirable for the petrochemical and pulp and paper industries as it would give them a direct quantitative measurement. This could apply to all other Industries of the Future that have flow measurement needs to temperatures as high as 500°C. Sensing and intelligent processes are call out as areas needed to be focused on by OIT.

Significance of the Results: In this research, computational thermodynamic and kinetic modeling was used to determine if the kinetics of $L1_2$ ordered γ' precipitates might be leading to rapid strain aging in the heat-affected zone. The results showed that by modification of the transformation kinetics through composition and thermal cycle modifications, it is possible to reduce the tendency for strain age cracking. This shows it is indeed possible to use high-temperature and corrosion-resistant nickel-base superalloys in chemical industries, thereby achieving high-energy efficient process cycles.

Objective: To accurately measure liquid mass flow at other than very low rates using a thermal based sensor, the thermal resistance (R_T) between the sensor and liquid media must be low (<1°C/w). The surface mounted sensor developed through this project will have sufficiently low R_T to perform measurement necessary for the development of the new instrument.

Results: The objective of this project was to use the flat-bed infrared furnace to determine the optimum temperature-versus-time profiles to provide bonding of the alumina resistance temperature detectors (RTDs) (both microheater RTD and temperature reference RTD) to the Glass-Mica substrate as well as to hermetically seal

RTD leads from the substrate outer surface (Fig. 1). A special fixture, as shown in Fig. 2 was developed to hold the assembly of different components together during the heating trials.

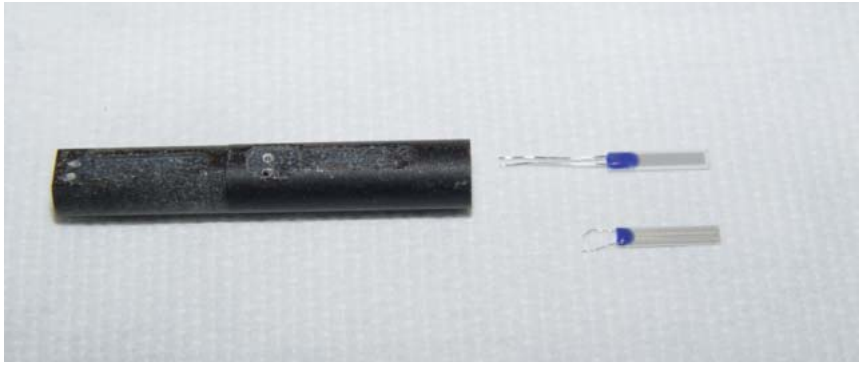

Figure 1: Glass-Mica substrate, microheater resistance temperature detector (RTD) and temperature reference RTD.

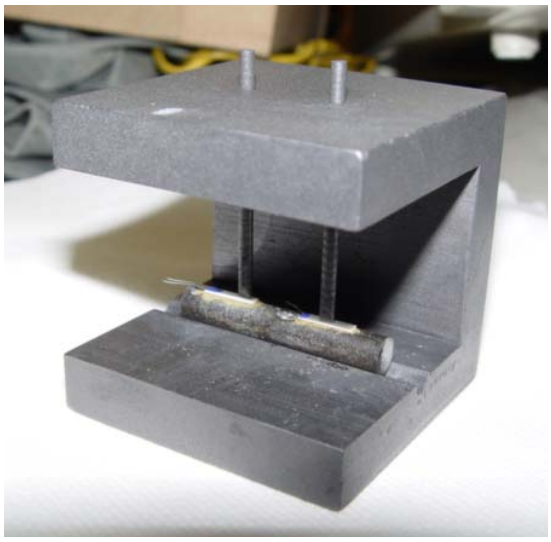

Figure 2: Fixture developed to hold the assembly of different components of the thermal probe.

Sealing of the RTDs and leads was tested with two types of proprietary low-temperature melting glasses. The experimental procedure consisted of recording temperature-time profiles indicating the heating rate (°C/min), soak temperature (°C), soak time (min) and cooling rate during heating trials followed by insulation resistance tests of the sealed surfaces to determine sufficient sealing and microscopic examination to determine sufficient wetting of the glass. Out of the two glasses, one glass failed the resistivity test indicating improper sealing. Scanning electron microscope micrographs (Fig. 3) at the

glass-RTD interface indicated existence of cracks. Cracks appear to generate due to thermal expansion mismatch between the glass and the RTDs and the substrate.

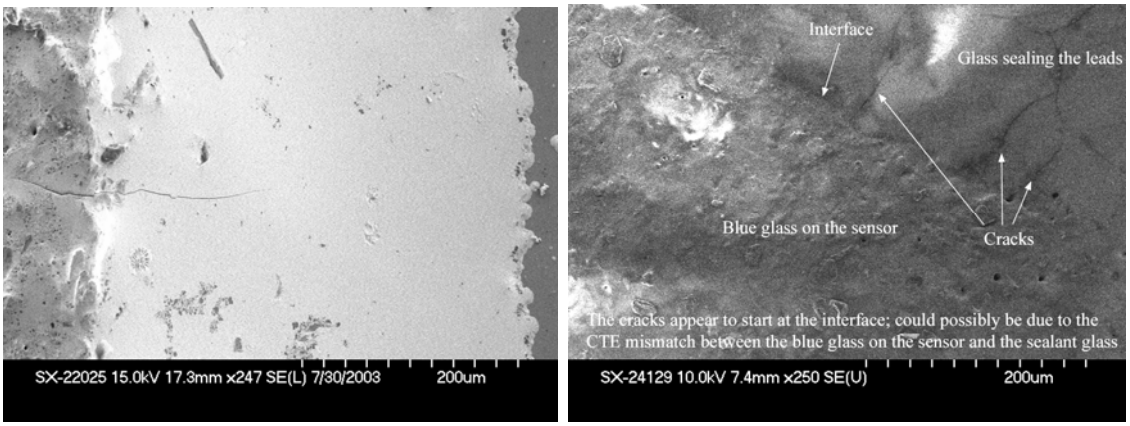

Figure 3: Scanning electron microscopy micrographs at the glass-RTD interface.

Based on this analysis, a second glass with coefficient of thermal expansion closer to the RTD and substrate was used to perform proper sealing. A series of experimental trails proved this new glass to be insensitive to the heating and the cooling rates and developed crack-free sealing with required resistance values. Figure 4 represents one of the time-temperature profiles used to seal this glass. Infrared heating was also proven to be a very efficient and controlled means to perform quick sealing of glasses.

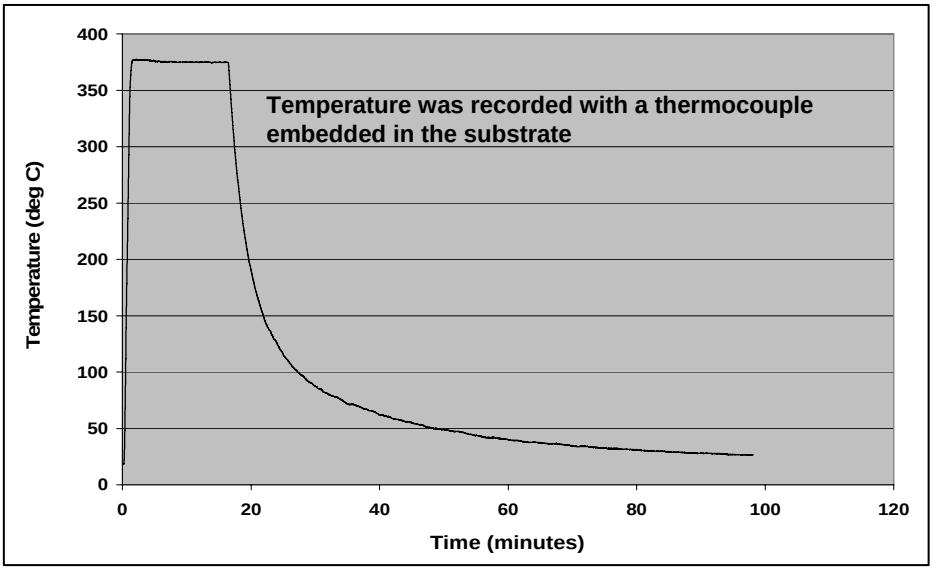

Figure 4: Time-temperature profiles for glass sealing (heating rate = 175°C/min; soak temperature = 375°C; soak time = 15 min; sensors were allowed to cool in furnace).

Conclusion: Processing parameters to produce rugged and low-resistance hermetic seals using a low-melting vitreous glass were identified. The sensors or flowmeters developed using these new seals offer a new generation instrument bringing economical, low maintenance and lower energy usage flow metering to the process industries. Their very low pressure drops at moderate to high flow rates as compared to the instruments currently available will allow significant energy reduction for many processes where they will be used.

Reports/Publications/Awards:

Reg McCulloch, Craig A. Blue, and Puja Kadolkar, “Development of a Process to Hermetically Seal a Thermal Sensor using a Vitreous Sealing Glass,” Final MPLUS report, June 2004.

MPLUS No.: MC-03-010

Title: Development of Hot-Rolling Fabrication Parameters for Aluminum-Boron-Carbide Metal-Matrix Composite Materials

Metamic's Donald Wiggins measuring dimensions of hot-rolled aluminum-boron-carbide metal-matrix composites

User Organization: Metamic L.L.C.
Lakeland, FL 33811

User Contacts: Thomas G. Haynes, 863-709-9448
metamicllc@msn.com

Donald Wiggins, 804-233-6201
Dwig2262@aol.com

ORNL R&D Staff: Craig A. Blue, 865-574-4351
blueca@ornl.gov

Puja Kadolkar, 865-574-9956
kadolkarp@ornl.gov

Relevance to ITP: The aluminum industry is one of the IOFs and this work will aid in the efficient production and utilization of aluminum metal matrix composites.

Objective: The objective of this project was to develop the hot-rolling fabrication technology to process aluminum metal-matrix composite materials to develop and expand potential market applications. If successful, Metamic would be supplying test samples to potential customers for evaluation for potential production applications in the nuclear, aerospace, and other potential commercial applications.

Results: The purpose of the project was to develop hot rolling reduction schedule for three different aluminum/boron metal matrix composite compositions. Metamic L.L.C. supplied the aluminum composite material with boron carbide loadings varying from 25 to 40%. The composite materials were prepared using cold isostatic and vacuum sinter powder metallurgy technology.

Sheets of boron-carbide-loaded composite material were heated up to 1000°F in a conventional air furnace and rolled with varying reduction schedules a number of times to produce a thin-gauge sheet suitable for production applications. A 2-high United rolling mill (Fig. 1) with roll dimensions 12.5-in. wide by 14-in. long was used for hot rolling. Eight-pass schedules such as that shown in Table 1 were identified as suitable reduction procedures for producing thin-gauge composite sheets. Among the three boron-carbide-loading compositions, composite material with loadings of 25 wt % was identified to roll with less difficulty and less cracking.

Figure 1: Oak Ridge National Laboratory's Kenneth Blakely performing hot-rolling of aluminum-boron-carbide composite material.

Table 1: Rolling schedule for 25 wt % boron-carbide-loaded composite material

Rolling Schedule	Thickness of the compact		Reduction (%)
	1000th of an inch	mm	
0	450	11.43	---
1	423	10.74	6
2	385	9.78	9
3	345	8.7	11
4	305	7.74	11
5	260	6.58	15
6	220	5.6	15
7	145	3.69	34
8	90	2.29	38

ORNL's United rolling mill was successfully used for hot-rolling of aluminum boron carbide composite materials. With 25% boron-carbide loadings, reductions as much as 38% were made possible. Based on the results, efforts are currently underway to scale up the rolling schedules for production.

Reports/Publications/Awards:

C. A. Blue, P. Kadolkar, T. G. Haynes, and D. Wiggins, "Development of Hot-Rolling Fabrication Parameters for Aluminum-Boron-Carbide Metal-Matrix Composite Materials," Final MPLUS report, August 2004.

MPLUS No.: MC-03-015

Title: Development of Welding Process to Join Aluminum Alloy Sheets Coil to Coil

User Organization: Commonwealth Industries, Inc.
Lexington, KY 40511

User Contact: Zhong Li, 859-514-4951
zhongli@ciionline.com

John Moore, 252-212-3102
JMoore@alflex.com

ORNL R&D Staff: Robert W. Reed, 865-574-4843
reedrwJR@ornl.gov

Jeff McNabb, 865-574-4811
mcnabbjd@ornl.gov

Stan A. David, 865-574-4804
davidsa1@ornl.gov

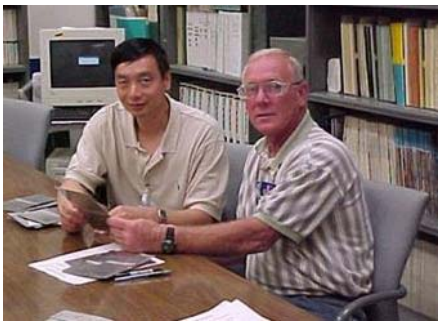

Zhong Li from Commonwealth Industries, Inc. with Robbie Reed (ORNL)

Relevance to ITP: The purpose of this project was to develop a welding process and parameters to improve the acceptance rate of weldments at Commonwealth Industries, Inc. (CII), after joining aluminum alloy sheets coil to coil. After a preliminary evaluation on three welding processes, namely, Laser, Gas Tungsten Arc (GTA) and Gas Metal Arc (GMA), successful procedures were developed by Oak Ridge National Laboratory (ORNL) for coil to coil welding using GTA process that is also the process of choice at CII. After implementing the suggested solution from ORNL, the welds have improved dramatically with regard to weld quality and consistency at the slitter. The weld beads were uniform, narrow, thin, and clear. The penetration also improved without any burnout at the beginning and at the end of the weld without use of any tabs. The weld failure rate decreased 13%. This project has immensely benefited CII, a goal within the scope of IMF.

Objective: The objective was to develop a welding process and parameters to improve the acceptance rate of weldments for the joining of aluminum alloy sheets coil to coil. The three processes investigated were GTA, GMA, and laser welding. The aluminum alloys to be welded were 0.015-in.-thick 3004 alloy, 0.025-in.-thick BH22 alloy, and 0.015-in.-thick BH23 alloy. Aluminum alloy 5356, 0.030-in.-diam wire was used as filler. The joint was a 6-in.-long butt-type joint. The current equipment and process that CII used for joining is GTA. So our primary focus was to develop better welding parameters and fixture for successful welding of the three alloys.

Results: The three aluminum alloys as well as the filler wire were supplied by CII. Welds were made using automatic GTA welding process shown in Fig. 1. Weldments were made using DC straight polarity and a 3/32-in.-diam thoriated tungsten electrode. The development of the welding parameters consisted of several attempts using various mixture of argon and helium, current, voltage, wire feed, and torch travel speeds for all three alloys. It was realized at the beginning that a flat chill plate would be needed on the backside of the joint to be welded to prevent burn-through. This was something that was not being done at CII. A chill fixture using a flat plate with hold-down clamps to hold the joint together and tight against the backing plate was fabricated here in the lab and shown in Fig. 2. Automatic voltage control unit to maintain a certain voltage throughout the weld was necessary. This is important in welding thin aluminum. Parameters were developed for successful welding of aluminum sheets without defects. Weldments passed bend tests required by CII (Figs. 3 and 4). Less build-up of weld metal on the surface was also obtained eliminating the need for grinding of the weld surface.

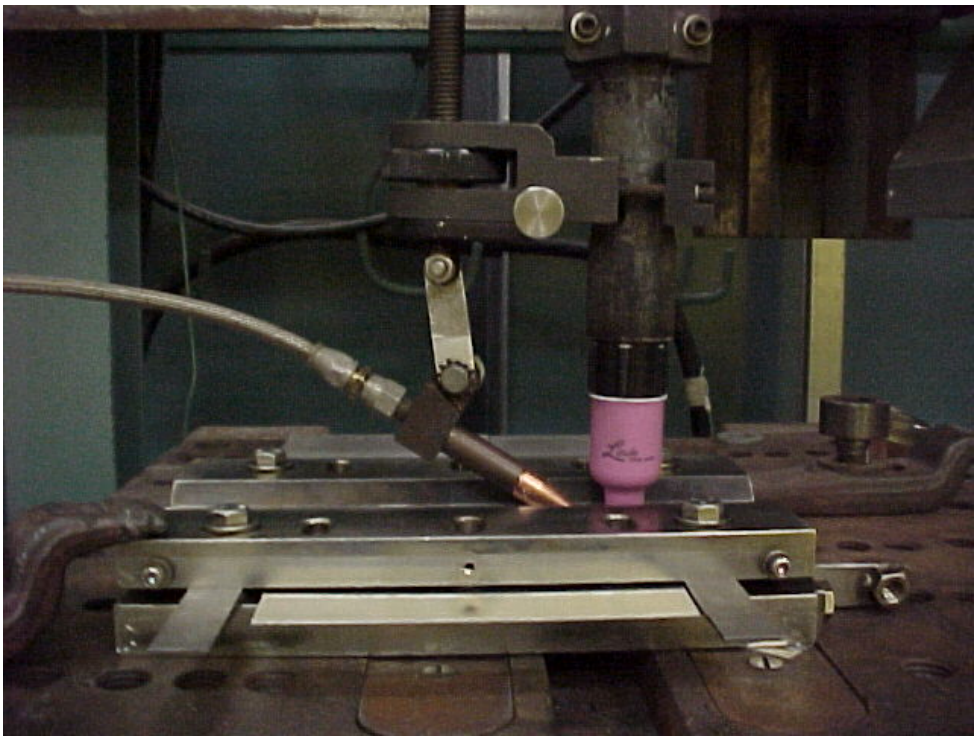

Figure 1: Automatic gas tungsten arc process.

Also, laser welds were successfully developed that were acceptable but the cost of buying a new laser welding system was a concern for CII. They decided to continue with their existing equipment and process, namely GTA welding.

GMA welds were also attempted on the three alloys and found to be very difficult to obtain a consistent weld along the entire length of the weldment.

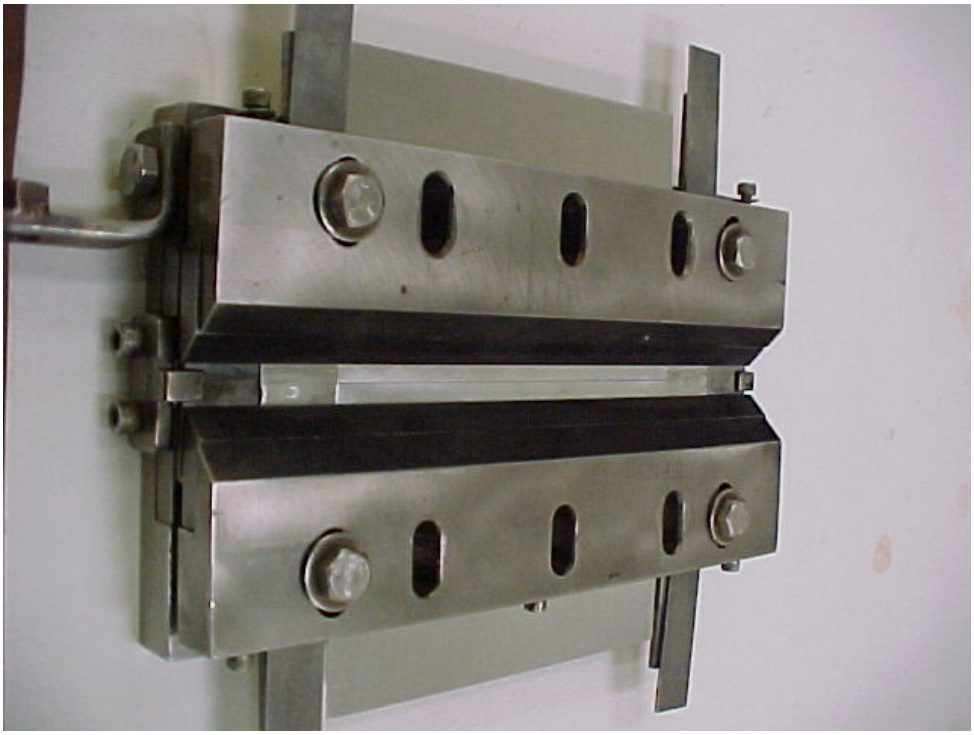

Figure 2: Hold-Down and Chill Fixture used for welding aluminum alloys.

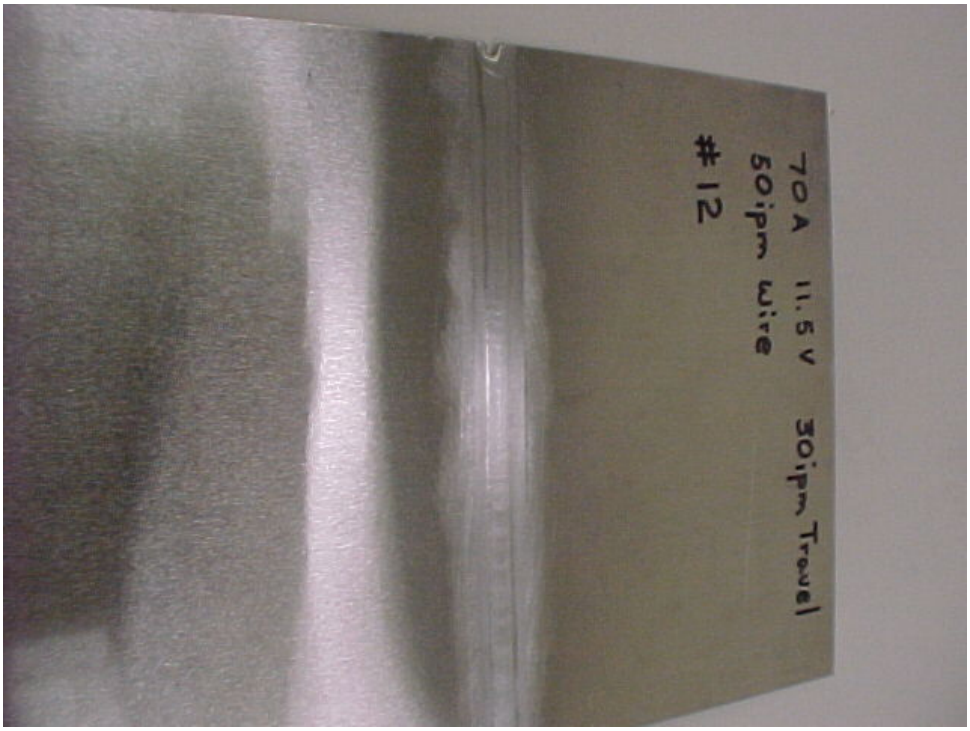

Figure 3: Successful weld made on aluminum alloy BH22.

Figure 4: Bend tests made on aluminum alloy BH22 weldment.

The results clearly show that by using the GTA process with the implementation of the chill fixture and the parameters developed at ORNL, successful coil-to-coil welds can be made at CII with a substantial increase in acceptance rate and be economically advantageous to CII.

Reports/Publications/Awards:

Zhong Li, John D. Moore, Robert W. Reed, Jeff McNabb, and Stan A. David, “Development of Welding Process to Join Aluminum Alloy Sheets Coil to Coil,” Final MPLUS report, April 2004.

MPLUS No.: MC-03-003

Title: Effect of Processing/Microstructure on the Corrosion Polarization Response of a Corrosion-Resistant Alloy: Phase II

John Pridgeon from ALLVAC

User Organization: ALLVAC
Monroe, NC 28111-5030

User Contact: John Pridgeon, 704-289-4511
John.pridgeon@allvac.com

ORNL R&D Staff: Dane F. Wilson, 865-576-4810
wilsondf@ornl.gov

Edward A Kenik, 865-574-5066
kenikea@ornl.gov

Steven J. Pawel, 865-574-5138
pawelsj@ornl.gov

Vinod K. Sikka, 865-574-5112
sikkavk@ornl.gov

Relevance to ITP: Corrosion performance of materials of construction is critical to the efficiency of many of the Office of Industrial Technologies industries of the future (forest products, chemical, and petrochemical). Localized corrosion such as pitting and crevice corrosion are common forms of corrosion found in these industries. Alloyed steels such as type 304 SS, type 316 SS, and alloy 734 are used in application where resistance to localized corrosion is needed. Alloy 734, while resistant to corrosion, demonstrates large variability in its corrosion response. This MPLUS investigated microstructural and microchemical variations that may contribute to this variability in corrosion response.

This task was designed to understand the microstructural and microchemical variables that would improve corrosion performance and allow U.S. industry to compete with the foreign producer of equivalent material that exhibited better corrosion performance. Better corrosion performance allows U.S. industry to be more energy efficient from reduced scrap and reduced in-house recycle, and be more competitive from reduced production cost and improved productivity.

This project is directly related to chemical, petrochemical, and forest product industries.

Objective: An alloy (734) high in nitrogen, similar to type 304 stainless steel, is well known for its resistance to pitting and crevice corrosion and corrosion fatigue. However, its corrosion performance is highly inconsistent. The objective of this work was to

understand the microstructural and microchemical control required for consistent corrosion performance.

Results: The microstructure and microchemistry of a heat of ALLVAC 734, which demonstrated variability in corrosion performance, were compared to another commercial heat of 734 stainless steel that demonstrated significantly less variability in corrosion performance. Scanning electron microscopy (SEM), transmission electron microscopy (TEM), and X-ray microanalysis were used to compare these two materials.

SEM examination showed that both heats contained similar-sized, coarse (1-10 μm diam) precipitates that were enriched in Nb and Cr and depleted in Fe and Ni relative to the matrix. Overall, the alloy and matrix composition for the two heats were similar.

TEM examination revealed that the ALLVAC 734 had a significantly larger grain size and less twinning than the other material. The lower grain boundary area could result in higher impurity concentrations at grain boundaries for elements that might segregate. In addition, the difference in grain size could indicate a different in the crystallographic texture of the two heats. There is an increasing body of information that texture can impact both mechanical and corrosion properties of metals.

TEM confirmed the presence of coarse, (1-10 μm) precipitates enriched in Nb and Cr in both heats as indicated earlier by SEM. Moderate-sized (0.2-1 μm) precipitates with similar composition were also present in the two materials. The presence of minor elements (Mo, V and Ti) in these precipitates was revealed by the higher sensitivity and spatial resolution of X-ray microanalysis in the TEM. The minor element content of the precipitates varied with size and location (e.g., intergranular versus intragranular precipitates).

Quantitative comparison of the heat compositions was performed with an electron microprobe analyzer (EMPA). Multiple areas were analyzed and the average composition (wt %) and standard deviation are given in Table 1. The composition is not normalized to 100% in order to judge the accuracy of the analysis (both heats gave ~102% totals). The major elements (Fe, Cr and Ni), as well as Mo, in the two heats are identical within the standard deviation. The Si level of the other 734SS is slightly higher than the ALLVAC 734, whereas the average Nb level (and standard deviation) of the ALLVAC 734 is slightly higher. However, this latter difference probably reflects the inclusion of several measurements where the analyzed volume contained small (Nb, Cr)-enriched particles. Though Si can influence the corrosion behavior of austenitic alloys, the required levels are usually higher than measured in the current two heats.

Table 1. Heat composition (wt %)

Alloy	Fe	Mn	Si	Cr	Ni	Nb	Mo
ALLVAC	63.9	4.2	0.2	22.2	9.6	0.2	1.8
7344	±1.01	±0.1	±0.01	±0.34	±0.22	±0.25	±0.08
Other	63.6	4.4	0.3	22.3	9.3	0.1	1.8
734SS	±0.71	±0.1	±0.01	±0.22	±0.17	±0.03	±0.07

There were several slight differences in the microstructure of the two heats including the presence of fine (<0.1 μm) precipitates, more dislocations and slip bands in the comparison material. The fine precipitates were enriched in Nb and Cr in a similar fashion to the largest precipitates and were presumed to be the same phase. None of these differences individually account for the variability seen in the ALLVAC material. It is possible that in the absence of the fine precipitates, compositional gradients adjacent to the large particles or grain boundary segregation at the larger grains dominate the corrosion performance. However, earlier results indicted no relationship between grain size and corrosion performance.

Reports/Publications/Awards:

D. F. Wilson, S. J. Pawel, V. K. Sikka, and H. F. Longmire, “Effect of Processing/Microstructure on the Corrosion Polarization Response of a Corrosion Resistant Alloy,” Final MPLUS report, August 2002.

MPLUS No.: MC-03-021

Title: Effect of Processing Parameters on Fabrication of Mo Sheet by Powder Metallurgy

Evan Ohriner (left) from ORNL, Sunil Jha (center) representing MET Group Inc., and G. Muralidharan (right) from ORNL

User Organization: MET Group Inc.
Dayton, OH 45415

User Contacts: Howard I. Sanderow, 937-832-1583
metgroup@earthlink.net

Sunil Jha, 520-878-9596
sjha@phelpsdodge.com

ORNL R&D Staff: G. (Murali) Muralidharan, 865-574-4821
muralidharag@ornl.gov

Evan K. Ohriner, 865-574-8519
ohrinerek@ornl.gov

Vinod K. Sikka, 865-574-5112
sikkavk@ornl.gov

Relevance to ITP: This project will evaluate alternate, potentially low-cost processing methods for the production of Mo sheets from nanosized Mo powders. Molybdenum is widely used in various industries including glass IOF for high temperature applications. It is also used as reflectors and heat shields in vacuum furnaces. Availability of low-cost Mo sheets with improved properties will benefit the steel, and aluminum industries along with supporting industries such as heat treating and metal forming.

Objective: The purpose of this study was to do evaluate the feasibility of processing, and determining the processing conditions necessary to prepare a fully dense molybdenum sheet from molybdenum powder. A thickness of 0.04 in. was set as a goal for final thickness. Issues to be evaluated include the thickness of sheet that can typically be processed using the developed technique/s, microstructure of the sheets, and any necessary intermediate heat-treatment temperatures and times.

Results: Nanoscale molybdenum powder was hot-pressed, sintered, and supplied by the user in the form of cylindrical disks measuring 0.43-in. diam and about 0.186-in. thick. One of these disks, as a first processing trial, was warm-forged at a temperature of 200°C with a molybdenum cover, and a thickness reduction of 43% was achieved. Visual examination following this operation showed that there were no cracks formed in the disk. A stress-relief annealing treatment was carried out in a hydrogen atmosphere at a temperature of 900°C for 1 h. Following this treatment, further rolling was attempted at a temperature of 200°C. However, the sample cracked during the rolling operation. The final thickness of the sample was observed to be 0.081 in. which was

short of the targeted thickness. Figures 1 and 2 show the samples before and after processing. Note the presence of cracks in the processed sample shown in Fig. 1.

Figure 1: Surface of as-received sample and deformed sample (Trial 1).

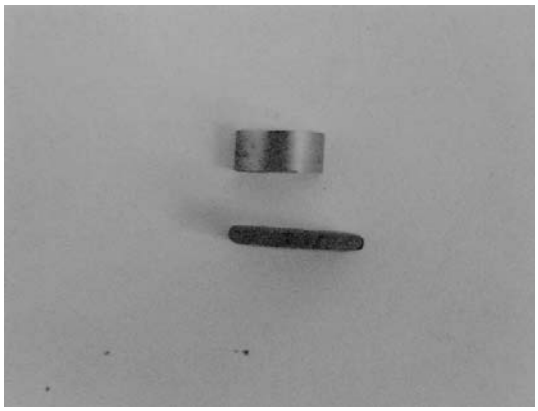

Figure 2: Cross-sectional view of as-received sample and deformed sample (Trial 1).

Cross-sections of the samples were prepared and studied using optical microscopy and scanning electron microscopy (SEM). Figures 3 and 5 show optical micrographs obtained from the as-received sample while Figures 4 and 6 show optical micrographs from the samples, respectively. Figures 7 and 8 show SEM micrographs of the same samples. As can be seen from Figs. 3 and 5, equiaxed grains were typically observed in the hot-pressed sample. A distribution of grain sizes is observed with sizes ranging from less than 1 μm to greater than 10 μm. Additionally, very little porosity was observed in the sample in the as-received condition. Optical micrographs from the rolled sample clearly show breakdown of the equiaxed structure, and an elongated structure with a much finer grain size is observed in these samples.

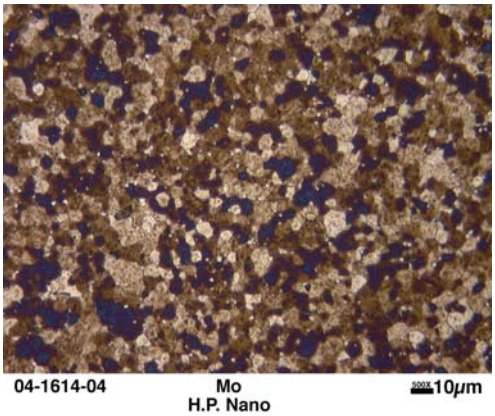

Figure 3: Optical microstructure of as-received sample (Trial 1).

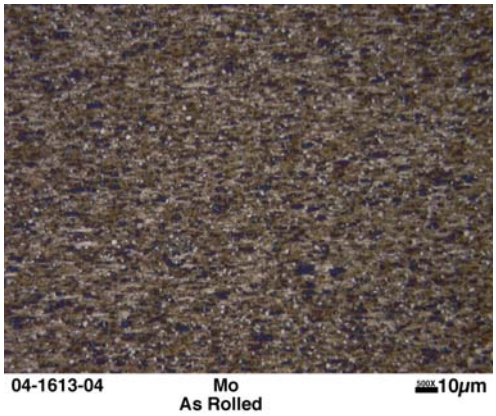

Figure 4: Optical microstructure of the deformed sample (Trial 1).

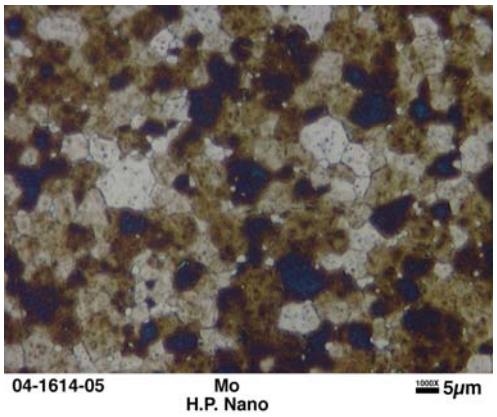

Figure 5: Optical microstructure of as-received sample at a higher magnification (Trial 1).

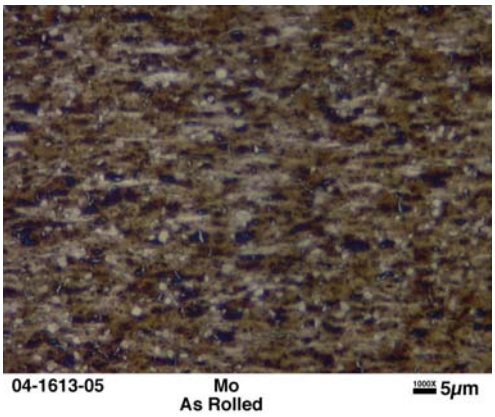

Figure 6: Optical microstructure of the deformed sample at a higher magnification (Trial 1).

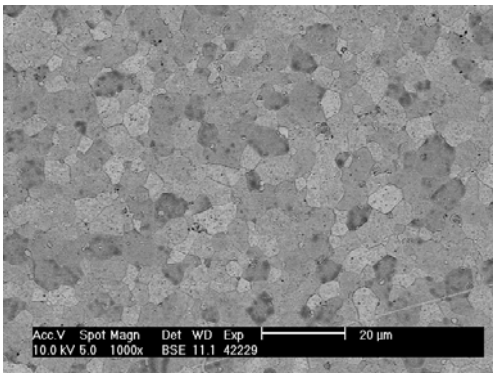

Figure 7: Scanning electron micrograph of as-received sample at a higher magnification (Trial 1).

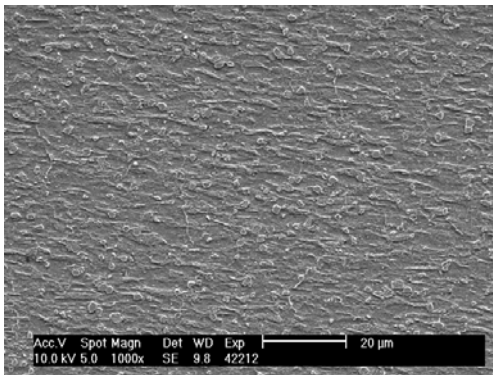

Figure 8: Scanning electron micrograph of the deformed sample at a high magnification (Trial 1).

Following this initial trial, a second attempt was made at processing the samples. However, the temperature of the intermediate anneal was changed to 950°C and the rolling temperature was raised to 400°C. Using the new processing conditions, the samples were successfully initially warm-forged from a 0.147-in.-thick disk to a thickness of 0.066 in. and finally rolled down to a thickness of 0.039 in. The samples were devoid of cracks as shown in Figs. 9 and 10. Thus, it has been clearly demonstrated that molybdenum sheets can be successfully processed to desired thicknesses (less than 0.040 in.) from nanoscale molybdenum powders.

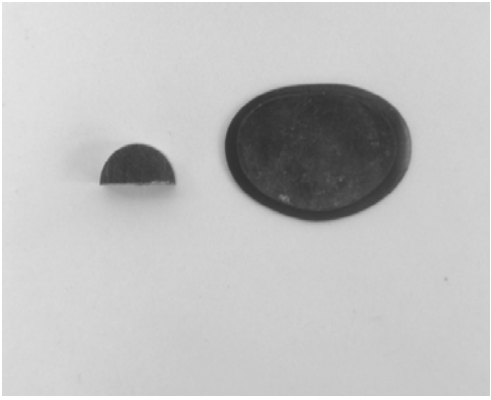

Figure 9: Surfaces of as-received sample and deformed sample (Trial 2). No cracks were observed.

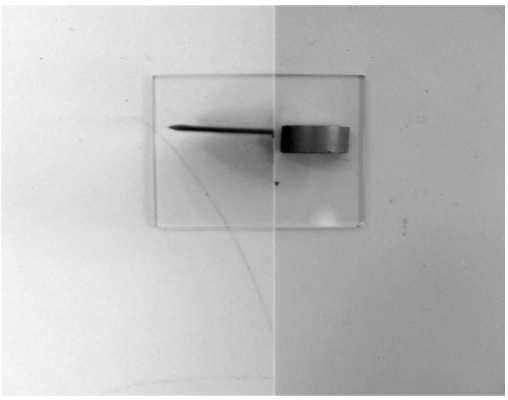

Figure 10: Cross-sectional view of deformed sample and as-received sample (Trial 2).

Reports/Publications/Awards:

G. Muralidharan, Evan K. Ohriner, Vinod K. Sikka, Howard I. Sanderow, and Sunil Jha, “Effect of Process Parameters on Fabrication of Mo Sheet by Powder Metallurgy,” Final MPLUS report, June 2004.

MPLUS No.: MC-03-039

Title: The Evaluation of Various Cladding Materials for Down-Hole Drilling Applications using the Pin on Disk Test

User Organization: Stoody Company
Bowling Green, KY 42101

User Contacts: Ravi Menon, 270-781-9777, ext 2009
menon@thermadyne.com

ORNL R&D Staff: Peter J. Blau, 865-574-5377
blaupj@ornl.gov

Ravi Menon from Stoody Co.

Relevance to ITP: This effort provides important material selection data for controlling the friction of wear resistant materials which are used in the petroleum industry for oil exploration.

Objective: The objective of this project was to evaluate the frictional performance of newly-developed metallic alloy overlays for mining and petroleum exploration equipment under controlled laboratory conditions that simulate certain aspects of the drilling mud environment.

Results: Eleven candidate claddings were evaluated using a pin-on-disk sliding friction testing system. Tests were conducted in a specially formulated sand and clay slurry that simulated down-hole 'drilling mud', and the same batch of slurry was used for all tests. The pin material for all tests was AISI 4130 steel hardened to HRC 45. Test pins were 6.4 mm in diameter with hemi-spherical tips.

Two sliding speeds and two test loads were used. Selected friction data for one of the test loads is shown in Fig. 1. Friction coefficients ranged between about 0.30 and 0.40. This friction range represents a 33% difference in friction from one cladding to another, and that could impact the drilling efficiency and mitigate seizure problems.

The test-to-test repeatability for the first series of runs was about +/- 5% for the same cladding material. However, later tests showed less material-to-material differences and small variations in the slurry could have had an effect on the results as well. More comprehensive data, correlations with material properties, and detailed analysis are contained within the 14-page project report.

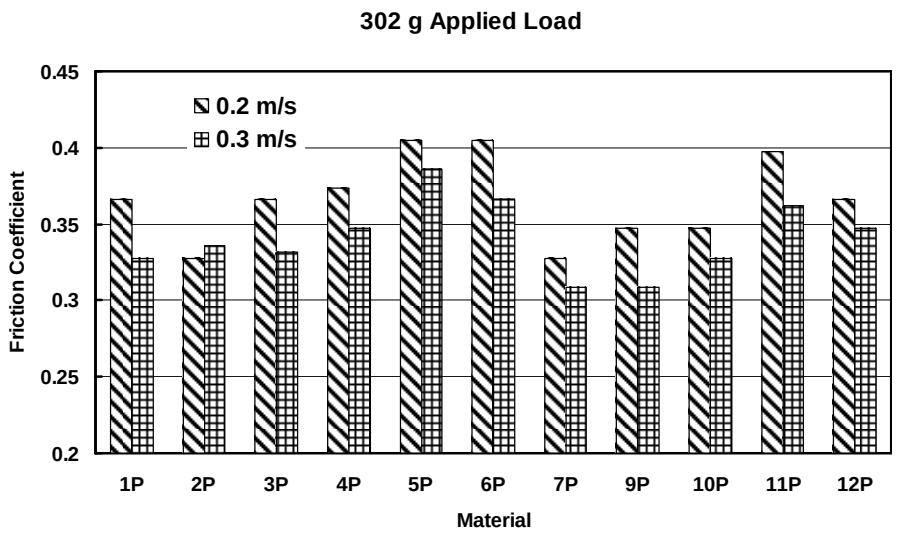

Figure 1: Effects of sliding speed on the friction of cladding materials tested in a silica sand and clay slurry. Similar trends in behavior were observed at the other two test loads.

Reports/Publications/Awards:

Ravi Menon, Daya Singh, John J. Truhan, and Peter J. Blau, "The Evaluation of Various Cladding Materials for Down-Hole Drilling Applications using the Pin-on-Disk Test," Final MPLUS report, 2004.

In addition to the final report, plans are to submit this work for presentation at the next International Conference on Wear of Materials, San Diego, California, April 2005.

MPLUS No.: MC-03-004

Title: High-Density-Infrared (HDIR) Densification of Thermal Spray Coatings for Spherical Surfaces

User Organization: F.W. Gartner Thermal Spray Co.
Houston, TX 77023

User Contacts: Jimmy Walker Jr., 713-225-0010
jwalkerjr@fwgts.com

John. B. Williams Jr., 281-449-0291
jwilliams@mogas.com

ORNL R&D Staff: Craig A. Blue, 865-574-4351
blueca@ornl.gov

Puja Kadolkar, 865-574-9956
kadolkarp@ornl.gov

Relevance to ITP: Development of this process into daily production will enhance valve performance and life significantly. This will translate into higher plant efficiencies and improved productivity in general.

Objective: The objective of this project was to determine if high density infrared (HDIR) process could be used to melt and fuse advanced metallic and ceramic coatings on spherical surfaces. This study will allow utilization of advanced coatings on steels that are currently impractical to use and would help improve general valve performance and increase plant production efficiency.

Results: Spherical ball valve components (viz. ball and valve seat) of 410 SS material (Fig. 1) were supplied by Mogas Industries, Houston TX. These components were thermally sprayed by F.W. Gartner using their 69SC coatings before they were sent to the MPLUS facility at Oak Ridge National Laboratory (ORNL). The HDI facility located in the Materials Processing Group at ORNL is a 300-kW, single-source, plasma arc lamp (Fig. 2) with power densities on the order of 3.5 kW/cm^2. When the arc lamp is energized, it is capable of producing plasma with a temperature in excess of 10000 K and a radiant spectrum from 0.2 to 1.4 μm. The lamp is also coupled with a six-axis robot and a rotating lathe to assist processing samples with complex and circular shapes in a shorter amount of time. In association with the robot, the lamp can be operated either in a continuous scan mode or in a single pulse burst mode, depending on the type of application. Tables 1 and 2 show the coating trials performed on the seat and ball components of various sizes.

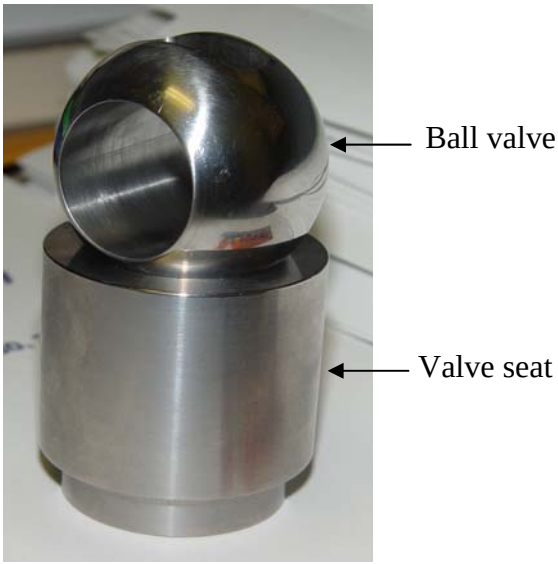

Figure 1: Ball valve components (uncoated) supplied by Mogas Industries.

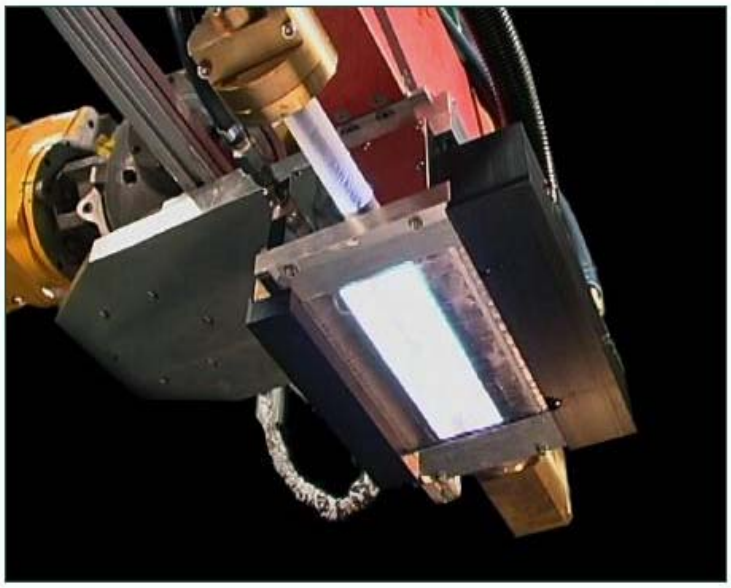

Figure 2: High density infrared (HDIR) plasma arc lamp in the Materials Processing Group's MPLUS facility at the Oak Ridge National Laboratory.

Table 1: Coating trials on valve seat

Component	Diameter Size (in.)	Processing Conditions		
		Amperage (Amps)		Scan rate (mm/s)
		Step I	Step II	
Valve seat	2.370	500 A	800 A	10
Valve seat	2.370	600 A	900 A	8
Valve seat	2.370	600 A	700 A	7
Valve seat	1.850	600 A	900 A	10
Valve seat	1.850	600 A	900 A	7
Valve seat	1.850	600 A	900 A	7
Valve seat	1.280	600 A	900 A	7
Valve seat	1.280	600 A	900 A	7

Table 2: Coating trials on ball valve

Component	Diameter Size	Processing Conditions		
		Amperage (Hold time) Amps (secs)		Rotation speed (RPM)
		Step I	Step II	
Ball valve	Small	500 (120)	-	3
Ball valve	Medium	500 (40)	700 (20)	3
Ball valve	Medium	400 (40)	600 (20)	3
Ball valve	Large	500 (40)	700 (20)	3
Ball valve	Large	5 rotations each with a different amperage setting and hold time		3
		500 (60)	-	6

Based on the appearance, three of the best coated components were chosen from the above test trials for microstructural and hardness characterization. Figures 3, 4 and 5 represent micrographs of the densified coating, showing a well-bonded interface with the substrate. Fine cracks extending from the surface of the coating to the interface are due to the thermal stresses developed due to the rapid heating and cooling and the thermal coefficient mismatch between the coating and the substrate materials. Cracking can be easily controlled by understanding the thermal property-processing relationship and modifying the existing heating pattern.

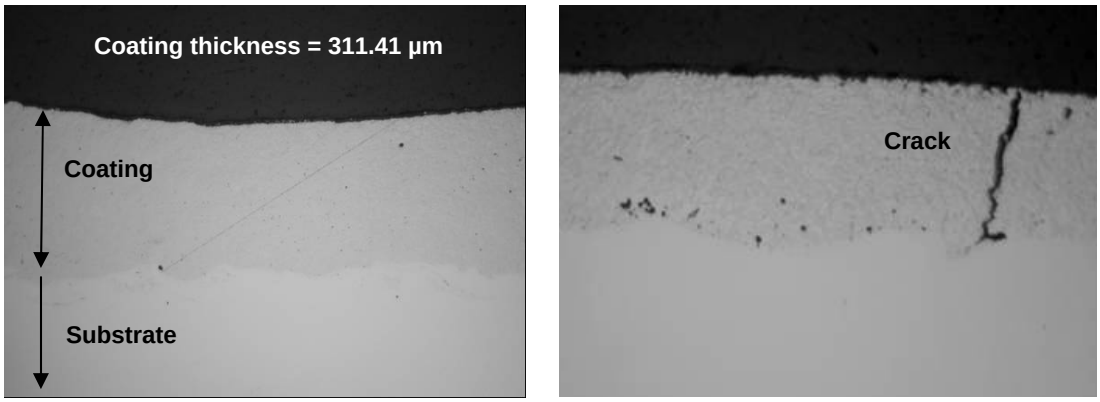

Figure 3: Coating on 1.28-in. valve seat.

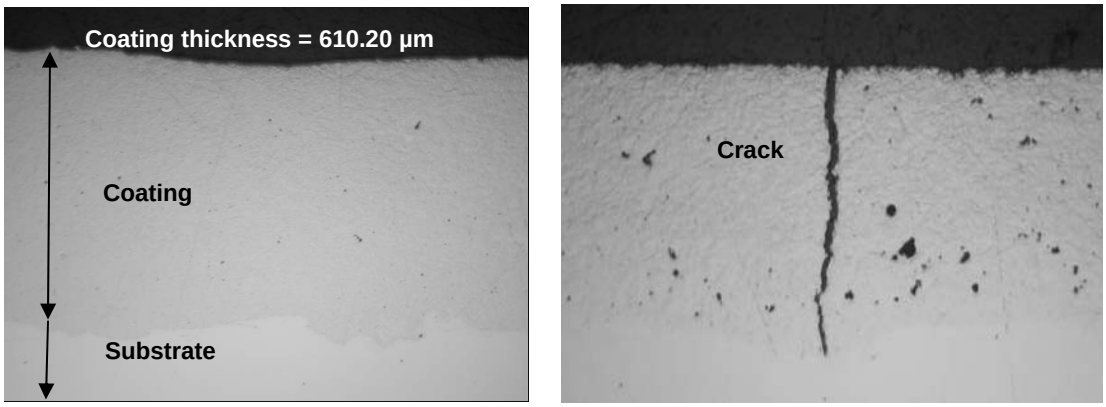

Figure 4: Coating on 1.85-in. valve seat.

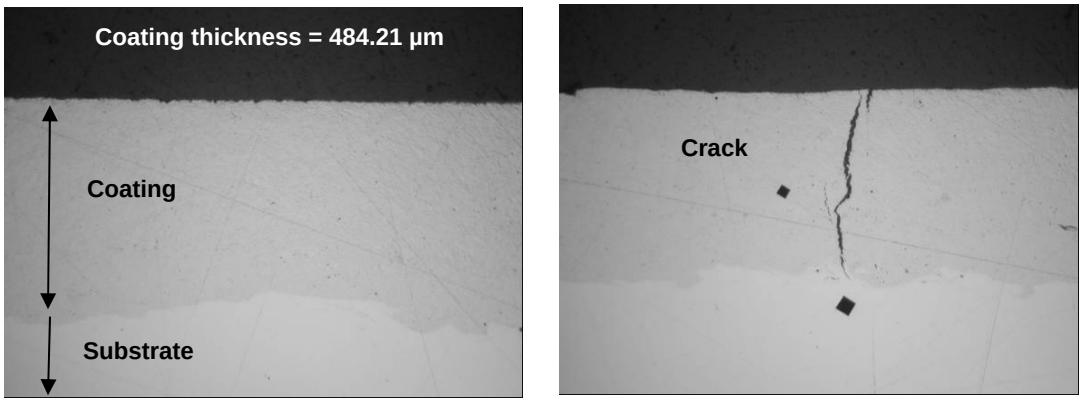

Figure 5: Coating on smaller diameter ball valve.

Hardness measurements of coatings and substrates were performed using a DM-400 Leco Hardness Tester with a load of 300 g. Indents were taken starting from the surface of the coating moving perpendicular in to the coating approaching the substrate. Measurements in Table 3 indicate a decreasing trend in the hardness values from the surface in to the substrate without a sudden drop at the interface, thus suggesting formation of the heat affected zone.

Table 3. Hardness measurement of coating and substrate

Hardness in the coating (1.28-in. valve seat)						
Indent No.	**Location**	**Hardness (HV)**	**Location**	**Hardness (HV)**	**Location**	**Hardness (HV)**
1	Top of seat	666	Seat area	757	Bore	962
2	“	680	“	746	“	887
3	“	710	“	720		
4	“	710	“	798		
5	“	738	“	862		

Hardness in the base material under coating (1.28-in. valve seat)				
Indent No.	**Not cracked**		**Under crack**	
	Distance from interface (inches)	**Hardness (HV)**	**Distance from interface (inches)**	**Hardness (HV)**
1	0.1	530	0.1	516
2	0.2	395	0.2	429
3	0.3	255	0.3	257
4	0.4	247	0.4	254
5	0.5	252	0.5	252

Hardness in the coating (1.85-in. valve seat)						
Indent No.	**Location**	**Hardness (HV)**	**Location**	**Hardness (HV)**	**Location**	**Hardness (HV)**
1	Top of seat	469	Seat area	728	Bore	966
2	“	659	“	769	“	999
3	“	641	“	901		
4	“	685	“	982		
5	“	722	“	901		

Hardness in the base material under coating (1.85-in. valve seat)				
Indent No.	**Not cracked**		**Under crack**	
	Distance from interface (inches)	**Hardness (HV)**	**Distance from interface (inches)**	**Hardness (HV)**
1	0.1	542	0.1	523
2	0.2	449	0.2	463
3	0.3	242	0.3	246
4	0.4	246	0.4	245
5	0.5	250	0.5	242

Table 3: (Continued)

Hardness in the coating (smaller diameter ball)				
Indent No.	**Hardness (HV)**	**Indent No.**	**Hardness (HV)**	**Average hardness (HV)**
1	862	6	810	840.9
2	962	7	814	
3	846	8	801	
4	814	9	792	
5	901	10	807	
Hardness in the base material under coating (smaller diameter ball)				
Indent No.	**Not cracked**		**Under crack**	
	Distance from interface (inches)	**Hardness (HV)**	**Distance from interface (inches)**	**Hardness (HV)**
1	0.1	402	0.1	398
2	0.2	396	0.2	339
3	0.3	288	0.3	274
4	0.4	269	0.4	270
5	0.5	260	0.5	268

Conclusion: High-density-infrared (HDIR) processing was successfully used to fuse advanced coatings such as 69SC on spherical surfaces. Higher hardness values in the coating suggest a stronger wear-resistant coated surface that would improve the performance and increase the life of valves. Formation of the heat-affected zone implies the coating to be an integral part of the component without forming a sharp interface between different fusing materials

Reports/Publications/Awards:

C. A. Blue, P. Kadolkar, J Walker Jr., and J. B. Williams Jr., “High-Density-Infrared (HDIR) Densificationof Thermal Spray Coatings for Spherical Surfaces,” Final MPLUS report, August 2004.

MPLUS No.: MC-03-027

Title: Heat Transfer Modeling of Continuously Cast Aluminum Slab

User Organization: Commonwealth Aluminum Concast, Inc.
Uhrichsville, OH 44683

User Contact: Zhong Li, 859-514-4951
Zhong.Li@ciionline.com

Paul Platek, 740-922-8329
Paul.Platek@ciionline.com

Zhong Li from Commonwealth Aluminum Concast, Inc.

ORNL R&D Staff: B. Radhakrishnan, 865-241-3861
radhakrishnb@ornl.gov

Relevance to ITP: In the continuous casting (CC) technology for the production of aluminum hot bands, the slab after exiting the casting machine cools significantly before it enters the finish hot rolling, resulting in not only a significant loss of energy but also a variability of the slab temperature prior to hot rolling. Providing insulation between the casting and the rolling stations could result in significant energy savings. Providing an auxiliary heating source could increase in overall energy efficiency for the process because less energy is required for finish hot rolling, and a higher coiling temperature may lead to complete recrystallization in the coil, thereby eliminating the need for subsequent annealing of the coil. Since the CC route for producing aluminum hot band has a roughly 25% energy savings compared to the conventional DC casting route, any process modification to improve the energy efficiency of the CC product line will further increase this energy saving. Realizing such energy savings is directly related to the Office of Industrial Technologies mission.

Objective: The objective of the project is to model the heat transfer between the CC slab and the surrounding air in order to determine the effect of auxiliary heating or insulation on the slab temperature prior to entering the tandem mill, thus providing inputs to the design of an appropriate heating/insulation unit that will result in the proper management of the slab temperature during processing.

Results: The commercial code Fluent™ was used to model the heat transfer between the moving slab and the surrounding which is either a free stream of air at the ambient temperature, an external heat flux, or an insulating shroud. Initially, the convective heat transfer coefficient between the moving slab and the air was tuned to fit the experimentally measured and the computed slab temperatures at various distances from the caser end, as shown in Fig. 1.

The same coefficient was used to model the convective heat transfer in all of the subsequent computations. The effect of variations in the ambient temperature (during

different seasons) on the slab temperature prior to entering the rolling mills was then computed, as shown in Fig. 2. It can be seen from this figure that decreasing the ambient temperature from the nominal 300K (27°C) to 250K (-23°C) decreased the mill entry temperature by about 16°C. Increasing the ambient to 350K increased the mill entry temperature by about 10K.

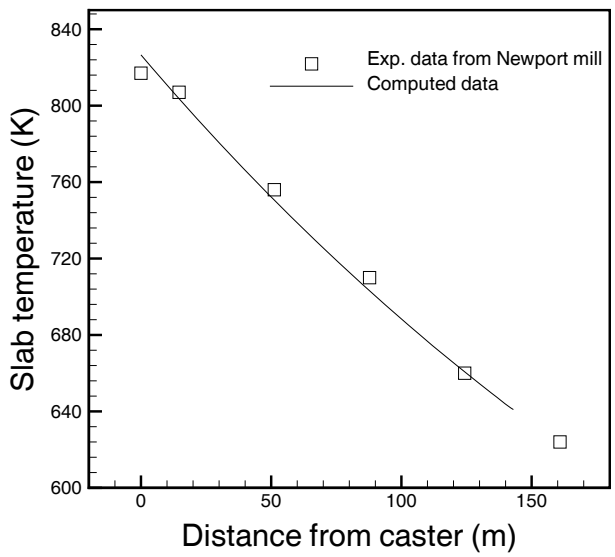

Figure 1: Comparison of experimental cooling data obtained for CC A13105 slab and computational data.

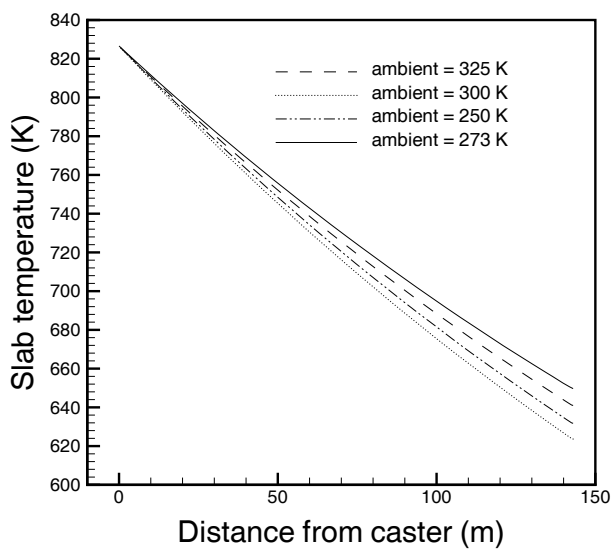

Figure 2: Effect of ambient temperature on slab entry temperature into the hot mill.

The effect of providing insulation at various positions between the castor and the rolling mill is shown in Fig. 3. Providing complete insulation over a distance of 143 m drops the slab temperature by only 20°C. When an 80-m insulator was provided from the caster end, a significant drop in temperature occurred between the insulator exit and roll entry. A 63-m insulator from the roller side resulted in a rapid initial drop of the temperature followed by a moderate decrease in the insulated region. The model therefore provides temperature profiles for various insulation scenarios and an appropriate design can be implemented based on cost and other production related factors.

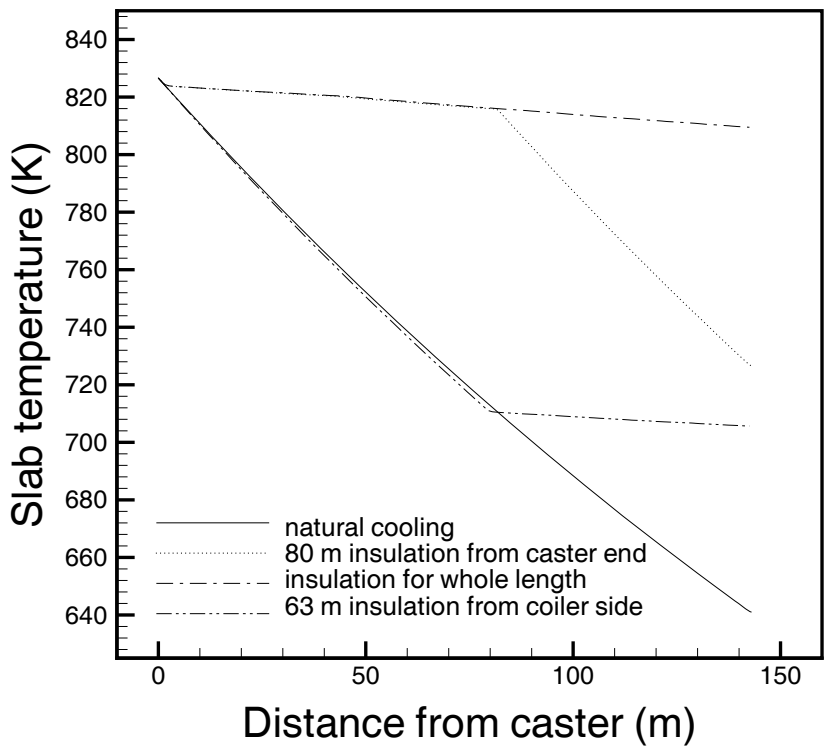

Figure 3: Effect of thermal insulation on slab entry temperature into the hot mill.

The effect of providing an external heat source on the slab temperature is summarized in Fig. 4. The external heat source was positioned at the hot rolling end of the slab for various lengths shown. Without auxiliary heating, the slab temperature prior to entering the hot rolling mill is about 640K. Figure 4 shows the temperature rise for various input heat fluxes and heater lengths. The data can be used to design a heater that will heat the slab to the required temperature subject to other cost and production related factors.

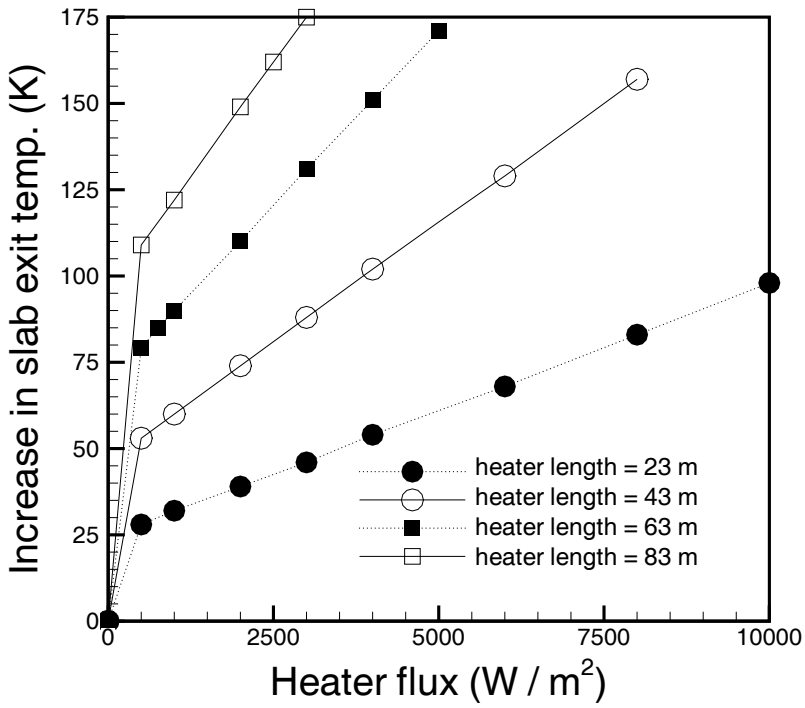

Figure 4: Effect of heater length and heater flux on the temperature rise of the slab prior to entry into hot mill.

Reports/Publications/Awards:

B. Radhakrishnan, "Heat Transfer Calculations to Aid the Design of an Auxiliary Heating/Insulating Unit for the Continuously Cast Aluminum slab," Final MPLUS report, 2003.

MPLUS No.: MC-03-007

Title: High-Energy Efficiency Wire Annealing Method

User Organization: Ametek
Wallingford, CT 06492-7607

User Contacts: Jack Easley, 202-265-6731
jack.easley@ametek.com

Clive Scorey, 203-949-8828
clive.scorey@ametek.com

ORNL R&D Staff: Vinod K. Sikka, 865-574-5112
sikkavk@ornl.gov

Yogesh Bhambri, 865-576-6031
bhambriy@ornl.gov

Clive Scorey from Ametek

Relevance to ITP: A wide range of materials are processed into wire for application in welding, brazing, heating element, etc. These wires are produced by cold drawing with intermediate annealing steps. The strand equipment currently used for these annealing operations is very inefficient from an energy perspective, and throughput rates are low. This MPLUS project led to demonstrating that tungsten halogen infrared-based heating can improve heating efficiency and throughput. Furthermore, the process is easily adaptable in a commercial production setting. The outcome of the project has benefits across weld wire production, wire and heat treating, and heat element wire production industries.

Objective: The objective of this MPLUS was to explore the use of tungsten halogen-based infrared heating of wires in both Inconel and quartz tubing. Inconel tubing is currently used, which oxidizes and needs frequent replacement. The quartz tube is resistant to oxidation and transparent to infrared heating and, thus, has the potential of saving frequent replacement. The overall objective of this project was to design a more energy efficient annealing system that occupies smaller floor space and operates at higher speeds.

Results: The 0.034-in.-diam wire of phosphor bronze brought by Dr. Clive Scorey of Ametek was thermocoupled and heated in the flatbed, tungsten-halogen infrared heater available in the MPLUS facilities. Wire samples were heated side-by-side in quartz and Inconel tubes. The heating profiles for two power settings of 70 and 90% of the infrared system are shown in Fig. 1. The following conclusions were possible from these data:

1. The wire heated faster in quartz tubing as opposed to Inconel tubing for both power settings. This is the case because Inconel tube absorbs part of the infrared radiation

as opposed to quartz, which is totally transparent to infrared radiation and thereby supplies all of its energy to the wire.

2. Use of 90% of the power setting as opposed to 70% reduces the wire heating time by nearly a factor of 2.

Based on these data, Ametek concluded that they can replace their Inconel tubes with quartz and their gas-fired heating by infrared-based heating. These changes accomplish the project's objectives of higher energy efficiency, smaller floor space, and higher throughput.

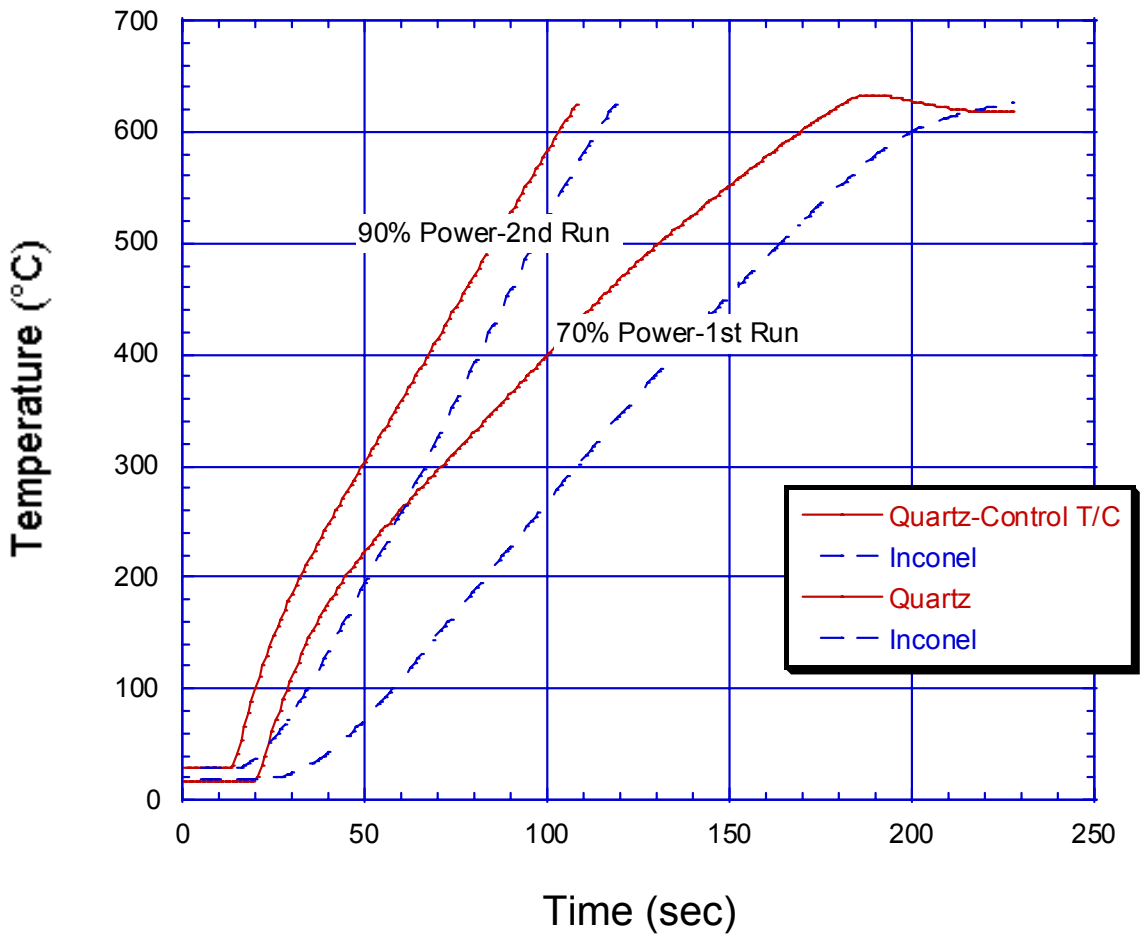

Figure 1: Heating profile for 70 and 90% of infrared system.

Reports/Publications/Awards:

V. K. Sikka and C. R. Howell, "Heating Profiles using Infrared heater for Wires Supplied by Ametek," Final MPLUS report, 2003.

MPLUS No.: MC-03-036

Title: The Measurement of Moisture/Water Content in Recycled Aluminum Scrap and RSI

User Organization: IMCO Recycling Inc.
Rockwood, TN 37854

User Contact: Ray D. Peterson, 865-354-6375
rpeterson@imcorecycling.com

ORNL R&D Staff: Qingyou Han, 865-574-4352
hanq@ornl.gov

Ray D. Peterson (left) from IMCO Recycling with Joe Vought (ORNL)

Relevance to ITP: Moisture/water in recycled scrap aluminum and remelt secondary ingot (RSI) represents a safety issue for the aluminum industries. Currently, there is no faster method to measure the water content in scrap aluminum alloys and RSI. The scrap metal and RSI have to be dried in furnace for extended time before they can be charged into melting furnace to void water-induced aluminum explosion. Still the Aluminum Association reports cases of aluminum explosion every year. The Aluminum Industry Roadmap lists moisture detection as one of the high priority R&D areas.

Objective: The purpose of this MPLUS research was to test whether neutron gauge can be used for fast measurement of water content in scrap aluminum alloys and RSI. The objectives included identifying suitable neutron gauge for moisture detection and testing the sensitivity of moisture detection using neutron source. The results of the proposed research may lead to a new method that can be used for avoiding explosion during aluminum melting due to the presence of moisture/water in the scrap aluminum metals.

Results: The basic idea is that fast neutrons can react with hydrogen in moisture inside metals and tend to become slow neutrons which are detectable by a slow neutron read-out device. The moisture content in metal can be deduced from the hydrogen content detected using neutron. Fast neutron source of 18 ug cf-252 was chosen because of its long half-decay life and low cost. Polyethylene beans, which contain hydrogen, were mixed mechanically into 2 kg of Al scrap. Polyethylene beans were used instead of water because the beads can be mixed uniformly in scrap metal. The results of the project indicate that neutron hydrogen detection can be used in aluminum industry as a rapid, non-destructive method to determine the moisture/water content in aluminum scrap and in RSI.

Figure 1 illustrates the experimental apparatus. A fast neutron beam from the 252Cf source is directed to the bottom of bucket (the distance is 15 in.). H2O (H: 11%) or polyethylene beans (H: 14.3%) mixed with Al scrap of varying ratios are contained inside the top bucket. A slow (thermal) neutron detector (Q-2824-1, counts/cm2/sec) is positioned at the bottom of bucket. Hydrogen (moisture) content can be detected within a few seconds.

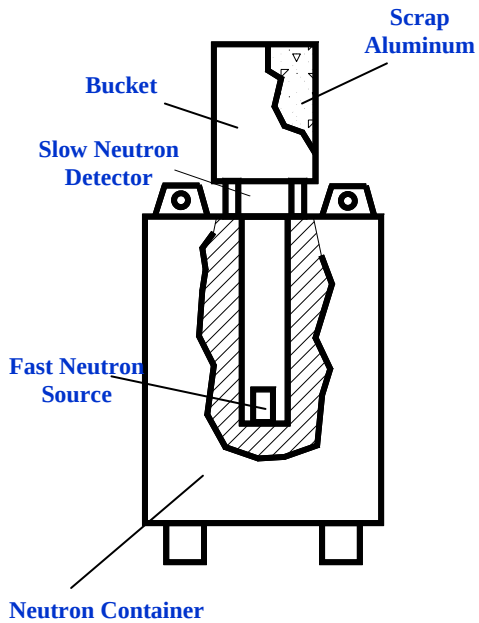

Figure 1: The experimental apparatus detecting moisture content in scrap metals using neutron source.

Figure 2 shows the relationship between the slow neutron counts detected and the weight fraction of the Poly-beans added in scrap metal. The slow neutron counts increases with increasing weight fraction of the Poly-beans. Since the weight fraction of the Poly-beans can be translated into the moisture content, the detected slow neutron counts can be correlated to moisture/water content in metal.

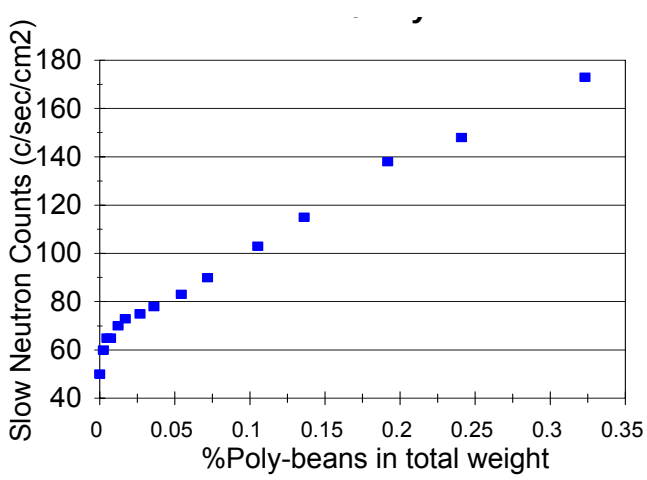

Figure 2: The relationship between the slow neutron counts detected and the weight fraction of Poly-beans added in scrap metal.

Reports/Publications/Awards:

Ray Peterson, Qingyou Han, and Miting Du, “The Measurement of Moisture/Water Content in Recycled Aluminum Scrap and RSI,” Final MPLUS report, March 14, 2004.

MPLUS No.: MC-03-031

Title: The Mechanism by which Boron and Zirconium Improve the Resistance of Haynes 214 Alloy to Strain Age Cracking

User Organization: Haynes International Inc.
Kokomo, IN 46904

User Contact: Mark. D. Rowe, 765-456-6228
mrowe@haynesintl.com

ORNL R&D Staff: S. S. Babu 865-574-4806
babuss@ornl.gov

M. K. Miller 865-574-4179
millermk@ornl.gov

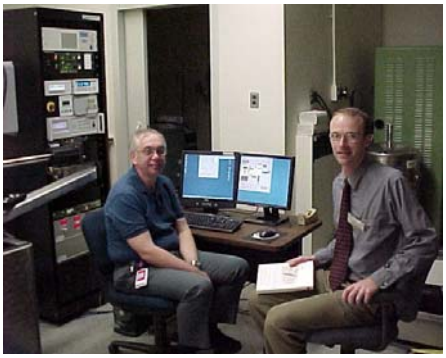

Mark Rowe (Haynes) and Mike Miller (ORNL) in front of the Local Electrode Atom Probe

Relevance to ITP: Glass, Steel, Aluminum and Chemical

Objective: The objective of this research was the fundamental understanding of boron and zirconium addition on the microstructural evolution in Haynes 214 alloy using high-resolution characterization techniques.

Results: Strain age cracking is a problem that can occur in alloys that strengthen by precipitation of gamma prime phase. Typically, these are nickel-based alloys that contain aluminum and/or titanium, either for high-temperature strength or oxidation resistance. Cracking occurs when an alloy that contains gamma prime forming elements in solid solution is heated into a temperature range where gamma prime precipitates, about 1100 to 1800°F. Due to the precipitation of gamma prime, the ductility of the alloy drops to a very low level, and cracking can occur if the alloy is subjected to a level of strain that exceeds the available ductility. Two alloys were studied in this research. One alloy (EN1001) was made with intentional additions of boron and zirconium, similar to commercial HAYNES 214 alloy, while the other alloy (EN1101) was made without boron or zirconium. The solution annealed specimens were heated to 1100°F, held 10 s at 1100°F and then heated to 1400°F and then quenched to room temperature. The samples in the as-received condition were also evaluated. The microstructural characterization was performed with a state-of-the-art local electrode atom probe instrument at Oak Ridge National Laboratory.

Transmission electron micrographs in Fig. 1 indicated that the samples after the heat treatment contain very fine (<10 nm) scale gamma prime precipitates. Therefore, atom probe analyses of samples in all conditions were performed and are summarized in Fig. 2. Interestingly, the atom probe analyses showed that these precipitates are already present in the normalized condition, in contrast to original hypothesis that these precipitates form during heat treatment. This result is indeed significant and further

analyses are being continued to evaluate the extent of precipitation. The implications of this result will be considered in the formation of strain-age cracking through computational models and future experimental work.

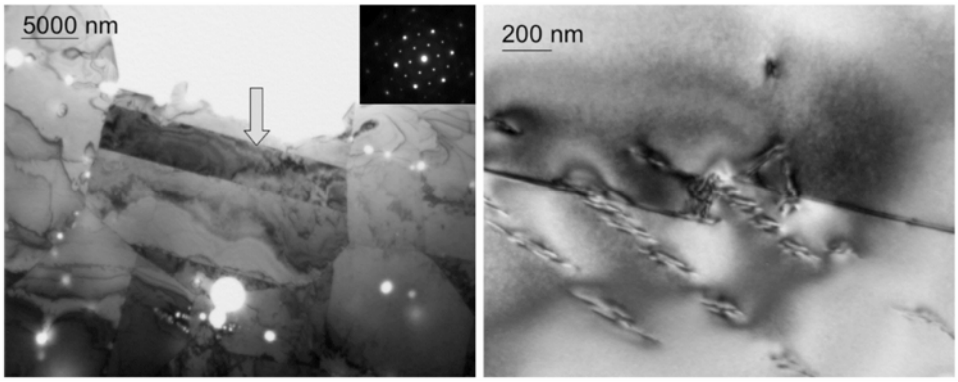

(a) (b)

Figure 1: Transmission electron micrographs show: (a) the microstructure and electron diffraction from L12 ordered precipitates and (b) fine-scale precipitates.

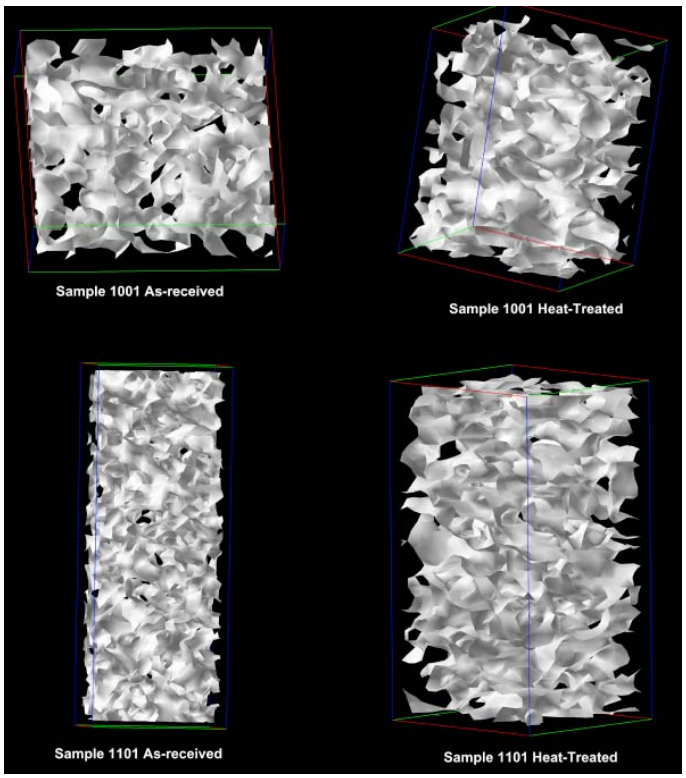

Figure 2: Overview of atom probe tomography results from samples in the (a) as-received and (b) heat-treated conditions are illustrated with iso-concentration surfaces of 10 at. % Al showing the presence of fine-scale phase separation in the sample.

Reports/Publications/Awards:

M. D. Rowe, S. S. Babu, and M. K. Miller, “The Mechanism by which Boron and Zirconium Improve the Resistance of Haynes 214 Alloy to Strain Age Cracking,” Final MPLUS report, June 2004.

A research paper summarizing all MPLUS research is being prepared.

MPLUS No.: MC-03-029

Title: The Mechanisms of Oxide Formation Found in Solidified Aluminum 5182 Alloy RSI

User Organization: IMCO Recycling Inc.
Rockwood, TN 37854

User Contact: Ray D. Peterson, (865) 354-6375
rpeterson@imcorecycling.com

ORNL R&D Staff: Qingyou Han, (865) 574-4352
hanq@ornl.gov

Ray D. Peterson from IMCO Recycling Inc.

Relevance to ITP: During recycling of aluminum scrap, a large amount of high-quality aluminum is turned into dross leading to substantial equivalent energy losses. Minimizing dross formation in aluminum remelt secondary ingots (RSI) can result in a significant energy savings in aluminum industry. In this MPLUS project, the mechanisms of dross formation were further investigated. The results have the potential of leading to the development of cost effective method of RSI processing with minimum dross formation.

Objective: In a previous MPLUS project, we observed a huge amount of dross formation during remelting of RSI. However the mechanisms of dross formation in the RSI are still arguable. The purpose of this MPLUS research was to carry out controlled experiments to investigate the mechanisms of dross formation. Aluminum 5182 alloys were melted both in air and under vacuum. The melt was cast and solidified under the cooling conditions identical to that of 2000 lbs industrial RSI. The results of the proposed research can be used to distinguish if the dross formation is mainly due to hydrogen porosity or due to oxide film formation at the surface of melt before casting or oxide formation during melting.

Results: Two types of recycling materials, light gauge materials and buttons, were melted both in air and under vacuum. The molten aluminum was then cast in a heated mold and cooled either in air or under vacuum at rates identical to that of 2000 lbs industrial RSI. The ingots made were about 5 lbs. The experimental results indicated the following:

- No substantial amount of dross formation was observed in ingots regardless of the atmospheres used during melting and solidification processes
- The material type had little effect on dross formation in the cast ingots.

These results suggest that the oxide films formed at the surface of the melt before casting or oxide formation during melting are not related to the dross formation observed during the remelting of 2000 lbs industrial RSI. Dross formation in those

industrial RSI is due to porosity formation and the low pressure exists in the center of a RSI towards the end of solidification when air is sucked into the center of the RSI, forming oxide layers on the surfaces of the growing dendrites.

Reports/Publications/Awards:

H. Xu, Q. Han, and R. D. Peterson, “The Mechanisms of Oxide Formation Found in Solidified Aluminum 5182 Alloy RSI,” Final MPLUS report, June, 2004.

MPLUS No.: MC-03-001

Title: Melting of Experimental Alloys for Corrosion Studies

User Organization: Lehigh University
Bethlehem, PA 18015

User Contacts: John DuPont, 610-758-3942
Jnd1@lehigh.edu

Jonathan R. Regina
Ryan M. Deacon

ORNL R&D Staff: Vinod K. Sikka, 865-574-5112
sikkavk@ornl.gov

John DuPont and Jonathan R. Regina (top, left to right) and Ryan M. Deacon (bottom) from Lehigh University

Relevance to ITP: Corrosion is one of the major causes that limit the continuous operation of many processes for several of the energy-intensive user industries. The corrosion is combated by many different methods including use of expensive materials, use of coatings, and weld overlays. The effectiveness of corrosion-protection methods depends on material composition used and the quality of the applied coating. The high-quality coatings require a good bond with the substrate and absence of any porosity. Such quality requirements can be met by weld overlay method for applying them. However, the selection of the proper weld overlay composition, detailed corrosion data of weld over composition. The nature of the weld overlay makes coupon testing for corrosion data rather difficult. Thus, it was decided to test drop-cast alloys for corrosion data, which closely simulates the weld overlay microstructure. The corrosion environments varied from high sulfidizing to oxidizing, and the test temperature was 500°C. It was shown that Fe-Al-Cr alloy, with aluminum of ≥ 19 at. % of Al + Cr of approximately 25 at. %, was essential to completely stifle many measurable weight gains during gaseous corrosion at 500°C in sulfidizing, oxidizing, and mixed gas environments. This MPLUS project led to alloy compositions that will need to be deposited as weld overlay for the desired corrosion protection.

Objective: The objective of this project was to prepare ten Fe-Al-Cr-X alloy compositions by nonconsumable-arc melting process and casting them into 1 × 0.5 × 5-in.-diam castings. The cast alloys were corrosion tested at 500°C in sulfidizing, oxidizing, and oxidizing/sulfidizing environments. High-temperature thermogrevinetric (TG) balance was used for measuring the corrosion kinetics. The alloys were prepared at the Oak Ridge National Laboratory and corrosion testing was carried out at Lehigh University.

Results: The ten alloy compositions studied during this project are listed in Table 1. The corrosion test environments were created by using three different gas chemistries given in Table 2. The corrosion data at 500°C for Fe-14.5Al and Fe-19Al series of alloys in sulfidizing, oxidizing/sulfidizing, and oxidizing environments are shown in Figs. 1 through 3. A detailed analysis of the data showed the following key observations:

1. Aluminum concentration of at least 19 at. % was needed in Fe-Al alloys in order to prevent rapid corrosion kinetics in all three test environments. Chromium additions were shown to help reduce the corrosion kinetics of FeAl alloys at 500°C.

2. A total alloy content (0 = at. % Al + at. % Cr) of approximately 25 was required to completely stifle any measurable weight change during gaseous corrosion testing at 500°C.

Based on these results, it is possible to use FeAl-based alloy as weld overlay for sulfidizing environment.

Table 1: Alloy compositions used for corrosion testing[a]

Alloy Designation	Fe	Al	Cr	Ti
Fe-14.5 Al	*b*	14.2	---	---
Fe-14.5Al-1Cr	*b*	14.3	1.0	---
Fe-14.5Al-2Cr	*b*	14.5	2.1	---
Fe-14.5Al-5Cr	*b*	14.8	5.0	---
Fe-14.5Al-2Cr-1.5Ti	*b*	14.9	2.2	1.8
Fe-19Al	*b*	18.8	---	---
Fe-19Al-1Cr	*b*	18.8	1.0	---
Fe-19Al-2Cr	*b*	19.0	2.1	---
Fe-19Al-5Cr	*b*	19.9	5.0	---
Fe-19Al-2Cr-1.5Ti	*b*	19.2	2.1	1.7

[a]All values are in atomic percent.
[b]Balance.

Table 2: Gas compositions used for corrosion testing[a]

Gas Component	Sulfidizing Gas	Mixed Oxidizing/ Sulfidizing Gas	Oxidizing Gas
O_2	---	---	2
CO	15	10	---
CO_2	---	5	15
H_2	3	---	---
H_2O	---	2	6
H_2S	0.12	0.12	---
SO_2	---	---	0.12
N_2	*b*	*b*	*b*
Log Po_2	-28	-19	-2
Log Ps_2	-6	-8	-46

[a]All values are in volume percent.
[b]Balance.

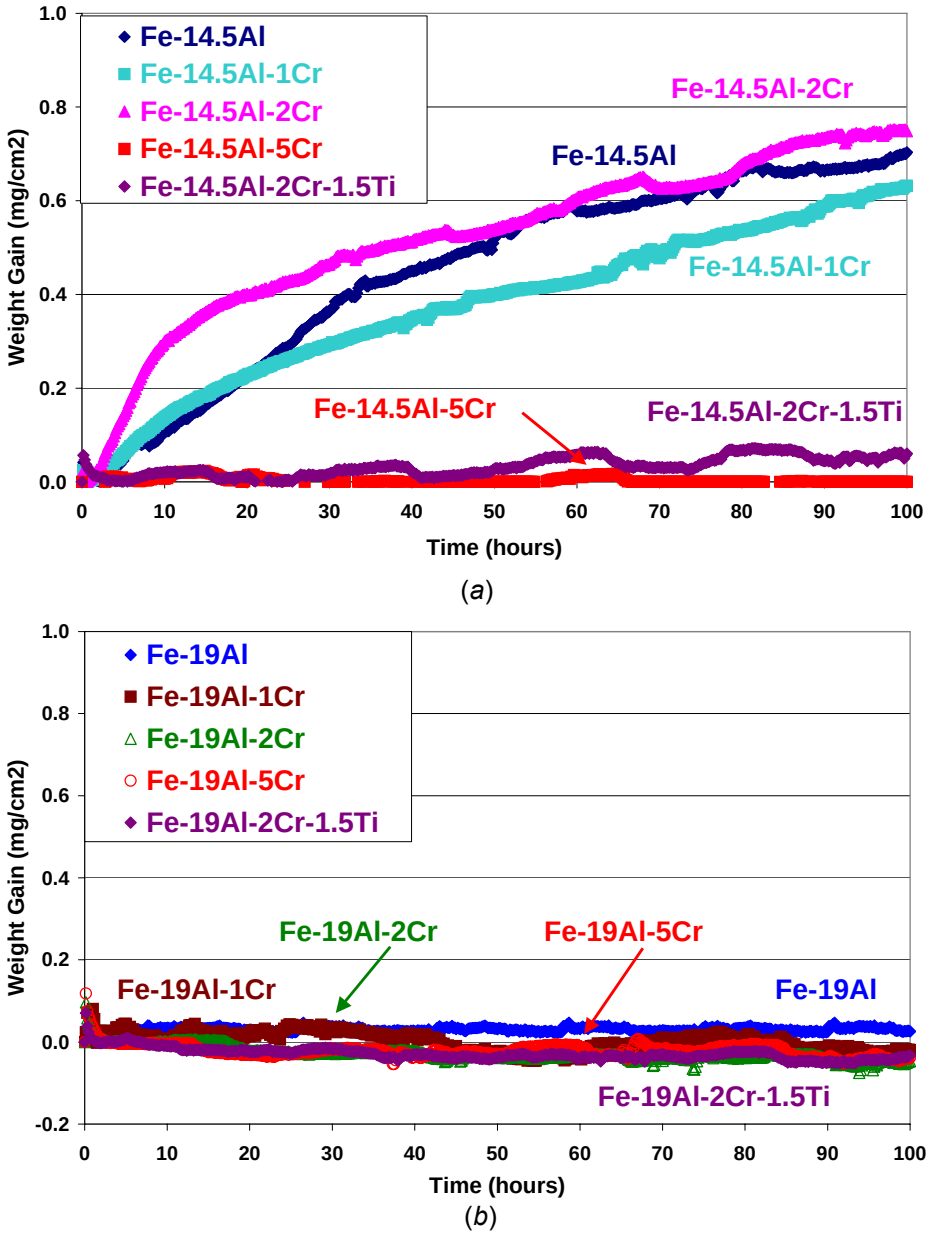

Figure 1: Kinetic results for (*a*) the Fe-14.5 at. % Al series and (*b*) the Fe-19 at. 5 Al series exposed to the sulfidizing environment.

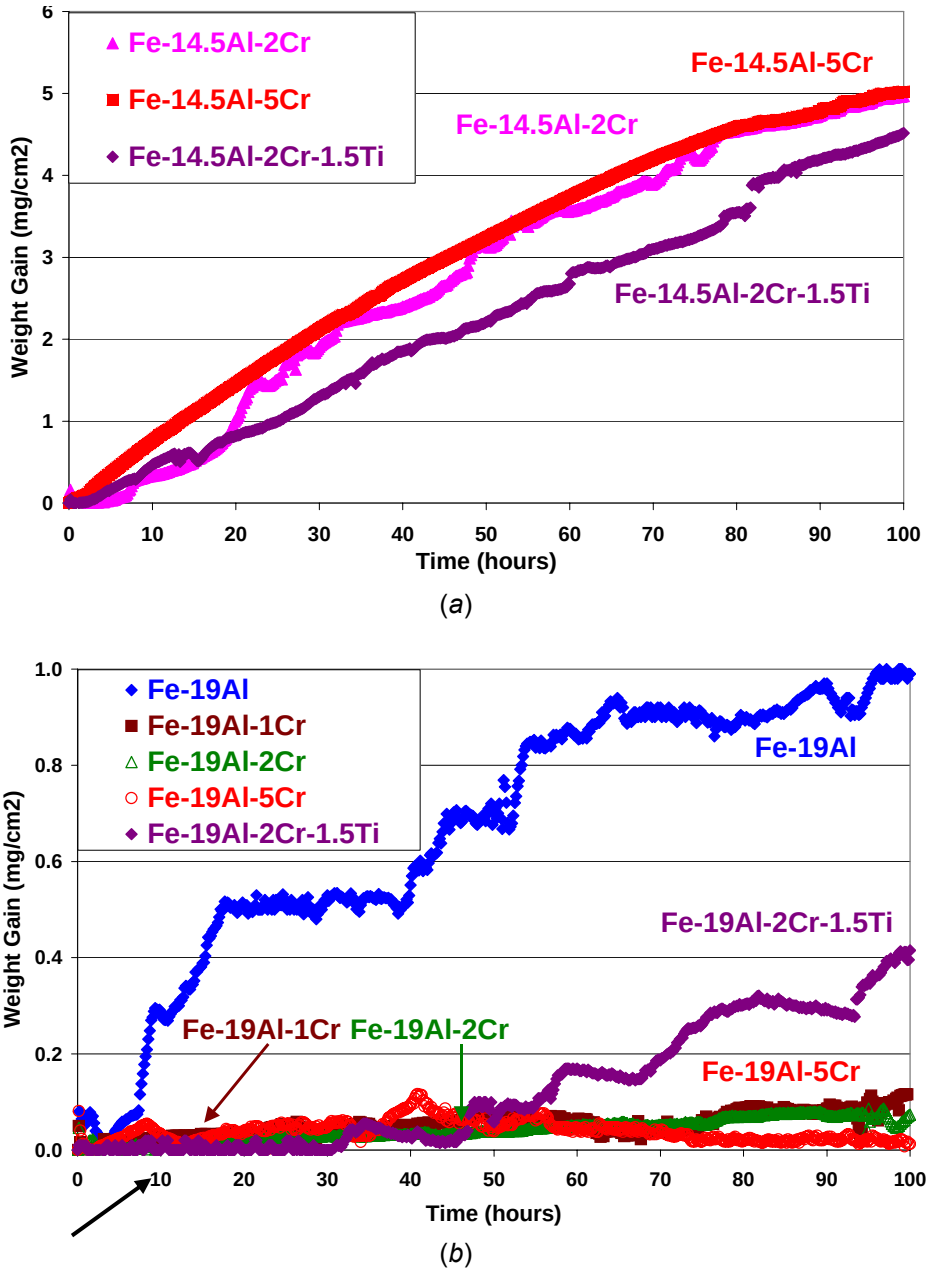

Figure 2: Kinetic results for (*a*) the Fe-14.5 at. % Al series and (*b*) the Fe-19 at. % Al series exposed to the mixed oxidizing/sulfidizing environment.

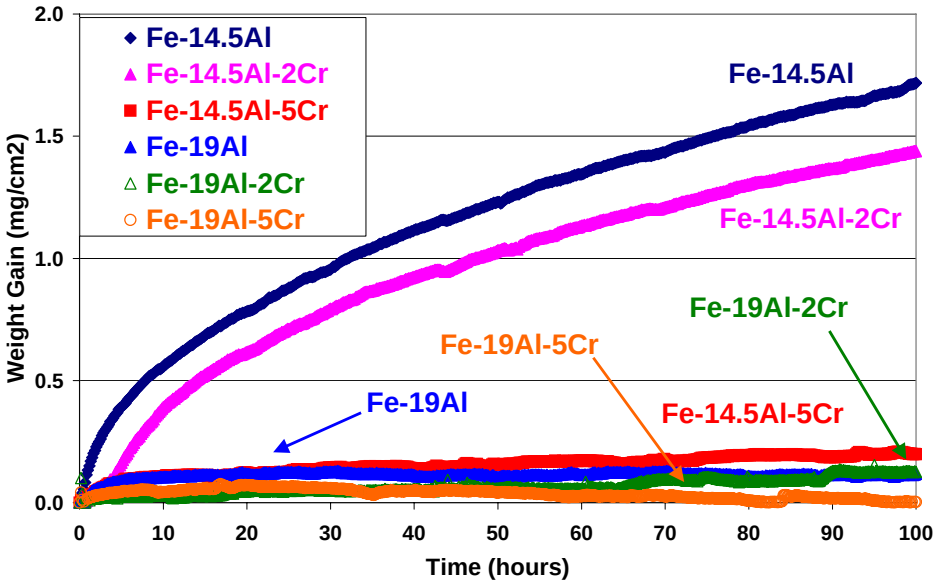

Figure 3: Kinetic results for alloys exposed to the oxidizing environment.

Reports/Publications/Awards:

J. R. Regina, J. N. DuPont, and A. R. Marder, "Gaseous Corrosion Resistance of Fe-Al Based Alloys Containing Cr and Ti Additions. Part 1 – Kinetic Results," Short title: "Fe-Al Alloy Corrosion Resistance – Part I," Final MPLUS report, December 16, 2003.

J. R. Regina, J. N. DuPont, and A. R. Marder, "Gaseous Corrosion Resistance of Fe-Al Based Alloys Containing Cr and Ti Additions. Part 1 – Kinetic Results," to be published in 2004.

J. R. Regina, J. N. DuPont, and A. R. Marder, "The Effect of Water Vapor on Passive Layer Stability and Corrosion Behavior of Fe-Al-Cr Based Alloys," *Oxidation of Metals*. Vol. 61, no. 1-2, pp. 69-90, Feb. 2004.

J. R. Regina, J. N. DuPont, and A. R. Marder, "Gas-Slag Corrosion Behavior of Fe-Al-Cr Alloys in Sulfur and Oxygen Rich Environments," *Corrosion*. Vol. 60, no. 5, pp. 501-512, May 2004.

J. R. Regina, J. N. DuPont, and A. R. Marder, "Gaseous Corrosion Resistance of Fe-Al Based Alloys Containing Cr and Ti Additions. Part I – Kinetic Results," Submitted to *Materials Science and Engineering A*, 2004.

J. R. Regina, J. N. DuPont, and A. R. Marder, "Gaseous Corrosion Resistance of Fe-Al Based Alloys Containing Cr and Ti Additions. Part II – Scale Morpholgy," Submitted to *Materials Science and Engineering A*, 2004.

MPLUS No.: MC-03-028

Title: Metal Filling of Lost Foam Castings

User Organization: University of Alabama – Birmingham
Birmingham, Alabama

User Contact: Wanliang Sun, 205-975-8839
swayne@uab.edu

Harry E. Littleton, 205-975-3890
hlittlet@eng.uab.edu

ORNL R&D Staff: R. B. Dinwiddie, 865-574-7599
dinwiddierb@ornl.gov

Wayne Sun from University of Alabama - Birmingham

Relevance to ITP: An understanding of the location of gas and liquid pyrolysis products escaping from the casting cavity is required to formulate a physical model of the metal/pattern replacement process. This will provide needed input for updating current commercial fill and solidification codes as well as providing insight to casting defect formation, such as folds.

Objective: Investigate the thermal events associated with metal (aluminum) replacement of lost foam patterns using a screened flask supplied by UAB. Viewing the screened area will provide data concerning the location of gas and liquid pyrolysis products escaping from the casting cavity. This understanding is required to formulate a physical model of the metal/pattern replacement process. This will provide needed input for updating current commercial fill and solidification codes as well as providing insight to casting defect formation, such as folds.

Results: This project consisted of a dual study to understand the content of folding defects typically found in lost foam aluminum castings and also to understand gas generation in the casting process. These items are intertwined since it is believed that folding defect content may originate from decomposition products of the lost foam pattern which include gaseous and liquid components.

We use the infrared imaging camera to observe a screened window set into the side of the ORNL casting flask. Hot gas is able to exit the window and be observed by infrared camera. In order to know the location of the metal front, several electrical contacts were placed in a single row horizontally across the middle of the foam pattern. As the metal reached each contact it allowed current to flow to a corresponding small light bulb located along the top edge of the image. The sequence of images in Fig. 1 shows the illuminated light bulbs lead the heat pattern of the sand. This indicates that the infrared (IR) camera is imaging the conductive heat transfer through the sand and not the gas flow as hoped. Several pours were undertaken but the gas was not easily observable. In

future work, it may be possible to image the hot gas using a hyperspectral attachment on the IR camera. However, this is beyond the scope of the current proposal.

The HTML SEM, Auger spectroscopy system and related equipment was successfully used to image and quantify the contents of several folding defects.

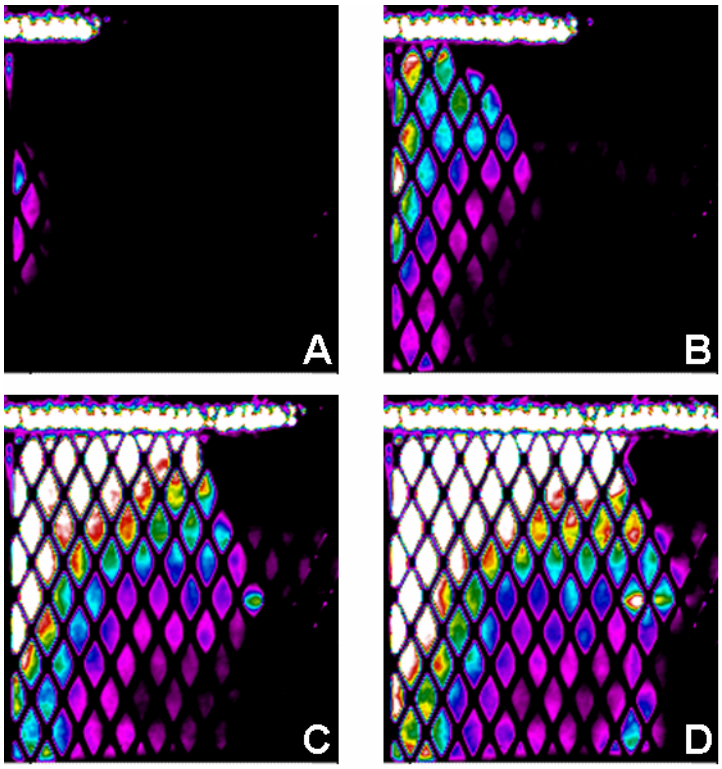

Figure1: Sequence of infrared images from Pour #2 clearly shows the metal position, as indicated by the light bulbs across the top of the image, is leading the hot pattern observed in the sand: (A) 3.4 s from the start of the pour, (B) 6.7 s, (C) 9.6 s, and (D) 10.8 s.

Reports/Publications/Awards:

W. Sun, H. E. Littleton, and R. B. Dinwiddie, “Metal Filling of Lost Foam Castings,” Final MPLUS report, June 2004.

Results from this project were presented at the Lost Foam Consortium Meeting in June 2004 and will be presented at the 2004 AFS Casting Congress in late 2004.

MPLUS No.: MC-03-024

Title: Methods to Improve Aluminum Smelter Hardware Materials

User Organization: Century Aluminum of West Virginia, Inc.
Ravenswood, WV 26164

User Contact: Richard O. Love, 304-273-6562
rlove@centurywv.com

ORNL R&D Staff: Vinod K. Sikka, 865-574-5112
sikkavk@ornl.gov

Yogesh Bhambri, 865-576-6031
bhambriy@ornl.gov

Richard Love from Century Aluminum of West Virginia, Inc.

Relevance to ITP: Aluminum smelters use salt mixtures during the smelting process. Some carbon dust from graphite anodes gets into the salt mixture. The sulfur in the carbon dust causes severe corrosion of steel hardware used in the smelter. One such hardware is a gusset. The Al addition to the surface of the steel is known to improve its sulfidation resistance of steel. This MPLUS project used a patented process developed at the Oak Ridge National Laboratory for enhancing the Al content of the surface of the gusset that becomes exposed to sulfidation environments. Two gussets with an Al-enhanced surface were shipped to Century Aluminum for testing in the Al smelter. The success in corrosion reduction of the gussets by Al enhancement will have very significant benefits in saving energy and cost of primary Al production.

Objective: The objective of the project was to develop a welding procedure for enhancing the Al content of steel used for gussets and validate the Al enhancement of the steel surface through microstructure analysis. The project objective also applied the developed weld procedure to enhance the Al content of two gussets for testing in smelter applications.

Results: The gas-tungsten-arc process was optimized to enhance the Al content on the surface. The welding wire was 1/16-in.-diam pure Al. The cover gas was 100% argon. Preheat was 100°F and the interpass temperature was 250°F max. The weld procedure was developed on a carbon steel block. The test plate cut from the weld procedure development is shown in Fig. 1. The etched end of the test weld plate showing the depth of Al enrichment is shown in Fig. 2. The microstructure of the Al-enriched region on the surface of the steel is shown in Fig. 3. The microstructure of the heat-affected zone (HAZ) and the base steel under the Al-enriched region are shown in Fig. 4, and the hardness profile in Fig. 5. The average hardness of the aluminum-enriched region is approximately 220 Vickers (~ R_C22). The base steel in the annealed condition is approximately 160 Vickers (~ R_C16). HAZ produced the highest hardness region because of transformation of austenite in this region to martensite during air

cooling after welding. The EDAX analysis of the Al-enriched region showed its Al content in the range of 8 to 10 wt %.

Figure 1: Test plate produced during weld procedure development.

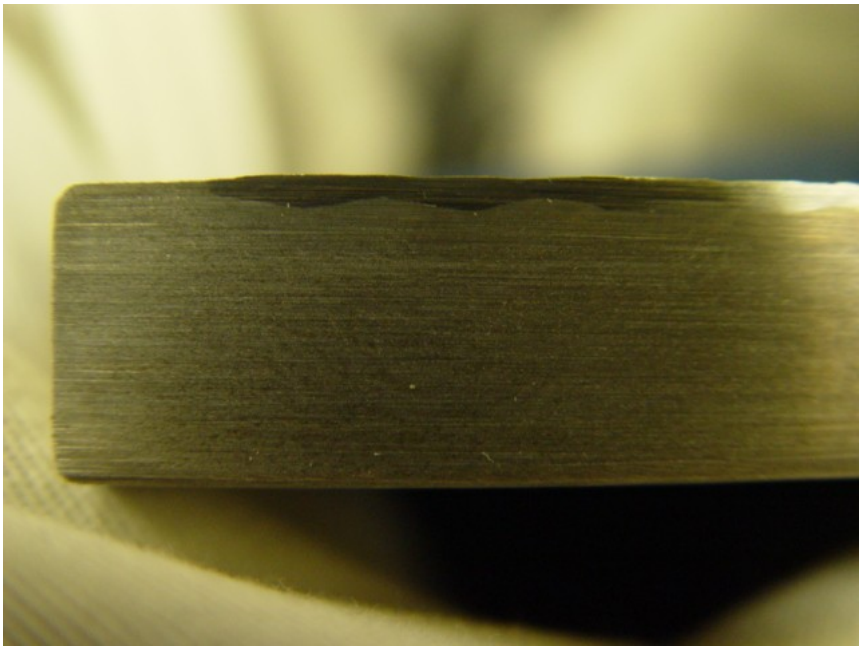

Figure 2: Etched end of the test weld plate showing the depth of aluminum enrichment.

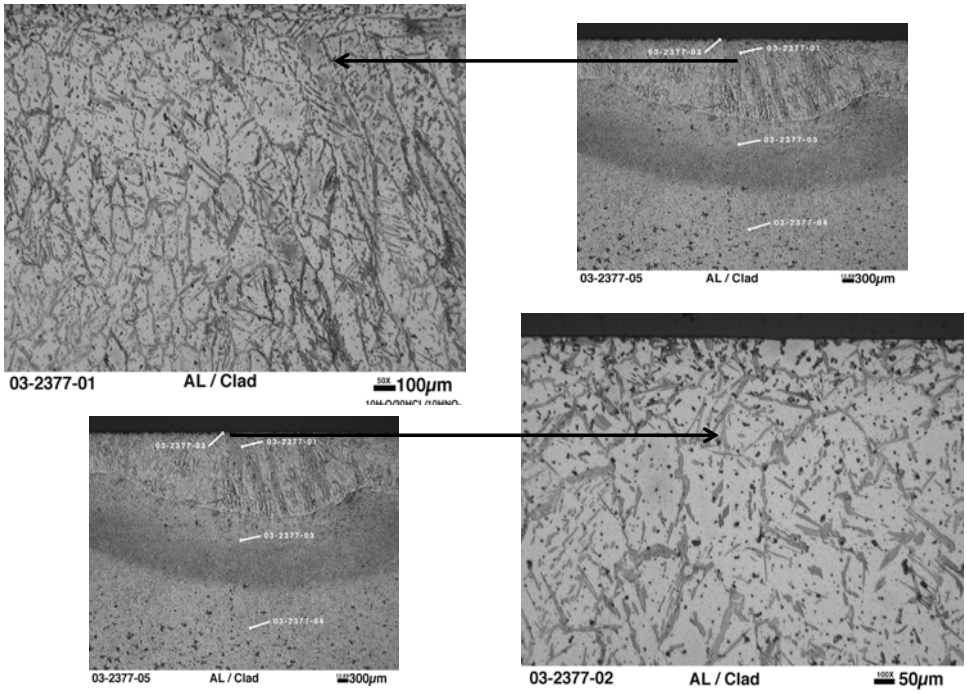

Figure 3: Microstructure of the aluminum-enriched region.

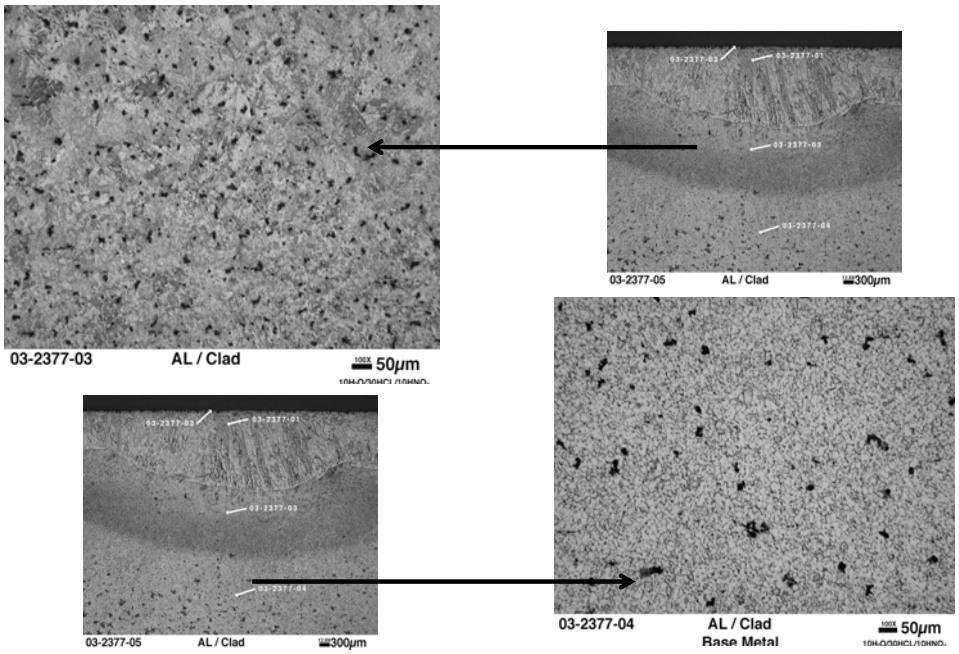

Figure 4: Microstructure of the heat-affected zone produced in the steel and of the base metal.

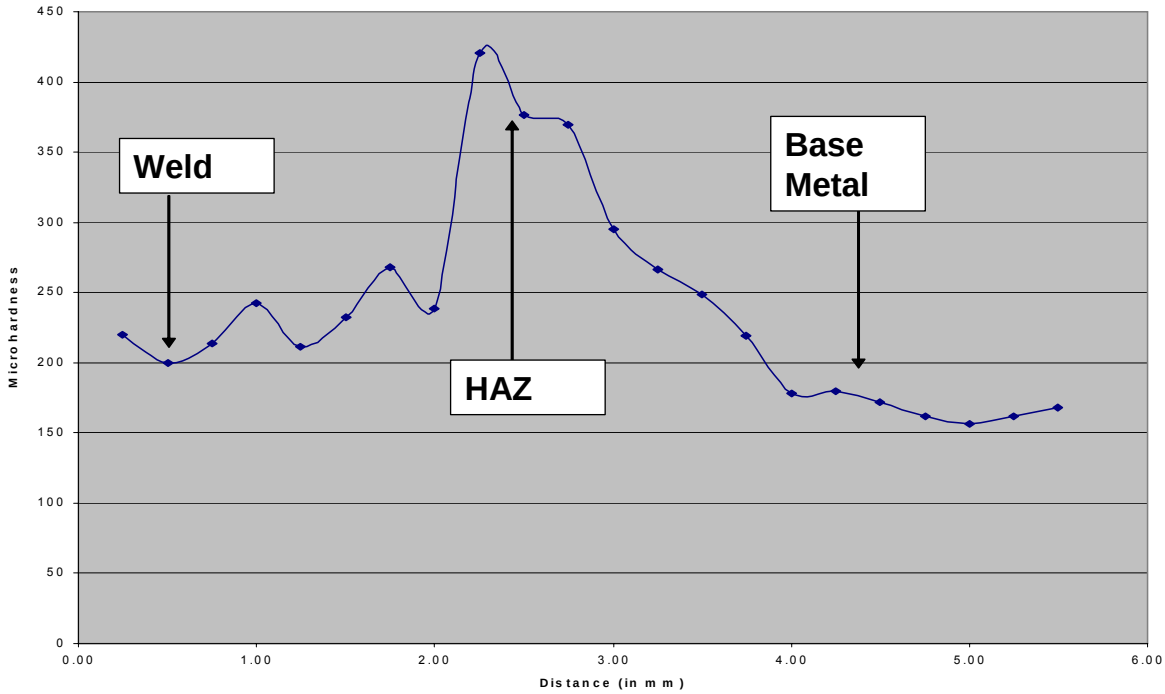

Figure 5: Hardness profile of the aluminum-enriched region, the heat-affected zone, and base metal.

Photograph of one of the gussets received from Century Aluminum is shown in Fig. 6. This photograph shows the overview of the gusset and a close-up showing marked areas that needed to be welded for Al enrichment. The weld parameters developed on the test plate were used to weld the two gussets. The photographs of the front and top surfaces of the two welded gussets are shown in Figs. 7 and 8. These welds show that the gussets could be successfully enriched with Al on the desired surfaces by the gas-tungsten-arc process under shop welding conditions. All of the gussets were welded at Specialty Welding and Machining, Inc. located in Harrison, Tennessee.

The welded gussets have been shipped to Century Aluminum for testing their corrosion performance in Al smelter furnaces.

The major conclusion of this MPLUS is that Al enrichment of the industrial component surfaces can be done under production conditions, and they are expected to produce a significant improvement in sulfidation resistance of these components in Al smelt furnaces. The actual smelter performance of the gussets will be known by the end of July 2004.

(*a*) (*b*)

Figure 6: One of the gussets received from Century Aluminum for aluminum enrichment: (*a*) overview and (*b*) close-up showing areas to be welded.

(*a*) (*b*)

Figure 7: Photographs showing aluminum enrichment by gas-tungsten-arc welding with 1/16-in.-diam aluminum on: (*a*) front and (*b*) top surface of the first gusset.

(*a*) (*b*)

Figure 8: Photographs showing aluminum enrichment by gas-tungsten-arc welding with 1/16-in.-diam aluminum on: (*a*) front and (*b*) top surface of the second gusset.

Reports/Publications/Awards:

Vinod K. Sikka, Yogesh Bhambri, and Richard O. Love, “Al Clad Steel Block,” MPLUS report, 2004.

Vinod K. Sikka, Yogest Bhambri, and Richard O. Love, “Methods to Improve Aluminum Smelter Hardware Materials,” Final MPLUS report, June 2004.

MPLUS No.: MC-03-030

Title: Methods to Improve Anode Rod Preheat Energy Requirements

Richard Love from Century Aluminum of West Virginia, Inc.

User Organization: Century Aluminum of West Virginia, Inc.
Ravenswood, WV 26164

User Contacts: Richard O. Love, 304-273-6562
rlove@centurywv.com

ORNL R&D Staff: Craig A. Blue, 865-574-4351
blueca@ornl.gov

Puja Kadolkar, 865-574-9956
kadolkarp@ornl.gov

Relevance to ITP: Anode rods are used in the process of changing carbon anodes during aluminum reduction process. During this process, the anode rod assembly is required to be connected to the carbon anode by casting iron around the stub area. Heating of the stub area prior to the pouring of cast iron is carried out to achieve a strong and low-resistant connection between the rod assembly and the carbon anode. A low-resistant stub-carbon cast iron interface will allow efficient transfer of low voltage electrical current from the hanger to the anode. The current heating techniques used at Century Aluminum of West Virginia, consists of a 24-ft-long stub drying unit operated by gas burners. Heating of stubs using this technique was found to be slow, inefficient and non-uniform. The objective of this project was to investigate new and efficient techniques for heating the stub area of an anode rod in a controlled manner. The outcome of this proposed work has strong potential for yielding an efficient process for rapid change of graphite anode to cast irons. Such a process will minimize the delay in continuing the aluminum reduction process and make it more energy efficient.

Objective: The objective of this project was to investigate infrared heating as a means to heat the stub area of an anode rod in a controlled manner.

Results: In this present study, a flat bed infrared furnace was used to heat the anode rod assembly. The flat-bed furnace is a 88-kW unit consisting of two halves, the upper half carrying an array of tungsten halogen quartz lamps and the lower half with a drop-down arrangement used to load specimens into the furnace. The main body of the upper and the lower halves is made of water-cooled stainless steel plates lined with fire brick. Figure 1 shows the anode rod assembly, and Fig. 2 shows the assembly loaded in to the furnace. Thermocouples were connected at four locations (one top and one bottom on each stub) over the surface of the stub area (see Fig. 3) to record temperatures while the heating was performed.

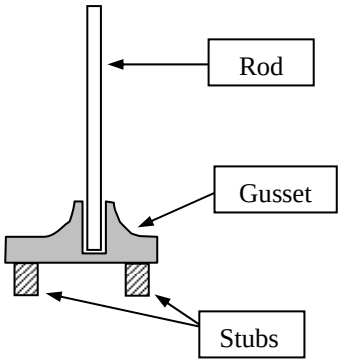

Figure 1: Anode Rod Assembly.

Figure 2: Anode Rod Assembly loaded in the flat bed furnace.

Figure 3. Location of thermocouples.

Preliminary heating trial at ORNL was performed to simulate the heating conditions employed at Century Aluminum. Figure 4 shows the flow diagram for the stub and the stub hole drying process used at Century Aluminum.

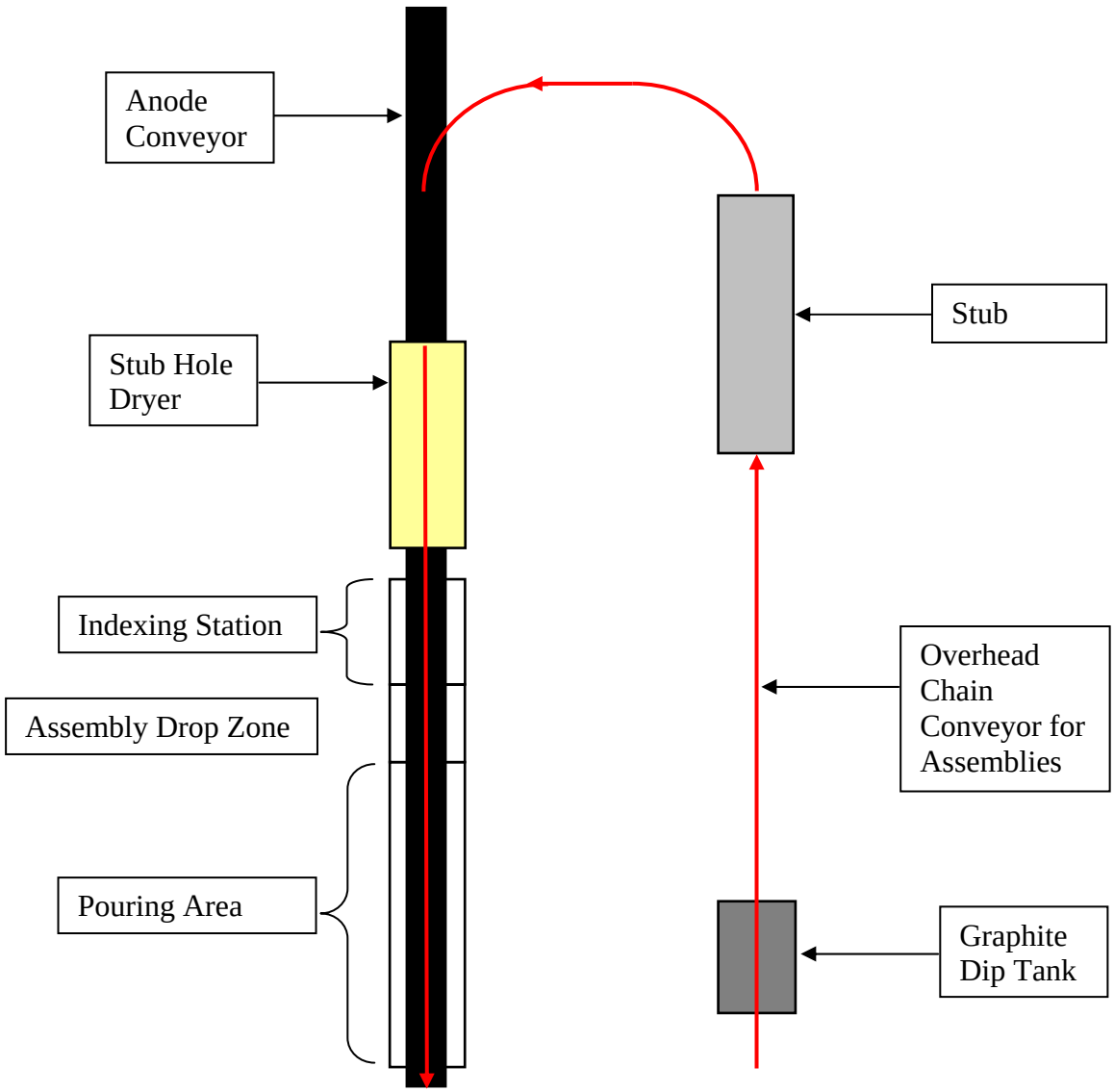

a. Temperature of the stub entering the stub dryer is 20°C.
b. Average time for which the stubs are in stub dryer = 7.5 min. Average temperature of the stub at exit = 110°C.
c. Time required for the assemblies to enter the stub hole dryer = 80 s + 60 s = 140 s = 2 min and 20 s.
d. Time for which the assemblies are in the stub hole dryer = 3 min.
e. Time to travel from stub hole dryer to the indexing station = 37 s. At the indexing station, temperature of the stub is anywhere from 80 to 190°C. Time for the stub assembly to spin and drop in to the anode = 28 s.
f. Expected temperature for the stub prior to pouring the cast iron = 135°C ± 10°C.

Figure 4: Flow diagram for the stub and the stub hole drying process.

Based on the flow diagram, the time taken by the stubs to travel from the exit of the stub dryer to the indexing station just prior to the pouring of cast iron is 80 + 60 + 180 + 37 + 28 s = 6 min and 25 s. It is assumed that no significant increase in the stub temperature

occurs while the assemblies pass through the stub hole dryer. The expected temperature of the stubs just prior to the pouring of cast iron is 135°C ± 10°C. Figure 5 shows the heating of the anode assembly using the flat bed infrared furnace whereas Fig. 6 shows the heating profile acquired during the preliminary test.

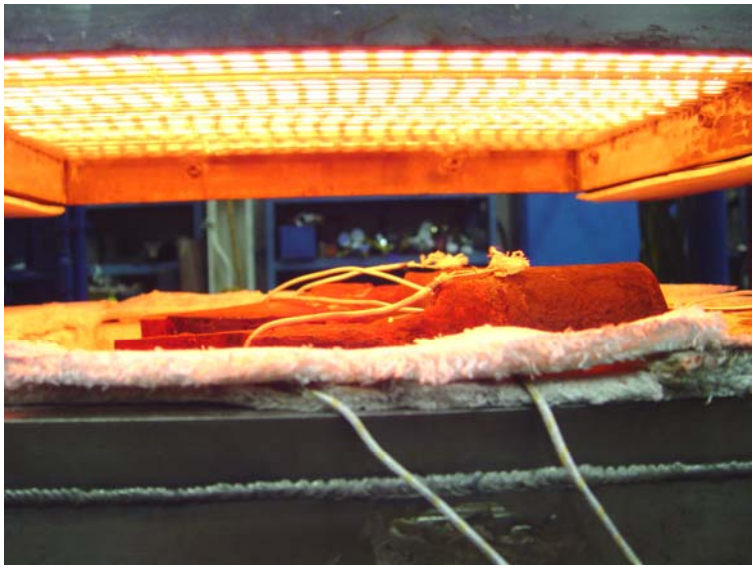

Figure 5: Anode assembly being heated using flat-bed infrared furnace.

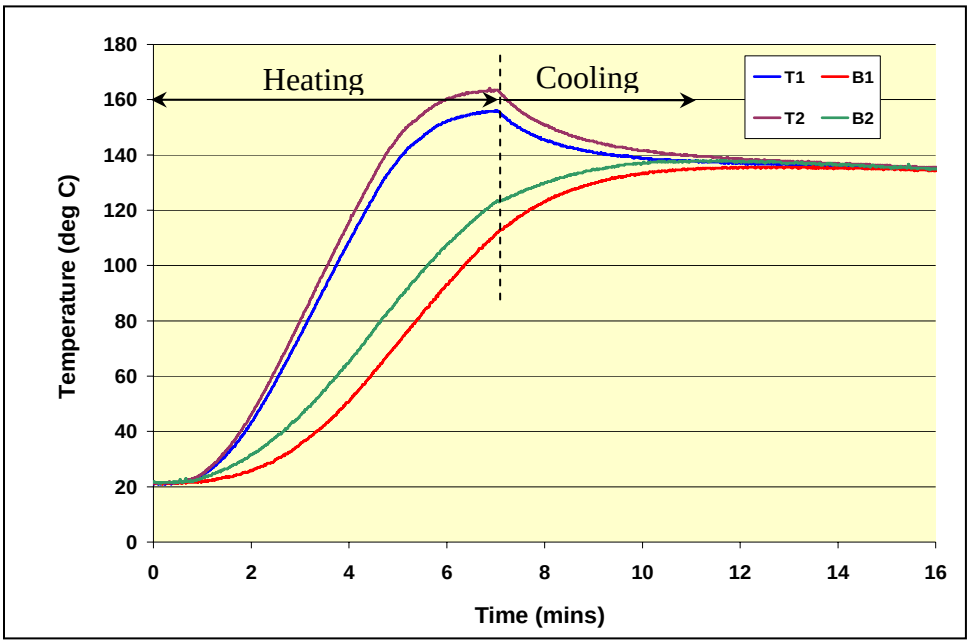

Figure 6: Temperature profile for anode stub preheating.

The furnace was set to heat the assemblies up to 150°C in 5 min followed by a hold time of 2 min at 150°C. After the hold time, the furnace was turned off and the anode

rod was allowed to cool. The cooling of the anode was performed to simulate the traveling of the assemblies from the stub dryer to the indexing station, which takes approximately 6.5 min (390 s).

Figure 6 clearly indicates the heating and cooling segments of the experiment. The difference in the T1 and B1 (and similarly T2 and B2) was due the cross section of the stub and one-sided heating of the furnace. At the end of the cooling cycle (just prior to pouring of the cast iron), the temperature of the entire stub assembly equalized to 135°C ± 3°C. The higher temperatures reached by the top surfaces and the overall heating time can be reduced using double-sided heating system for this kind of application.

Based on the preliminary results, additional tests were also carried out using the same one-sided infrared heating unit, to heat the anode stubs as fast as possible or in the shortest time possible. The furnace was operated with varying outputs viz. 60%, 70% and 80%, considering the fact that a full-scale production-based conveyor-type infrared heating unit would be less than 80 to 90% efficient. Temperature profiles recorded from thermocouples T1 and B1 for different outputs are shown in Fig. 7.

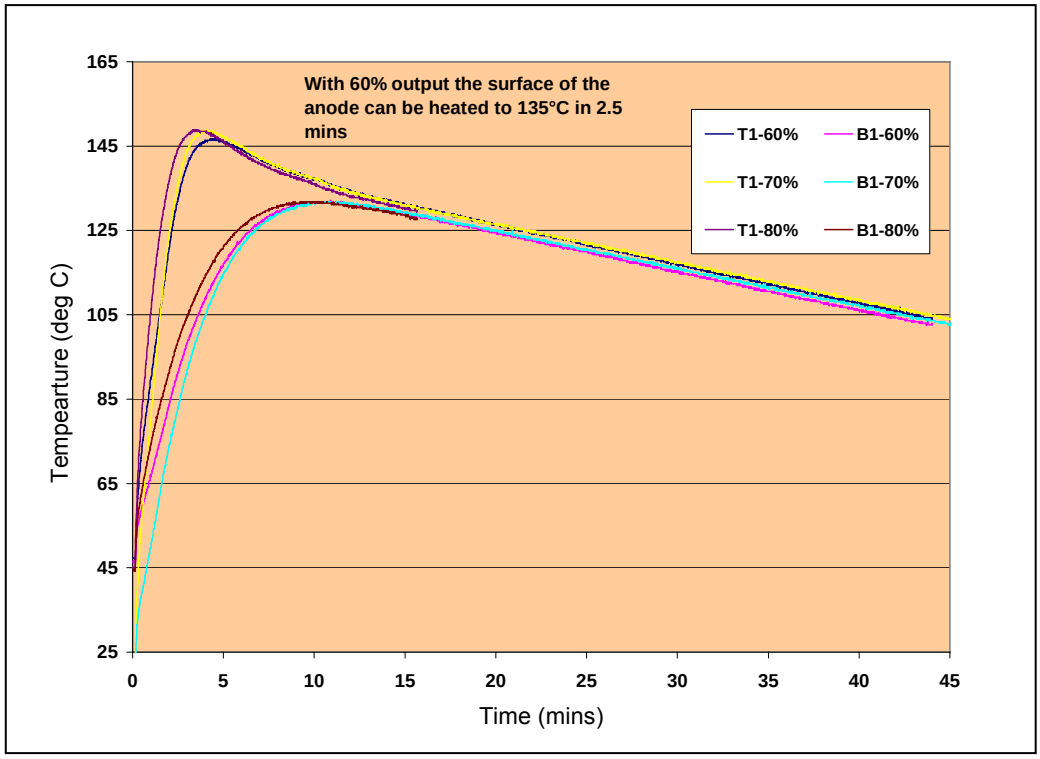

Figure 7: Heating of the stub using the infrared furnace with varying outputs.

It is interesting to note that heating of the stub is insensitive to the output of the furnace. It can also be noted that unlike conventional heating which takes 7.5 min, infrared

heating takes only 2.5 min with only 60% output to heat the surface of stubs to the desired temperature. Based on the above results, a double-sided heating furnace (as shown in Fig. 8) as a replacement to the existing stub hole dryer is proposed for uniform and efficient heating of the entire stub surface in 2.5 to 3min.

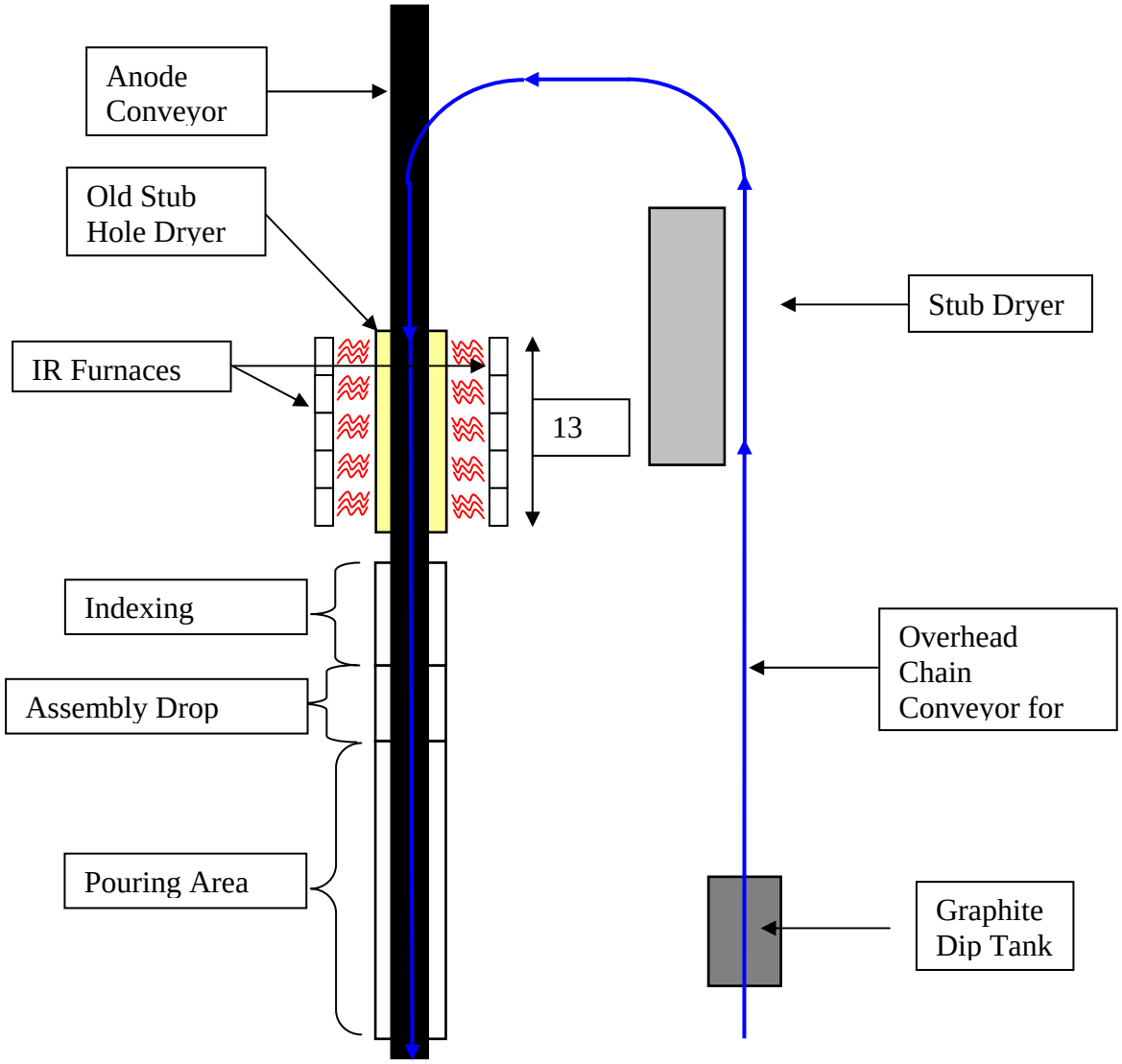

Figure 8: Replacement of stub hole dryer.

In summary, infrared heating provides uniform and controlled heating of stubs. Replacement of the conventional heating furnace with a double-sided conveyor-based

infrared furnace has been proposed. The furnace can be designed such that the same unit can be used to heat the anode stubs as well as carbon anodes simultaneously. Such replacement indicates a huge potential for energy savings in the anode rod preheating process.

Reports/Publications/Awards:

Craig A. Blue, Puja Kadolkar, and Richard Love, “Methods to Improve Anode Rod Preheat Energy Requirements,” Final MPLUS report, June 2004.

MPLUS No.: MC-03-040

Title: Microwave Activation of Catalysts

User Organization: Equistar Chemical Company
Cincinnati, OH 45249

User Contact: Emory A. Ford, 413-584-0512
eaford@comcast.net

ORNL R&D Staff: Alicia L. Compere 865-574-4970
compereal@ornl.gov

Emory A. Ford from
Equistar Chemical Company

Relevance to ITP: Catalytic cracking of heavy crude oils and petrochemical feedstocks is an energy intensive unit process which requires high temperatures and high pressures. Microwave-activated catalysis could greatly reduce process temperature and pressure required to crack crude oils because the catalyst, rather than the bulk of the material processed would be selectively activated. This would result in significant energy savings. In addition to the energy savings, microwave activation of cracking catalysts could increase U.S. energy security by permitting domestic refineries to make more efficient use of Western Hemisphere crude oils which are heavier (more cracking required), and higher in contaminants (sulfur and metals), and more viscous (may be processed in a supercritical fluid) than Arabian oils.

Objective: To determine, using small bench scale experiments, the feasibility of using microwaves to selectively activate catalysts for cracking crude oil and petrochemical feedstocks.

Results: The ability to selectively activate crude oil cracking catalysts using microwaves depends on: (1) the ability of microwaves to couple to the industrial catalysts used for crude oil processing, (2) the microwave absorption spectrum of the crude oil, and (3) whether the crude oils will form liquid states or whether dissolution in microwave transparent fluids (supercritical fluids) will be required to facilitate processing. Other measurements critical to scale up and use of a microwave activation process include the penetration depth, which provides a measure of the interior radius of processing equipment.

The crude oils which were supplied by Equistar were free-flowing and low in viscosity. This permitted their processing as liquids at low temperatures.

The most common cracking catalysts are cobalt-molybdenum oxides (CoMo) on an alumina carrier. Figure 1 shows dielectric properties for the alumina carrier (a) and for the CoMo catalyst on alumina (b). The dielectric constant for the CoMo catalyst is significantly higher than that of the alumina carrier, indicating that the catalyst centers are likely being selectively activated, or heated.

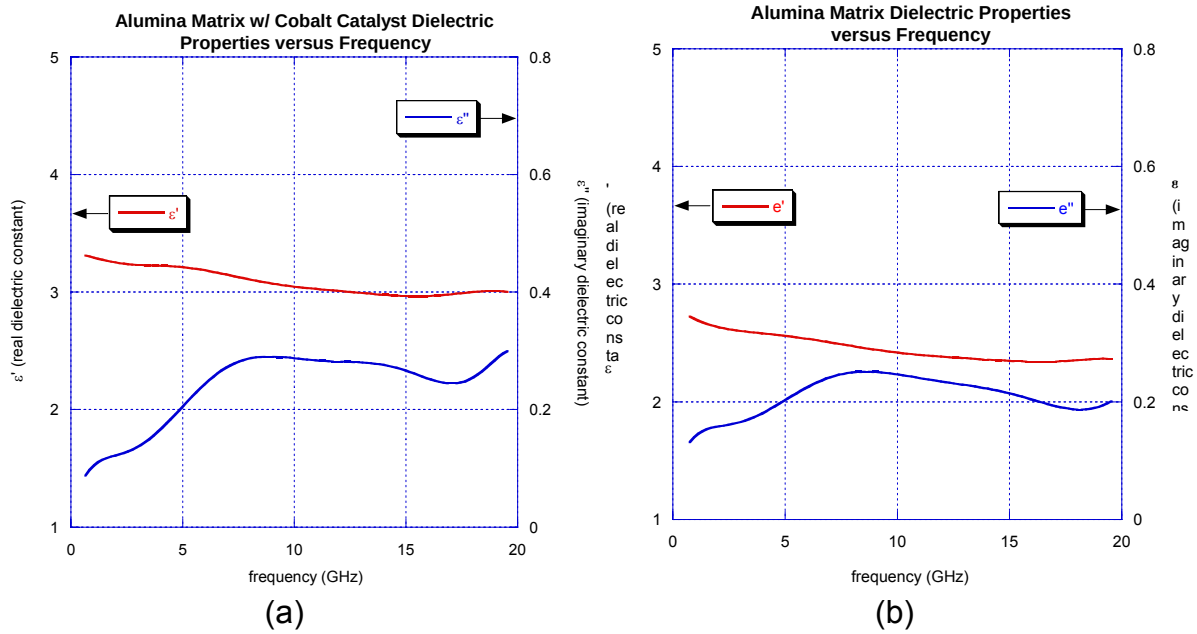

Figure 1: Dielectric constant vs. frequency for cobalt-molybdenum catalyst (left) and alumina support (right).

Similar measurements for three crude oils supplied by Equistar, Lamanaria, Sincor, and Tapis are shown in Fig. 2. Although the absorption bands for these materials are relatively complicated, they are well below those of the CoMo catalysts in typical industrial processing frequencies (950 MHz and 2.45 GHz).

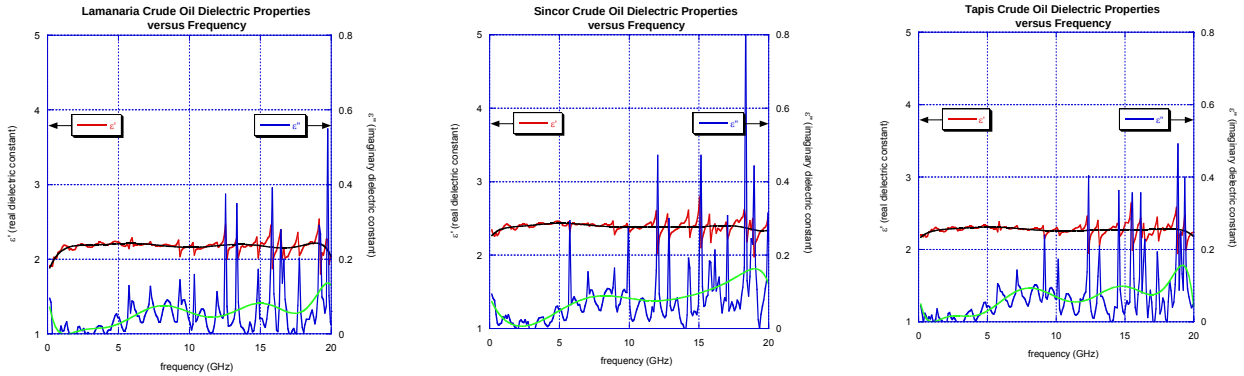

Figure 2: Dielectric constant vs. frequency for Lamanaria (left), Sincor (center) and Tapis (right) crude oils.

The next consideration is limitations on process equipment size. Penetration depth as a function of frequency is shown in Fig. 3 for the alumina carrier and the CoMo catalyst and in Fig. 4 for the crude oils. The penetration depth for solid catalyst would permit

even activation in a column of 160 cm (5 ft) in internal diameter. Larger diameters could likely be used for fixed or fluidized beds of supported catalyst shapes or for dispersed particulate catalysts.

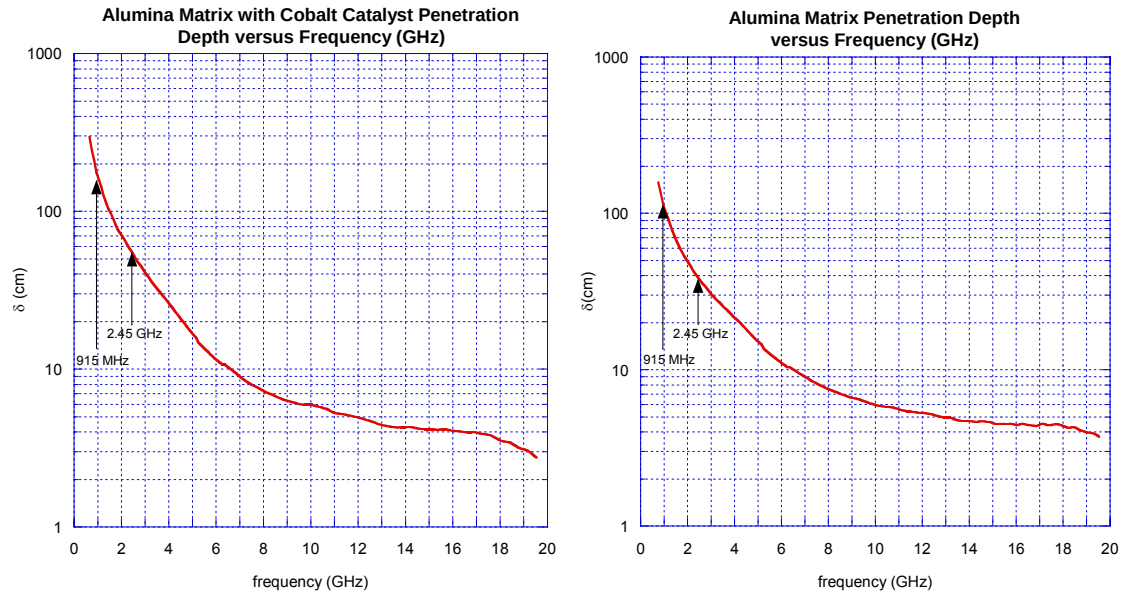

Figure 3: Penetration depth versus frequency for cobalt - molybdenum catalyst (left) and alumina support (right).

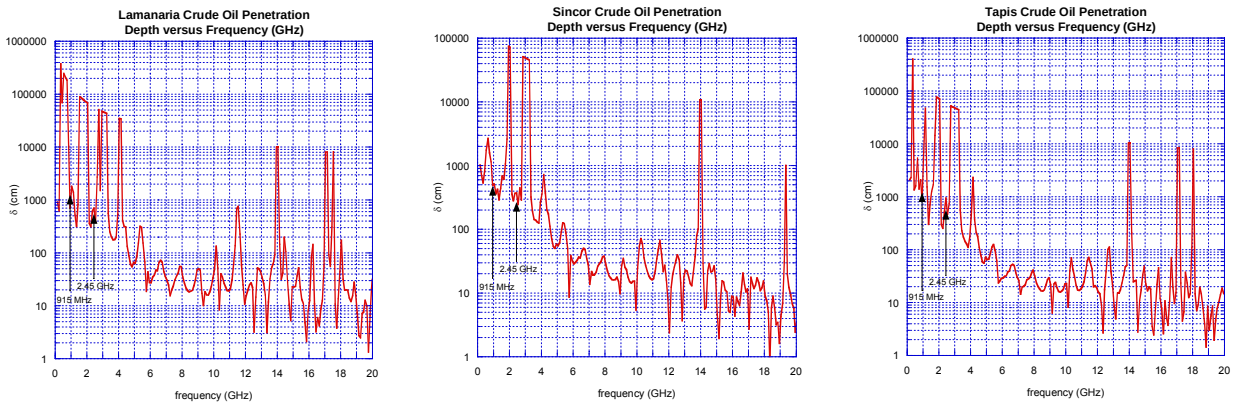

Figure 4: Penetration depth vs. frequency for Lamanaria (left), Sincor (center) and Tapis (right) crude oils.

Penetration depth for the three crude oils tested indicates that they are very unlikely to be a limiting factor in equipment design.

These results indicate that selective microwave activation of a conventional refinery catalyst, cobalt - molybdenum oxides on alumina, at permitted industrial frequencies, 950 MHz and 2.45 GHz, in the presence of crude oils is feasible.

Successful scale up and implementation of this technology could significantly decrease process energy required to crack crude oils by decreasing process temperature and pressure. It could also greatly improve the ability of U.S. petroleum and petrochemical producers to process crude oils from the Americas, which are typically heavier and more viscous than Arabian crudies. Thus, in addition to improving energy efficiency of refinery operations, this technology could improve U.S. energy security.

Reports/Publications/Awards:

A. L. Compere and Emory A. Ford, “Microwave Activation of Catalysts,” Final MPLUS report, June 2004.

MPLUS No.: MC-03-014

Title: Optimization of IR Imaging of the Lost Foam Metal Casting Process

User Organization: Foseco-Morval
Bessemer, Alabama 35022

User Contacts: Dennis Nolan, 519-763-7177
dennis.nolan@fosecomet.com

ORNL R&D Staff: R. B. Dinwiddie, 865-574-7599
dinwiddierb@ornl.gov

Dennis Nolan from Foseco-Morval

Relevance to ITP: A better understanding of the decomposition characteristics of the foam pattern in the lost foam casting process is needed to improve yield. Lost foam casting already has significant energy and environmental advantages over other metal casting processes. Yield improvements would increase these advantages and encourage further adoption of the process. Infrared (IR) imaging can provide unique insights into both the physical state and thermal behavior of the pattern decomposition products.

Objective: The objective of the project was to refine the IR imaging system for observing lost foam casting of aluminum and to analyze the effect of different tooling technologies and polymer compositions on the process.

Results: A new casting flask was designed and new procedures developed to allow more reliable imaging of castings. A new window material (Robax) was obtained and tested. In addition to being transparent in the wavelength band of the IR camera, this material was found to have superior thermal shock resistance and mechanical strength compared to Pyrex and Quartz. Robax windows also resulted in more detailed IR images. As a result, multiple pours were completed, allowing comparison of metal fill characteristics between different polymers.

In each of the videos created from the IR images, the formation of areas of coalesced polymer and their subsequent removal from the system is observed. This was a critical observation and supports recent theories concerning the nature of foam decomposition and behavior. These theories have suggested that liquid polymer products form a critical part of the system. Control of these is key in the production of high quality castings. Prior to this, it was assumed that the majority of the decomposition products formed was gaseous. This IR work confirmed these recent theories.

The following IR images (Fig. 1) taken from a pour show this phenomenon (Note areas labeled A and B):

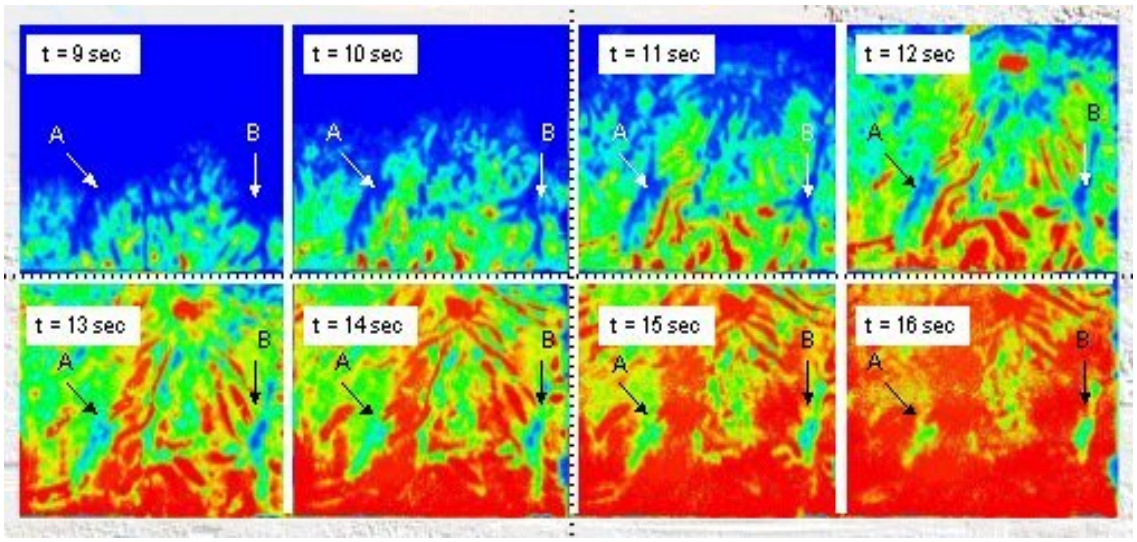

Figure 1: Polymer coalescence and residue removal.

The digital video taken in conjunction with the IR images also indicates the formation of liquid pockets of polymer. In many cases, we can see these pools form and disappear in the video.

In addition, noticeable differences in pour times occurred when different polymers were used for the patterns.

Reports/Publications/Awards:

Ralph Dinwiddie and Dennis Nolan, “Infrared Imaging of the Lost Foam Casting Process”, presented and published in the conference proceedings at the Paderborn Symposium on Lost Foam Casting, University of Paderborn (Germany), 2004.

Ralph Dinwiddie and Dennis Nolan, “Optimization of Imaging of the Lost Foam Metal Casting Process”, Final MPLUS report, 2003.

Dennis Nolan, “Update on IR Imaging” presented at the February meeting of the AFS/DOE Lost Foam Consortium, University of Alabama.

These results will also be presented in a panel discussion at the AFS Casting Congress, Rosemount, Illinois in June 2004.

MPLUS No.: MC-03-032

Title: Optimized Heat Treatment for Cast A356 Aluminum Wheels

Chuck Russo from Amcast Automotive

User Organization: Amcast Automotive
Southfield, MI 48034

User Contacts: Jagan Nath, 248-799-2207
jagan.nath@amcast.com

Chuck Russo, 260-495-5602, ext. 310
chuck.russo@amcast.com

Sara Chen, 248-799-2219
sara.chen@amcast.com

ORNL R&D Staff: Qingyou Han, 865-574-4352
hanq@ornl.gov

Relevance to ITP: Metal casting and heat treating industries. Wheels cast from A356 alloy are typically solution heat treated in large batch furnaces, capable of holding up to 320 standard wheels (16-in. diam). The nominal solution process requires a soak time of 5 hours at 995°F. Recent cost estimates at Amcast indicates a potential cost savings of approximately $125,000 per year at one plant alone (from reduced usage of natural gas) for each one-hour reduction in the solution hold time. This project aimed to develop computational methodology for the simulation of segregation and solution heat treatment of wheel castings. It addresses the priority research needs of the roadmaps of the heat treating industries and the metal casting industries. The research results can lead to minimization of the solution heat treatment time and thus substantial energy and cost savings.

Objective: The objective of this project was to use thermodynamic simulations to determine (1) the amount of Mg_2Si particles as a function of alloy composition, (2) the solubility curve of the magnesium in A356 aluminum alloy, and (3) the time required to complete dissolution of pre-existing Mg_2Si particles under the worst case conditions found in the industrial manufacturing environment.

Results: Thermodynamic modeling was carried out to the mole fraction of Mg_2Si phase that precipitates during solidification of A356 aluminum alloy. The solubility curve of magnesium, which defines the maximum magnesium concentration in the fcc aluminum phase at a given temperature, was also simulated. Based on the thermodynamic simulations, kinetic modeling was carried out to simulate the dissolution of Mg_2Si particles. Preliminary results indicate that the time required for complete dissolution of Mg_2Si particles might be much shorter than the normal solution heat treatment time used in the wheel industry (5 h at 995°F).

Figure 1 shows the mole percent of Mg_2Si particle as a function of magnesium concentration in A356 aluminum alloy. The amount of Mg_2Si precipitated during solidification increases linearly with increasing magnesium concentration of the alloy.

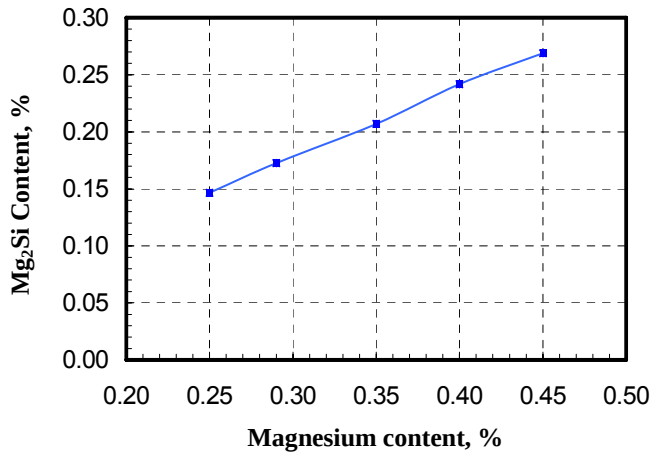

Figure 1: The amount of Mg_2Si particle precipitated during solidification of commercial A356 alloys with different Mg concentration.

Figure 2 illustrates typical dissolution curves of Mg_2Si particle in the primary aluminum dendrites. The size and volume fraction of the Mg_2Si particles decreases with increasing solution treatment time.

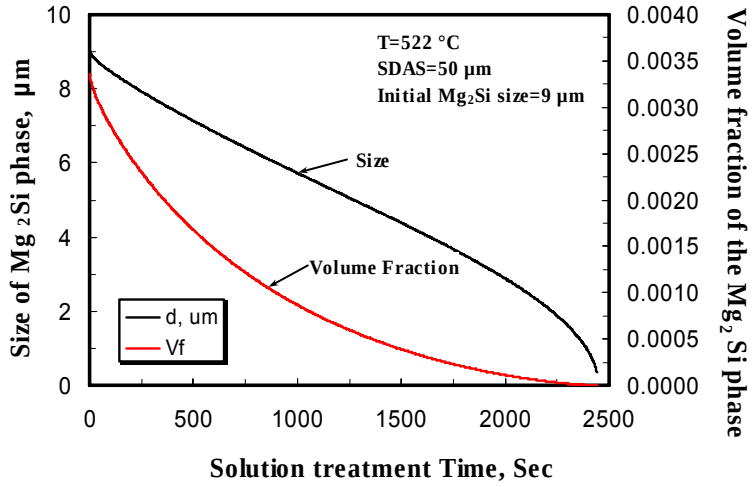

Figure 2: Typical curves of the dissolution of 9-µm Mg_2Si particle during solution treatment at 522°C when the secondary dendrite arm spacing is about 50 µm.

The dissolution time of Mg_2Si particle as a function of particle size and solution heat treatment temperature is illustrated in Fig. 3. 1 μm particles can be dissolved in less than 100 seconds under normal solution treatment temperature. Particles smaller than 9 μm require a solution heat treatment time much shorter than 5 h (18,000 s), the normal solution treatment time of aluminum wheels at 995°F (535°C).

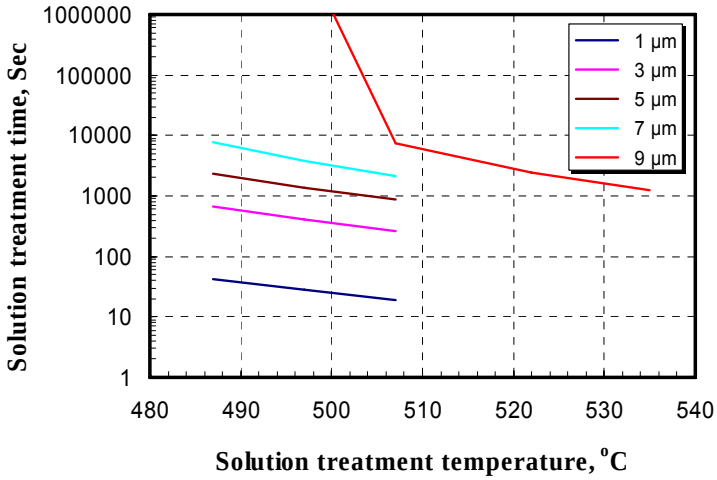

Figure 3: The predicted solution treatment time required to complete dissolution of Mg_2Si particle during solution treatment when the secondary dendrite arm spacing is 50 μm.

Reports/Publications/Awards:

C. Xu, Q. Han, C.J. Russo, and S. Chen, "Optimized Heat Treatment for Cast A356 Aluminum Wheels," Final MPLUS report, June 2004.

MPLUS No.: MC-03-013

Title: Optimizing Induction Heating to Obtain Profile Hardening of Gears

User Organization: Inductoheat
Madison Heights, MI 48071

User Contacts: Madhu S. Chatterjee, 248-629-5004
mchatterjee@inductoheat.com

ORNL R&D Staff: R. B. Dinwiddie, 865-574-7599
dinwiddierb@ornl.gov

Madhu S. Chatterjee from Inductoheat

Relevance to ITP: A high value gear requires a hard wear-resistant surface with a soft core. As a gear transmits torque, the teeth endure a combination of cyclic bending, contact stresses and different degrees of sliding or contact behavior. This makes it critical for a gear to have a proper case core structure. This condition can very readily be applied using an induction process. A MPUS program # MC-02-010 was used to define proper setup parameters using a single frequency system, known as DPIH and shown in Fig. 1.

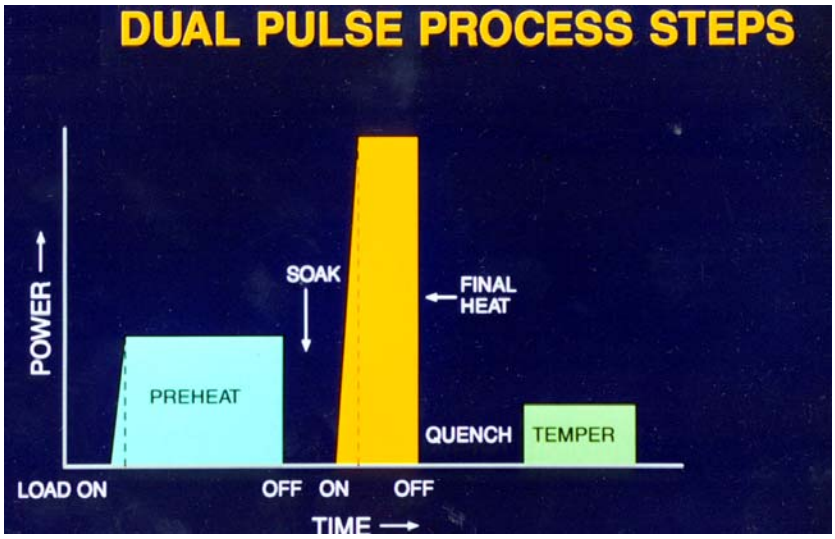

Figure 1: Steps in the DPIH process.

This project will further optimize single most economical and metallurgically superior process among all the profile gear hardening processes. The project will allow us to compare different systems of profile gear hardening to measure amount of energy saved. Other environmentally applications are smaller factory floor space, and higher production.

Objective: In this study, single frequency, known as DPIH process, was applied to profile hardening of our chosen gear geometry and compare hardness results. This comparison study was conducted in conjunction with a high speed infrared (IR) camera. The IR camera measured the gear tooth surface temperature during induction heating. This temperature study was correlated with a metallurgical evaluation for K-Factor and hardness.

Results: In MPLUS program the high speed camera measured temperatures at four critical areas of the gear. The DPIH process was altered at various levels of preheat time, soak time and power levels. By comparing the temperatures of the four areas and sectioning samples at different heat treat process variables, an optimum process setting was possible for that particular gear. The picture below is a color illustration of the temperature readings desired for this experiment.

After induction hardening, the case depths were measured at the tip and the root, and "k" Factor (ratio of Tip to Root thickness) was determined. An ideal situation is when a parts approaches uniform case depths (K Factor = 1) throughout the profiled region. Figure 2 shows the areas checked for Tip and root depths.

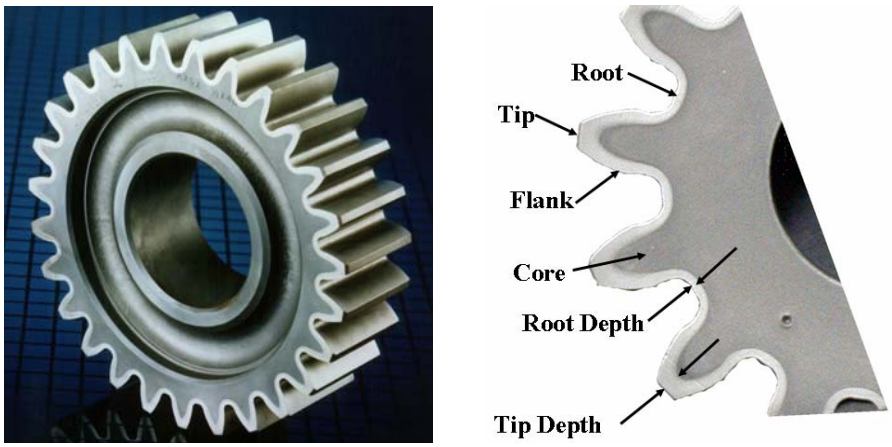

Figure 2: Gear showing hardening profile pattern and gear terminology.

The infrared (IR) camera was calibrated for temperature by imaging a gear tooth that was equipped with a thermocouple while undergoing steady state heating. The camera to gear distance, integration time, lens, and filters were kept constant during all measurements. Figure 3 shows the calibration data and resulting equation used to convert the IR signal from the camera into a temperature in degrees Fahrenheit.

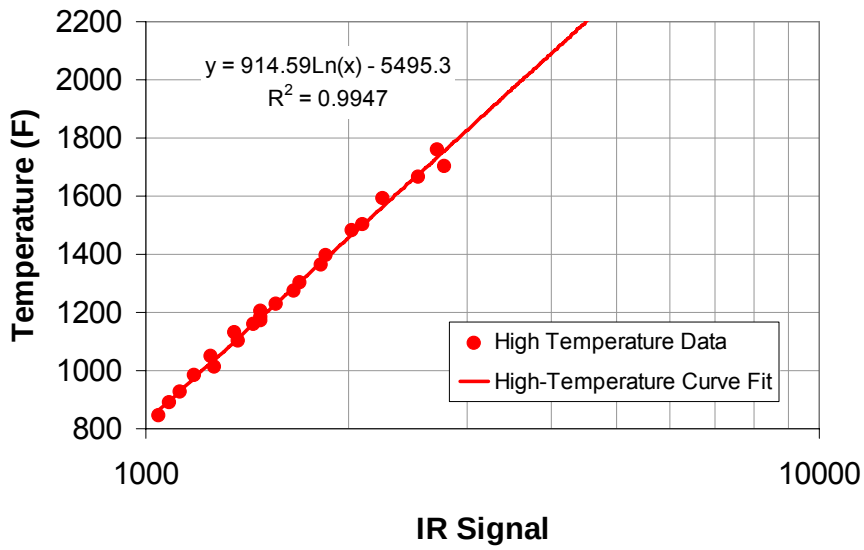

Figure 3: Temperature calibration used to convert the infrared signal data into temperatures.

A thermal image showing the locations of temperature measurements is shown in Fig. 4. This image was taken 0.007 seconds before the water quenching begins. The high-speed thermal imaging (142 images per second) also allowed the optimization of the timing signal sent to the quench valve.

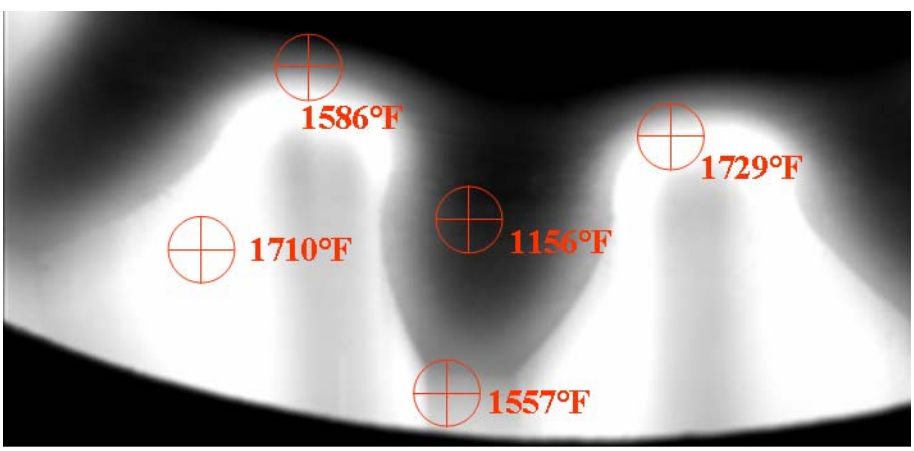

Figure 4: Thermal image of gear 0.007 s before water quenching begins.

Table 1 shows how the final heat and soak times varied for each gear sample, as well as, the results of the metallurgical evaluation for K Factor and hardness. Gears IR 15, 16, and 17 all have K factors close to 1. Gears IR 7, and 18 showed no hardening at the root and thus a K factor could not be determined.

Table 1. Metallurgical evaluation for K-factor and hardness

Sample ID#	Final Heat Power (KW)	Soak Time (sec)	Case Depth Root (mm)	Case Depth Tooth (mm)	K Factor	Hardness Root (HRA)	Hardness Tooth (HRA)
IR 1	181	5.0	0.9	1.1	0.818	82	83
IR 2	181	4.5	0.8	1.2	0.667	83	84
IR 3	181	5.5	0.8	1.0	0.800	83	83
IR 4	181	3.0	1.2	2.9	0.414	82	82
IR 5	181	7.0	1.0	0.7	1.429	84	82
IR 6	200	7.0	1.2	2.0	0.600	82	82
IR 7	170	7.0	0.9	0.0	#DIV/0!	82	82
IR 8	170	5.0	0.9	1.2	0.750	83	82
IR 9	200	5.0	1.2	3.5	0.343	82	83
IR 10	200	3.0	1.3	4.0	0.325	84	82
IR 11	170	3.0	0.9	2.4	0.375	83	84
IR 12	200	3.0	1.3	4.1	0.317	82	84
IR 13	200	7.0	1.4	2.5	0.560	82	83
IR 14	170	3.0	1.0	2.9	0.345	83	83
IR 15	170	5.0	0.9	1.0	0.900	82	82
IR 16	181	5.0	1.0	1.2	0.833	82	83
IR 17	181	7.0	1.1	1.3	0.846	82	82
IR 18	170	7.0	0.9	0.0	#DIV/0!	83	83
IR 19	181	7.0	1.0	3.1	0.323	84	82
IR 20	200	5.0	1.1	3.3	0.333	82	85

Reports/Presentations/Awards:

R. B. Dinwiddie and M. S. Chatterjee, “Optimizing Induction Heating to Obtain Profile Hardening of Gears,” Final MPLUS report, June 2004.

Ralph B. Dinwiddie and Madhu Chatterjee, “Infrared Imaging as a Diagnostic Tool for Powertrain Component Heat-Treat Process,” Global Powertrain Congress 2003, Ann Arbor, Michigan, September 23-25, 2003

MPLUS No.: MC-03-016

Title: Process Improvements for Complete Oxidation of Copper Chops for Ease of Production of Fine, Easily Compactable Cu and Cu Alloy Powders

User Organization: ACuPowder TN LLC
Greenback, TN 37742

User Contact: Krishna Patel, 865-856-3021
patel@acupowder.com

ORNL R&D Staff: Vinod K. Sikka, 865-574-5112
sikkavk@ornl.gov

Yogesh Bhambri, 865-576-6031
bhambriy@ornl.gov

Ed Fuch from ACuPowder using the ORNL-loaned infrared unit at the Greenback facility

Relevance to ITP: Production of fine powders of ductile materials such as Cu requires the following three steps:

Step 1: Cu (wire drops) + air (O_2) = Cu_2O + CuO

In this step, ductile wire chops of pure Cu or Cu alloys are oxidized in air or oxygen to form brittle oxides of Cu (Cu_2O + CuO). The stiochiometry of the oxides shows that Cu_2O contains 10 to 11% O_2 and CuO contains 22 wt % O_2.

Step 2: The brittle mixture of oxides of Cu_2O + CuO are crushed and milled to fine oxide particles. Because of their brittleness as opposed to pure Cu, they are easy to produce in fine particle sizes.

Step 3: In this step, the fine particle size powder of oxides is reduced by 25% H – 75% N gas mixture to Cu.

Although the three-step process above works, it is not optimized for its energy use. Some issues with the current process are as follows:

- It does not oxidize the entire wire – core still contains pure Cu
- Current oxidation process forms CuO on the surface, which contains 22% O_2 as opposed to desired Cu_2O, which contains approximately 10 to 11%. The reduction of CuO to Cu requires nearly the double amount of the reducing gas mixture and production rates are slower.

It is important to understand the oxidation kinetics of Cu wires and effects on these kinetics of variables such as heating methods of gas-fired versus infrared heating, prior treatments of a wire such as acetic acid wash, and addition of moisture in air during oxidation.

A systematic study of various variables showed that the heating of Cu wires by infrared heating system produces porous Cu_2O on the surface with internal oxidation of Cu core through rapid oxygen diffusion. If longer times are used, Cu_2O on the surface converts to dense CuO with reduced oxygen diffusion and internal oxidation of Cu.

The infrared heating of Cu wires with heating times of 15 to 30 min at 925°C was considered desirable for optimum brittleness during crushing and milling. These were also desirable because it required minimum amount of reducing gas for oxide reduction with high throughput of Cu powder.

A prototype infrared heating system supplied by MPLUS facilities to ACuPowder confirmed the laboratory results under production conditions. The project had major benefits of saving energy and increasing productivity. Similar concepts may also be applicable to powder production of other ductile metals and alloys.

Objective: The objective of this project was to determine the optimum processing parameters for oxidation of Cu + Cu alloy wires for ease of their milling and grinding to produce fine powders of Cu and Cu alloys. The process to be optimized included: method of heating wires, optimum temperature and time combination, effect of prior treatment of wires to maximize the oxidation process, and the effect of adding water vapor to air during the oxidation process.

Results: The oxidation kinetics of Cu wire in air is shown in Figs. 1 through 4. Effects of temperature for two heating methods are shown in Figs. 1 and 2. For the same test temperature, the effect of infrared heating versus conventional heating on oxidation kinetics is compared in Fig. 3. Effect of cleaning Cu wires with acetic acid and addition of water vapor to air on oxidation kinetics are compared in Fig. 4. Photomicrographs of Cu wire oxidized at 925°C for different times (15 to 50 min) are shown in Fig. 5. These micrographs clearly show that oxide for short exposure time is porous with significant internal oxidation of the core. For longer time, oxide is more dense and internal oxidation is somewhat reduced. It is expected that the longer exposure time results in not only dense but undesirable CuO, which has nearly double the oxygen content.

The effect of oxygen content on the crushing energy of oxidized Cu wires is shown in Fig. 6. It can be noted that even 5 wt % oxygen reduces the crushing energy of pure Cu by a factor of 3.

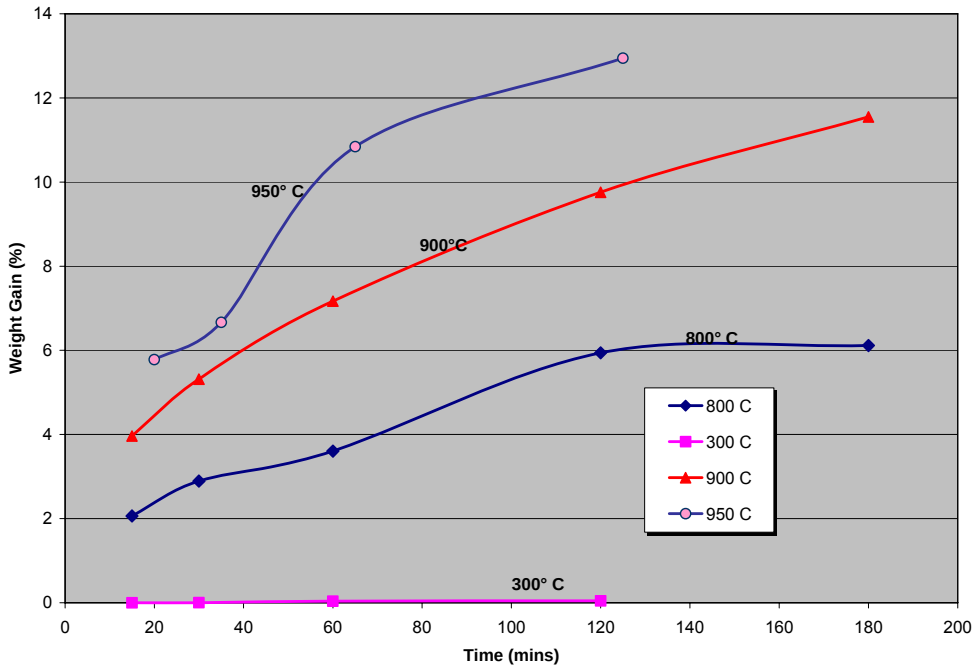

Figure 1: Plot illustrating copper weight gain as a function of time at various temperatures heat-treated in conventional furnace.

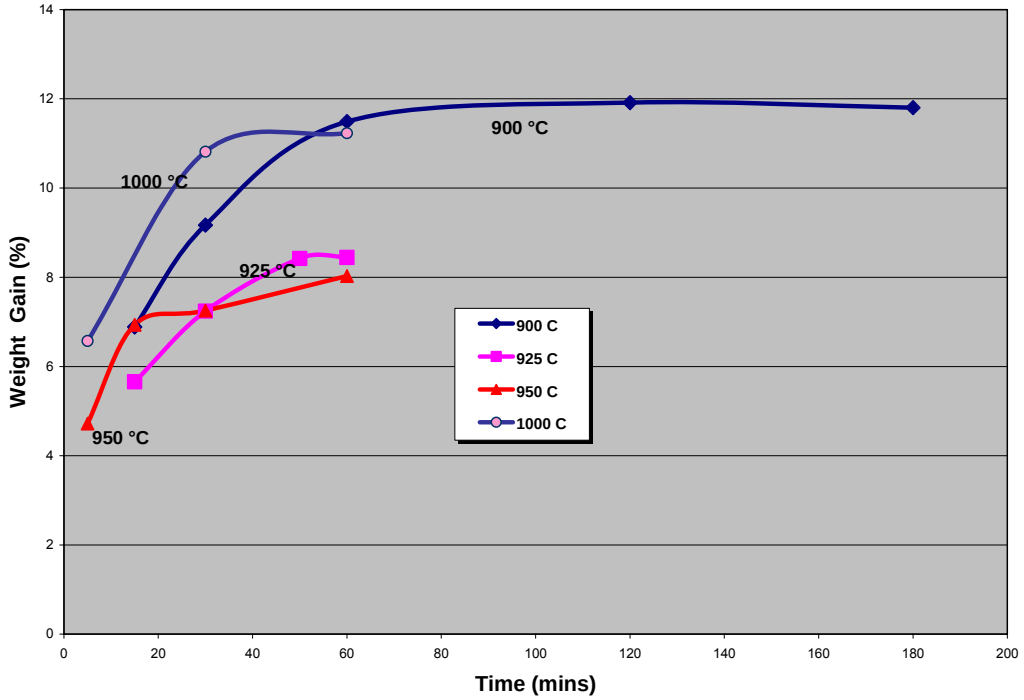

Figure 2: Plot illustrating copper weight gain as a function of time at various temperatures heat-treated in infrared furnace.

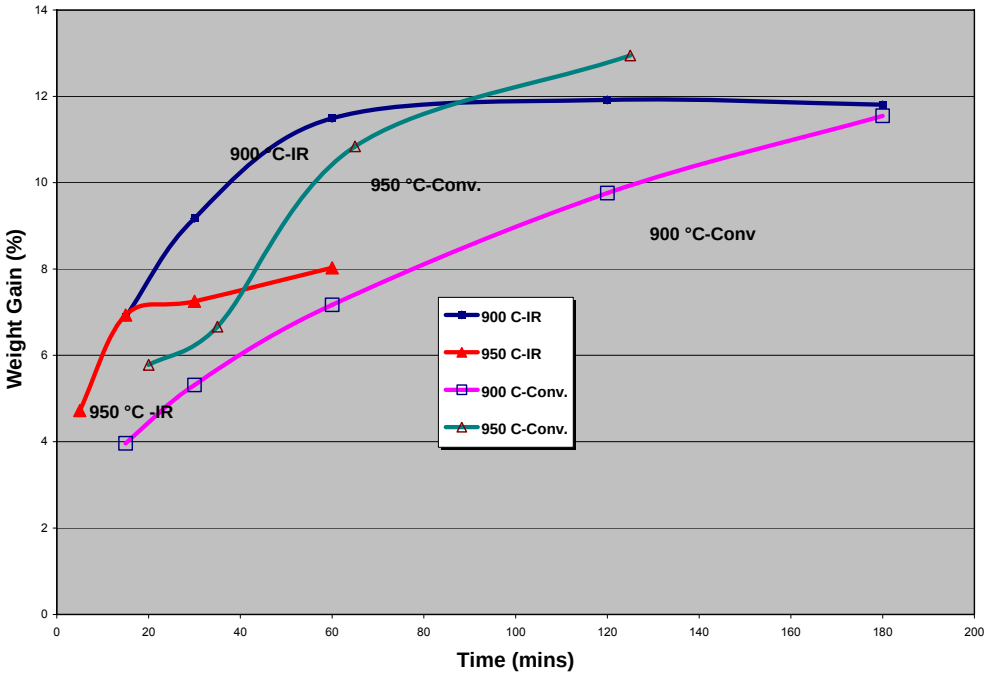

Figure 3: Plot illustrating copper weight gain comparison between infrared furnace and conventional furnace at 900 and 950°C.

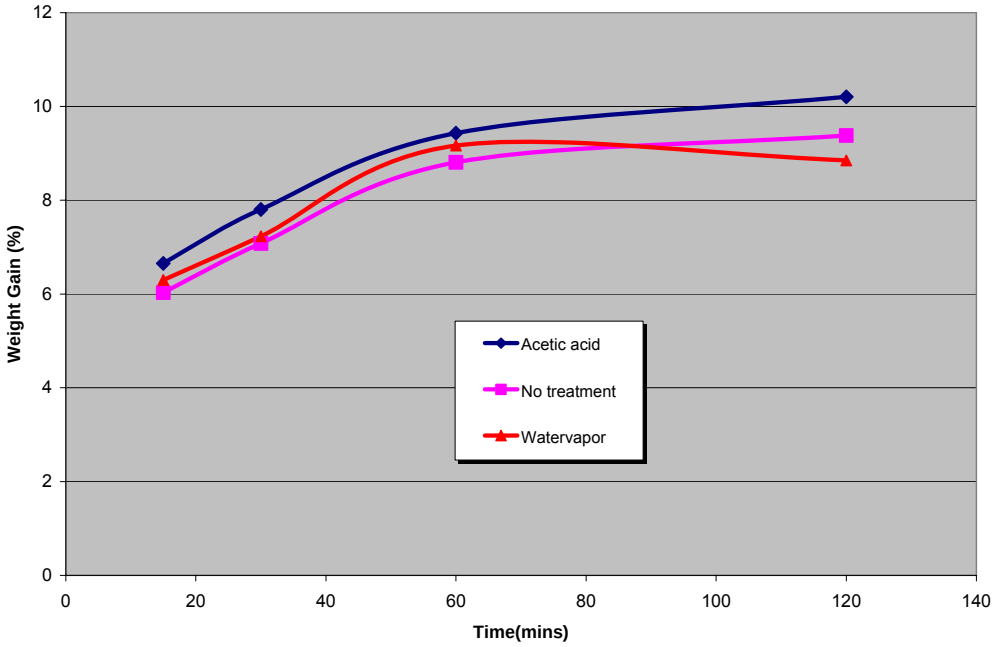

Figure 4: Plot illustrating copper weight gain comparison with different treatments at 900°C in infrared furnace.

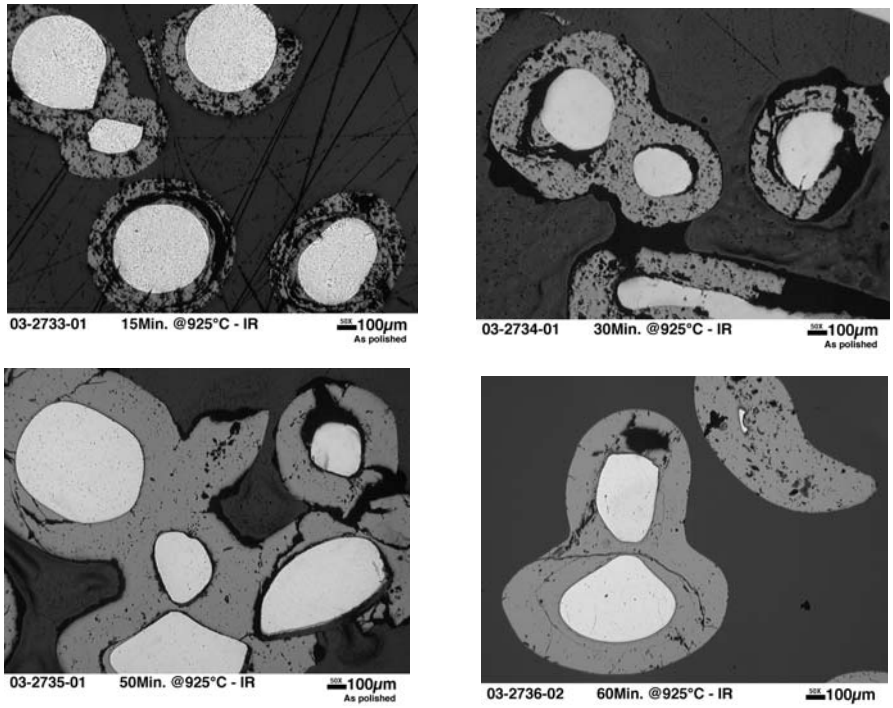

Figure 5: Copper oxidized samples at 925°C for different time intervals.

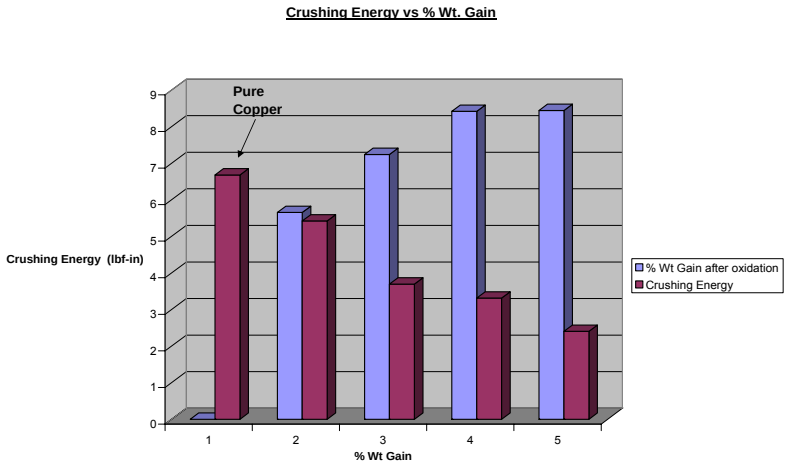

Figure 6: Plot of crushing energy as a function of percent weight gain after oxidation.

The following conclusions are possible from the data presented in Figs. 1 through 6:

1. Short-time oxidation of Cu wires in air at 925°C is desirable for formation of porous Cu_2O oxide on the surface and internal oxidation of Cu.

2. Even a pick-up of 5 wt % oxygen reduces the crushing energy of oxidized Cu wire by a factor of 3.

3. Infrared heating unit can potentially be used to accomplish the above goals.

An infrared heating unit loaned to ACuPowder was successfully demonstrated under production conditions. This unit is shown in Fig. 7.

Figure 7: Set-up of MPLUS supplied infrared heater for pre-oxidation of Cu wires at ACuPowder facility in Greenback, Tennessee.

Reports/Publications/Awards:

Yogest Bhambri, Vinod K. Sikka, and Krishna Patel, "Cu Oxidation Data: Report No. 1," MPLUS report, March 2004.

Yogest Bhambri and Vinod K. Sikka, "Cu Oxidation Testing Data: Report No. 2," Final MPLUS report, April 2004.

MPLUS No.: MC-03-012

Title: Quantifying and Correlating Lost Foam Pattern Properties with Metals Fill Casting Performance: Understanding the Process

User Organization: Metal Casting Technology, Inc.
Milford, New Hampshire 03055

User Contact: Qi Zhao, 603-673-9720 X2307
qzhao@mct-inc.com

ORNL R&D Staff: R. B. Dinwiddie, 865-574-7599
dinwiddierb@ornl.gov

Qi Zhao from
GM Metal Casting Technology, Inc.

Relevance to ITP: Understanding the true foam removal mechanism in the lost foam aluminum process is critical to the defects elimination and continuous process improvement (more efficient energy use). The project successfully acquired both mass and heat transfer during the process, visually confirmed the existence of a gas layer between metal and plastic foam residue, and visualized an interface controlled foam removal process. The results added more values to support GM lost foam production.

Objective: The objective of the project was to use the real time thermal imaging to visualize foam removal kinetics for a better understanding of the foam removal mechanism in the lost foam aluminum process.

Results: A steel sand flask with a glass window of Robox™ was used (Fig. 1A) to host a coated foam sprue assembly (Fig. 1B). The flask has a removable back cover to facilitate sand investment and vibration compaction (Fig. 1C). The back cover was tightly closed after sand compaction (Fig. 1D). The loaded steel sand flask was then reoriented and transferred to the scene for cast and monitored by an infrared (IR) camera (Fig. 1E). A356.2 aluminum alloy in a resistance heat furnace was heated to 732°C (1350°F) and manually poured 6 seconds before the infrared thermal imaging and recording started.

The real time infrared (IR) visualization of the mass and heat transfer was successfully acquired. A series of snap shots were presented in Fig. 2, which demonstrated foam collapse, coalescence, and removal orderly via an interface controlled mechanism. The results demonstrated the following:

1. Infrared thermal imaging is unique in acquiring real time process information of both heat and mass transfer in the lost foam aluminum process.

2. Thermal imaging visually confirmed the existance of a gas layer of 1 mm or less in width between the molten metal and entrapped platstic foam residues.

3. Thermal imgaging visually confirmed the presence of foam coalescence during the lost foam aluminum process. The event was observed as a lcoal foam residue redistribution.

4. Thermal imaging visualized the foam removal in the lost foam aluminum process. The visualization confirmed the interface controlled mechanism proposed by the model proposed in the final reports of MCT WA87821 and G305.

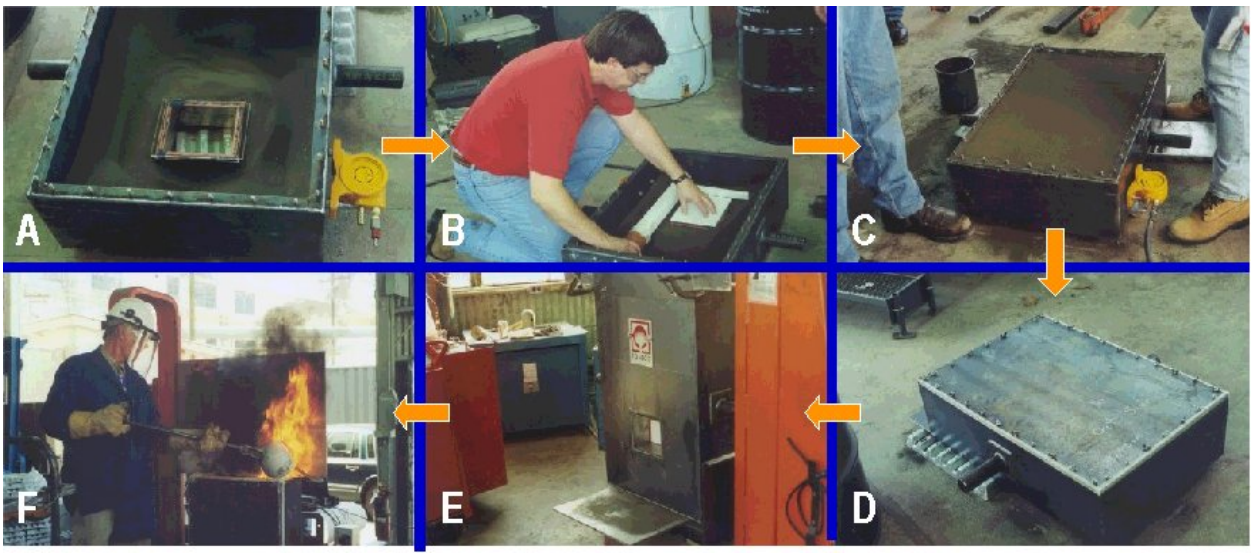

Figure 1: Foundry procedure for infrared imaging: (A) window setup on a steel sand flask, (B) foam sprue setup with a close contact between foam plate and glass window, (C) sand investment aided by vibration, (D) enclosure of mold/sand assembly, (E) loaded sand flask in standup position for metal casting and thermal imaging (on a selected view field of 5 x 5 in.), and (F) manual pour of molten A356.2 aluminum alloy.

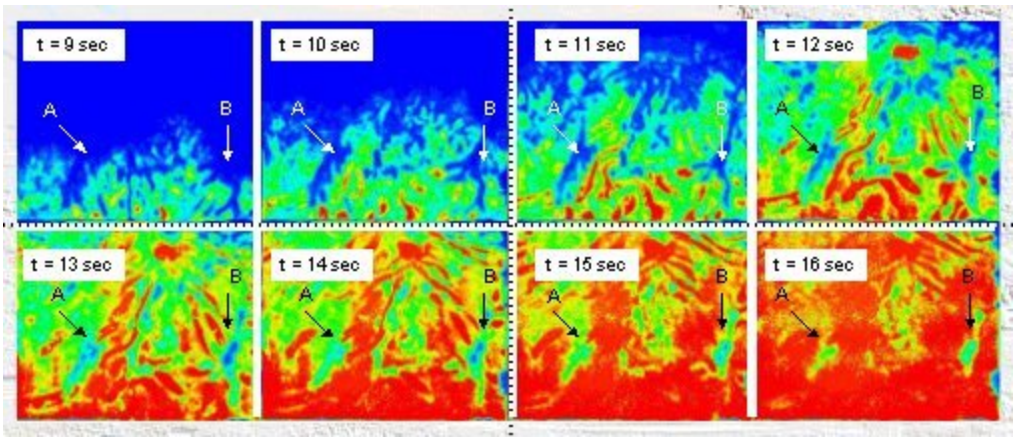

Figure 2: Globs (in green) on coating substrates during a lost foam aluminum casting from 9 to 12 s after the metal pour started. Thermal image sequence of molten aluminum burning nonuniformly into a low fusion foam pattern; thermal images of the foam removal (plastic globs in green) at points A and B by surrounding metal that were separated by gas phases (in yellow) during a lost foam aluminum casting from 13 to 16 s after the metal pour started. Two globs at points A and B (in green with blue cores) shrank in all directions as time increased from 13 to 16 s after the metal pour started.

Reports/Publications/Awards:

Qi Zhao, Tom Gustafson, and Ralph Dinwiddie, "IR Imaging of Foam Removal in Lost Foam Aluminum Process", *TMS Annual Meeting, Automotive Alloys*, Charlotte, NC, March 15-18, 2004.

These results will be also discussed in presentations at the 2004 AFS Casting Congress.

MPLUS No.: MC-03-033

Title: Qualifying Production Grade Foam and Coatings with Real Time X-Ray, Infrared and Capacitive Methods for the Lost Foam Casting Process

User Organization: GM Powertrain
Saginaw, MI 48650-5073

User Contacts: Jerry A. Barendreght, 989-757-0810
jerry.a.barendreght@gm.com

ORNL R&D Staff: Ralph B. Dinwiddie, 865-574-7599
dinwiddierb@ornl.gov

Jerry Barendreght from GM Powertrain

Relevance to ITP: This research will improve the Lost Foam casting process. These improvements in the casting process will reduce scrap and improve casting quality.

Objective: The objectives of this project were to compare and validate process measurement methods and improve understanding of the relationship between metals and lost foam pyrolysis locations. This level of measurement has not been previously performed and provides an unparalleled level of process understanding.

Results: The measurements were performed with a known series of patterns. Their performances were correlated with both the foam and coating properties. Foam patterns were tested before casting using optical analysis, gas permeability by standard and infrared techniques, water uptake, density scans, and optical fusion measurements. Coated foam patterns were then cast while simultaneously imaged by infrared and X-ray methods. Figure 1 shows the agreement between images taken with the infrared camera and real-time X-ray equipment. Coating failure against the window was the dominant controlling factor determining metal flow behavior. Smaller patterns and/or stronger coatings will be required in any future testing.

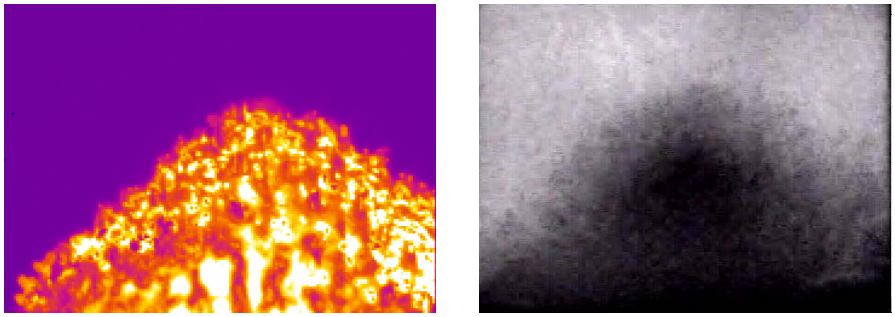

(*a*) (*b*)

Figure 1: Comparison of the infrared image (*a*) with the real-time x-ray image (*b*) for pour #7 taken at GM Powertrain on July 29-30, 2004.

Reports/Publications/Awards:

Ralph B. Dinwiddie, “Qualifying Production Grade Foam and Coatings with Real Time X-Ray, Infrared and Capacitive Methods for the Lost Foam Casting Process,” Final MPLUS report, June 2004.

Graham V. Walford presented the GM Powertrain MPLUS work at the Lost Foam Consortium Meeting on .

Presented at the 2004 AFS Casting Congress on June 12, 2004 in Rosemount, Illinois.

MPLUS No.: MC-03-022

Title: Study of Pyrolysis Product Generation and Behavior in the Lost Foam Casting Process

User Organization: Tennessee Technological University
Cookeville, TN 38505-0001

User Contact: Fred Vondra, 931-372-3527
fvondra@tntech.edu

Graham Walford, 865-482-4995
walfordgv@ornl.gov

ORNL R&D Staff: R. B. Dinwiddie, 865-574-7599
dinwiddierb@ornl.gov

Fred Vondra from Tennessee Technological University

Relevance to ITP: Understanding the decomposition of the foam during the lost foam casting process is critical if improvements are to be made in the process and increasing yield (more efficient energy use). The project successfully sampled the evolved gases and liquids during the thermal decomposition of polystyrene foam. Results indicate that helium gas significantly increases the rate at which the pyrolysis products are transported through the coating.

Objective: The objectives of the experiments include: (1) sample and analyze the pyrolysis products (evolved gases and liquids) resulting from the thermal decomposition of polystyrene foam, (2) learn to understand the removal of the pyrolysis through pressure, coating and other parameter control, and (3) understand if gas species effects the liquid decomposition product removal.

Results: We have constructed a burn chamber and observed and modified the burning process. The observations and measurement of foam in controlled burning conditions allows observation of bead differences (i.e., T185 and T170), differing coating permabilities and differing atmospheres and pressures. This has led to our process development using differing gases and elimination of liquid pyrolysis with our "heli-flow"* approach.

A study was made to directly observe the decomposition of expanded polystyrene foam as applicable to the metals casting process. An Infrared heat source with the equivalent heat energy capability of a molten aluminum front was used to heat a foam surface in a chamber with controlled atmospheres. The Decomposition of the foam was observed with an infrared camera with wavelength sensitivity different from the heat source. Therefore the heat transfer into the foam and the ensuing build up of heat in the decomposition products could be observed with minimal interference from the heat lamp or other sources.

We successfully observed the decomposition process with differing fusion levels of foam, foam chemistries, differing coating permeabilities and atmospheres to identify those conditions that resulted in the most effective removal of the foam products. Both liquid and gaseous product generation was observed.

Real time mass spectroscopy was performed on the decomposition products and static samples were collected for further analysis.

A concept previously considered by Currie* and Walford* was validated where the use of a helium atmosphere greatly enhanced decomposition of the foam was validated. This is now the subject of significant effort to apply the use of helium atmospheres to the lost foam casting process.

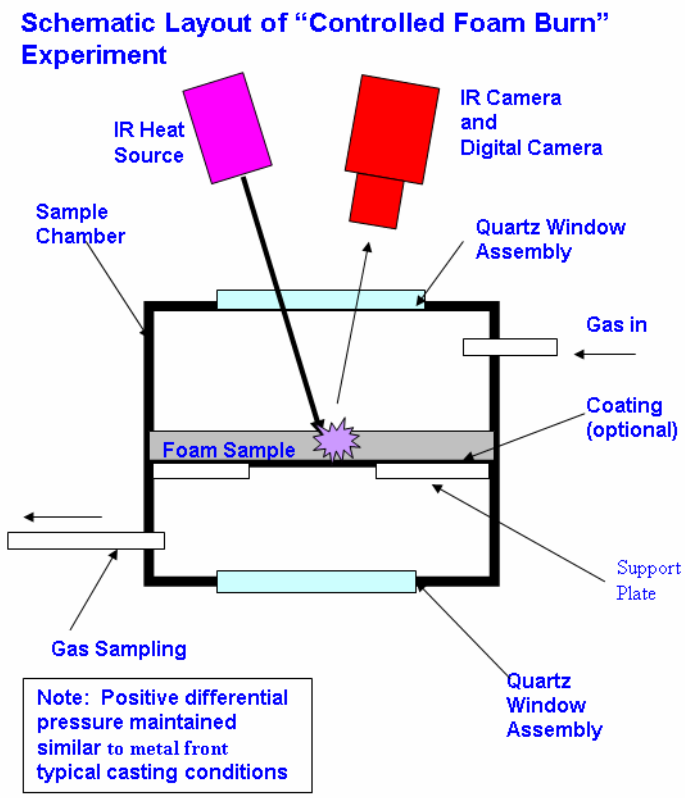

Figure 1: Diagram of the chamber developed to study the controlled thermal decomposition of polystyrene foam.

*Subject of a Walford Technologies patent application activity.

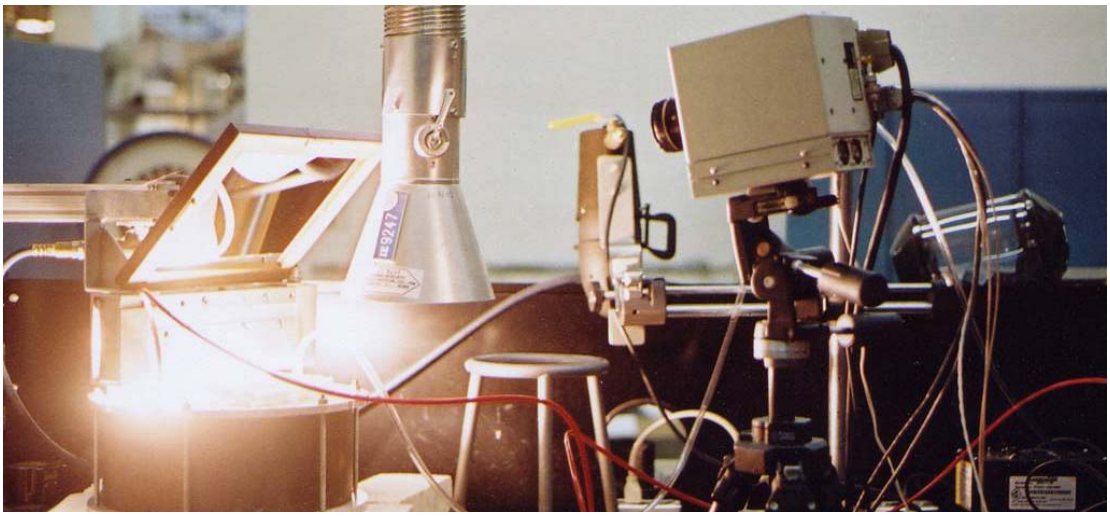

Figure 2: Photograph showing the experimental set-up with the infrared heating lamp on top of the burn chamber in the lower left corner and the infrared camera is in the upper right corner.

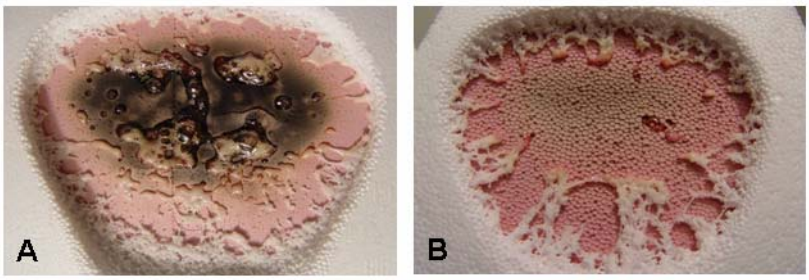

Figure 3: Foam samples after exposure to infrared heating: (A) in air, and (B) in helium.

Reports/Publications/Awards:

R. B. Dinwiddie, "Gas Flow Studies in the Lost Foam Pattern – Elimination of Pyrolysis Products from the Pattern Volume," Lost Foam Casting Consortium, October 2003, Des Plaines, Illinois.

Patent disclosure is in progress.

The results of this MPLUS project will be discussed in presentations at the June 2004 AFS Casting Congress.

MPLUS No.: MC-03-006

Title: Thermal Conductivity vs. Temperature Measurement of Nanostructured Insulating Materials

User Organization: Lawrence Berkeley National Laboratory
Berkeley, CA 94720

User Contacts: Arlon J. Hunt, 510-486 5370
ajhunt@lbl.gov

ORNL R&D Staff: Hsin Wang, 865-576-5074
wangh@ornl.gov

Arlon J. Hunt from Lawrence Berkeley National Laboratory

Relevance to ITP: Improve high-temperature industrial processing heating, lower cost, and save energy via development of new refractory materials.

Objective: To measure thermal conductivity and thermal diffusivity of nanostructured aerogel composites prepared at Lawrence Berkeley National Laboratory (LBNL) from room temperature to elevated temperatures.

Results: Nanostructured aerogel composite specimens were prepared at LBNL and shipped to ORNL for testing. The density of the aerogel can be from 0.003g/cm^3 to 0.35g/cm^3 with the most common density of 0.1g/cm^3. The aerogel is very fragile and could easily break into pieces. All of the specimen thicknesses were measured at LBNL. Any contact measurement is not suitable for these specimens. We chose to use the flash diffusivity method at room and elevated temperatures. The specimen thickness is 1.5 mm. At room temperature, thermal diffusivity is 0.0013cm^2/s. The diffusivity value is a bit higher than expected, probably because the uncertainty of thickness and possible light penetration into the specimen surface.

At elevated temperatures, two aerogel specimens were tested up to 500ºC. Due to its low thermal conductivity, the thermal transient after the laser shot took more than 2 s to reach its peak. Extra post-analysis was performed in order to obtain thermal diffusivity. The thermal diffusivity values at 100ºC were similar to that of room temperature. There was a slight decrease at 200 and 300ºC. Considering the slight increase in specific heat, the thermal conductivity of the aerogel stayed close to constant in this temperature range. At 400ºC and above, heat transfer to the specimen holder and the long measurement time (12 s) caused baseline shift of the sample. Thermal diffusivity values could not be obtained directly. Further testing requires better design of specimen holder and post analysis including

Thermal conductivity and thermal diffusivity of aerogel materials are very difficult to measure. Normal thermal conductivity measurements of insulating materials are contact in nature and not suitable for testing at elevated temperatures. The results obtained in this project are very important in understanding the high-temperature

thermal transport behavior of the aerogel composites. In the course of the project, we also found that the laser flash method may be another way to show the infrared opacity of the aerogel and further investigation may be needed.

Reports/Publications/Awards:

H. Wang and A. J. Hunt, “Thermal Conductivity vs. Temperature Measurement of Nanostructured Insulating Materials,” Final MPLUS report, July 2004.

MPLUS No.: MC-03-038

Title: Thermodynamic Simulation of Porosity Potential in Ductile Irons

User Organization: Citation Corporation
Birmingham, AL 35242

User Contacts: Al Alagarsamy, 205-271-7402
ala@citation.net

ORNL R&D Staff: Qingyou Han, 865-574-4352
hanq@ornl.gov

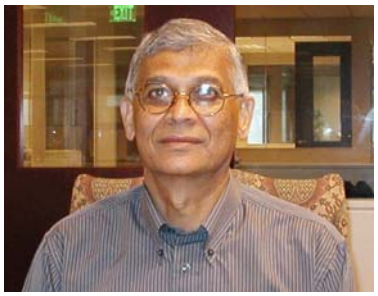

Al Alagarsamy from Citation Corporation

Relevance to ITP: Ductile irons suffer from porosity formation during solidification, which is detrimental to the mechanical properties, notably the fatigue life, and the pressure tightness of castings. In order to minimize porosity formation, large risers are normally used, which reduces porosity level sometimes but leads to a low mold yield in the range of 50 to 60%, meaning that only 50 to 60% of liquid metal is used for making the casting, the rest is used to form the gating and riser systems. Predictive tools that can simulate porosity potential in ductile irons can be used to increase the mold yield and save energy.

Objective: Carbon, Si, Mg, Mn, Cr, Mo, and P are the elements that affect porosity formation in ductile irons. Experiments have been carried out at Citation Corporation and a porosity index for ductile irons has been suggested. The purpose of this MPLUS research was to use computation thermodynamic tools to predict the porosity potential in ductile irons and to compare the thermodynamic simulation prediction with data obtained in ductile iron casting. It was expected that the results of this MPLUS project can lead to a predictive tool for reducing porosity formation in ductile irons.

Results: During solidification of ductile irons, the precipitation of graphite leads to volume expansion. Any element that promotes graphite formation, especially at the late stage of solidification, will be beneficial to reduce shrinkage porosity formation in castings. Based on this idea, thermodynamic simulations were carried out to predict graphite formation and the influence of alloying element on graphite formation. The results indicate that C and Si promote graphite formation while Cr and Mn retard graphite formation and promote carbide formation. This accounts for the fact that C and Si decrease the potential of porosity formation but Cr and Mn increase the potential of porosity formation. The results also indicate that the thermodynamic simulation alone can only predict the trend of porosity formation but not the porosity index obtained at Citation Corporation. Advanced kinetic models have to be developed in order to predict porosity formation in ductile irons more realistically.

Figure 1 shows phase precipitation during solidification of ductile irons. Graphite starts to form from early solidification. No carbide is formed under equilibrium conditions. However, under Scheil conditions which represents most of the solidification conditions, carbide forms at the end of solidification. The shrinkage of carbide formation is likely to promote porosity formation.

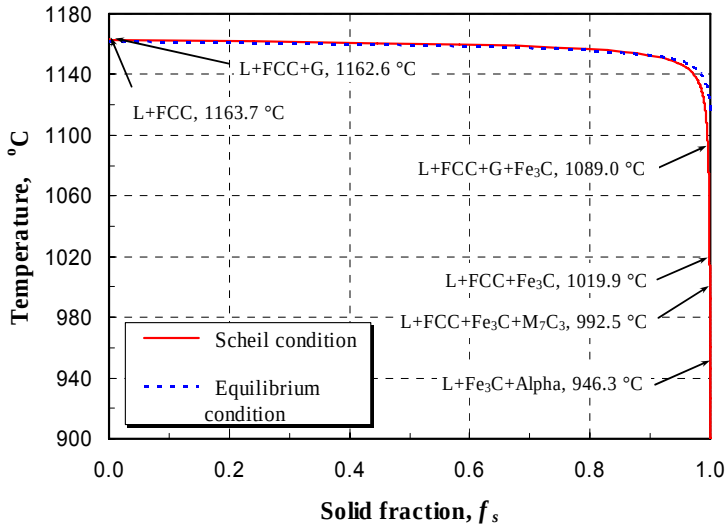

Figure 1: Phase evolution during solidification of ductile iron.

The influence of the elements in ductile irons on graphite formation was also systematically investigated. Figure 2 illustrates the effect of carbon on the mole fraction of graphite precipitated during solidification, where *N1.0* is the total amount of graphite formed and *N0.25* is the amount of graphite formed at a solid fraction of 0.25. *Neff* is the amount of graphite formed in the range of solid fractions between 0.25 and 1.0, where graphite expansion is believed to be effective in reducing porosity formation. The mole fraction of graphite precipitated increases with increasing carbon content.

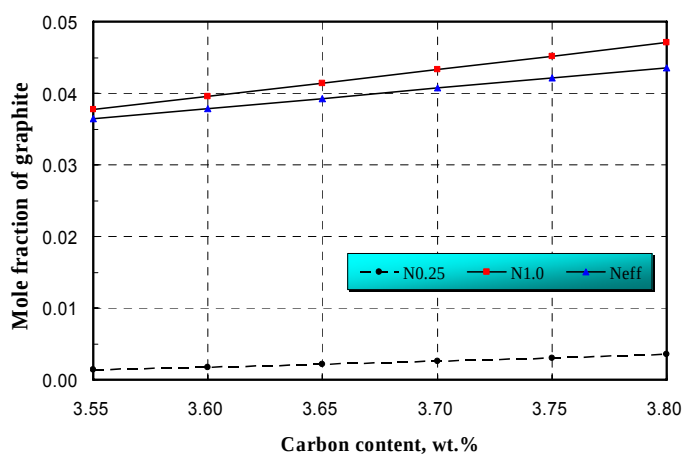

Figure 2: The relationship between the mole fraction of graphite and the carbon content of the irons.

In general, each element in ductile iron affects graphite formation to some extent. By using thermodynamic simulation, graphite precipitation can be maximized by adjusting the compositions of the alloy, leading to a minimization of shrinkage porosity formation.

Reports/Publications/Awards:

C. Xu, Q. Han, and Al Alagarsamy, “Thermodynamic Simulation of Porosity Potential in Ductile Irons,” Final MPLUS report, June 2004.

MPLUS No.: MC-03-017

Title: Utilizing Graphite Expansion to Compensate Solidification Shrinkage in High-Strength Gray Cast Iron

User Organization: HK Casting, Inc.
Weston, WV 26452

User Contact: Patricia Minehardt, 304-269-7809
plminehardt@aol.com

Roy Burkhammer, 304-269-7809

ORNL R&D Staff: Qingyou Han, 865-574-4352
hanq@ornl.gov

Qingyou Han (ORNL) with Patricia Minehardt from HK Casting, Inc.

Relevance to ITP: High-strength cast irons suffer from porosity formation during solidification, which is detrimental to the mechanical properties, notably the fatigue life, and the pressure tightness of castings. The porosity scrap rate can be as high as 40% in iron castings and usually does not show up until after heavy machining operations, wasting time and materials. In many cases in iron castings, the formation of porosity is due to inadequate riser/gating design. Often large risers are used in industry but porosity defects still exist in the casting, leading to low mold yield and high scrap/rework.

Objective: The purpose of this project was to investigate the effect of composition on graphite formation and the techniques of riser design to make full use of graphite expansion to compensate for the solidification shrinkage, which lead to porosity formation. The objective was to reduce the scrap rate for high-strength gray iron castings and to increase the mold yield by reducing the size of the risers.

Results: Thermodynamic simulations were carried out to determine phase evolution in the alloy (3.0-3.5%C, 1.8-2.4%Si, 0.09%S, 0.05%P, 0.5-1.2%Ni, 0.55%Mo-0.5%Cu, and 0.05%V). Simple calculations based on the principal of proportional solidification were made to estimate the riser neck size in order to make full use of graphite expansion to compensate for the shrinkage which occurs at the end of solidification. The following two main results were obtained:

- The sequence of graphite and carbide formation and their mole fraction as function of alloy composition.

- The estimation of the riser neck size such that when graphite expansion occurs in the casting, the riser neck freezes to avoid the feeding of a casting to a riser.

Figure 1 shows phase evolution in the alloy. Graphite (G) precipitates at the early stage of solidification (small solid fractions) where any volume shrinkage can be compensated for by the risers so the volume expansion due to the precipitation is not utilized to feed shrinkage. At the end of solidification, carbides (Fe_3C and MC) form and the formation carbides leads to volume shrink which cannot be fed using the liquid metal in the risers, giving rise to shrinkage porosity formation. If the graphite expansion can be utilized for compensating the shrinkage of the carbides, porosity can be reduced or eliminated.

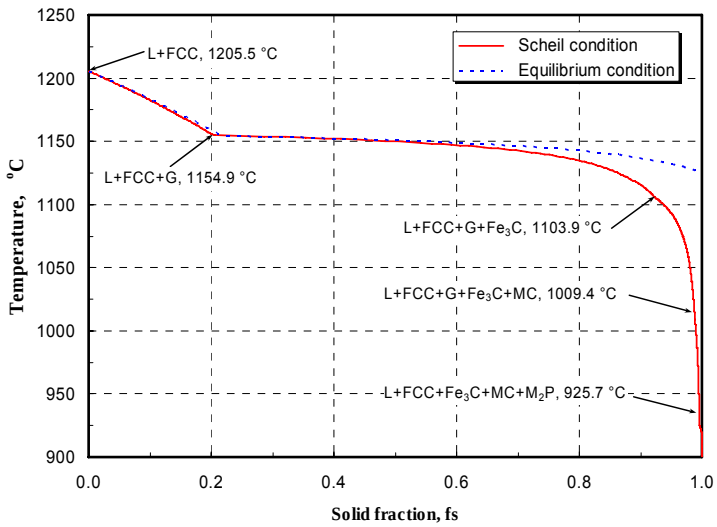

Fig. 1: Phase precipitation during solidification of high strength gray irons.

Table 1 lists the simulation mole fractions of graphite and carbides precipitated during solidification of high strength gray irons, where the carbon equivalent, CE, is defined as CE=C%+1/3Si%, and V_G, V_{Fe3C} and V_{MC} are mole fractions of graphite. Fe_3C, and MC respectively. The mole fraction of graphite increases and that of carbides decreases with increasing carbon equivalent of the alloy. The results suggest that increasing the carbon equivalent of the alloy tends to reduce shrinkage porosity level in the castings.

Table 1: Carbon equivalent of the alloy and the mole fraction of the phases predicted using thermodynamic simulations

CE	V_G	V_{Fe3C}	V_{MC}
3.60	2.834×10^{-3}	2.66×10^{-4}	8.50×10^{-6}
3.95	2.175×10^{-3}	3.58×10^{-4}	7.86×10^{-6}
4.30	1.676×10^{-3}	4.46×10^{-4}	7.34×10^{-6}

In order to utilize graphite expansion, which occurs at the early stage of solidification, to compensate carbide shrinkage towards the end of solidification, the riser neck, which links the risers to castings, has to be chocked-off so that pressure can be built up within

the casting. Calculations based on known principles of proportional solidification were performed and the size of the riser neck was determined. Using predicted riser neck size and some other technical modifications, HK casting is able to reduce the scrap rate of a piston casting to a much low level.

Reports/Publications/Awards:

C. Xu, Q. Han, and Patricia Minehardt, “Utilizing Graphite Expansion to Compensate Solidification Shrinkage in High Strength Gray Cast Irons,” Final MPLUS report, 2004.

MPLUS No.: MC-03-025

Title: Weld Pool Dynamics and Its Effects on Weld Profile and Properties of High-Strength Steels

User Organization: Ford Motor Company
Dearborn, MI 48124

User Contact: John Chiang, 313-323-1063
jchiang@ford.com

Cindy Jiang, 248-813-0130
Cindy.jiang@aet-integration.com

ORNL R&D Staff: Zhili Feng, 865-576-3797
fengz@ornl.gov

Jeff McNabb, 865-576-3797
mcnabbjd@ornl.gov

John Chiang from
Ford Motor Company

Relevance to ITP: Welding is a cross-cutting technology area, supporting the all the primary Industry of the Future (IOF) sectors of the Office of Industrial Technologies. The theme of the program is to understand the material flow in molten weld pool and weld pool shape produced with the MIG welding process. The MIG welding process studied here is one of the primary high-productivity welding processes widely used for construction and maintenance repairs of chemical plants, petroleum refineries, casting equipments, and agricultural machinery. Therefore, the findings from this work are expected to help improve the service life of the steel weld joints in those IOF applications where thermal and/or mechanical cyclic loading is critical to the operations of the plants or machineries. In fact, IMF's Caterpillar's virtual welding project has pointed out that the weld bead shape is perhaps the most dominate factor controlling the fatigue and other weld performance life. Furthermore, the proposed R&D work would ultimately help the steel industry to produce high-strength steels that are more weldable and have better fatigue properties.

Objective: To weld four types of steels under high-speed welding conditions, to determine the effects of steel grades and welding conditions on the weld profiles and the microstructures that are critical to the durability of high-strength steel welds.

Results: Four types of steels were investigated. Three of them were dual-phase high-strength steels with a strength level in the range of 100 ksi, but produced by three different steel suppliers with different compositions and processing routes. The fourth steel is mild steel for baseline comparison. Fillet lap joints were made with one filler wire chemistry and under the same shielding gas mixture of CO_2 and argon.

Welds were made under three welding speeds and three levels of joint gaps. It was found that the weld quality is greatly affected by the weld joint gaps. The type of steels was also a factor affecting the weld profiles. Compared to the baseline mild steel, all high-strength steels showed improved weld profile which indicates better weld performance under cyclic loading conditions (Fig. 1). One of the high-strength steels (Steel No. 1) consistently showed better weld profiles for all the welding conditions studied.

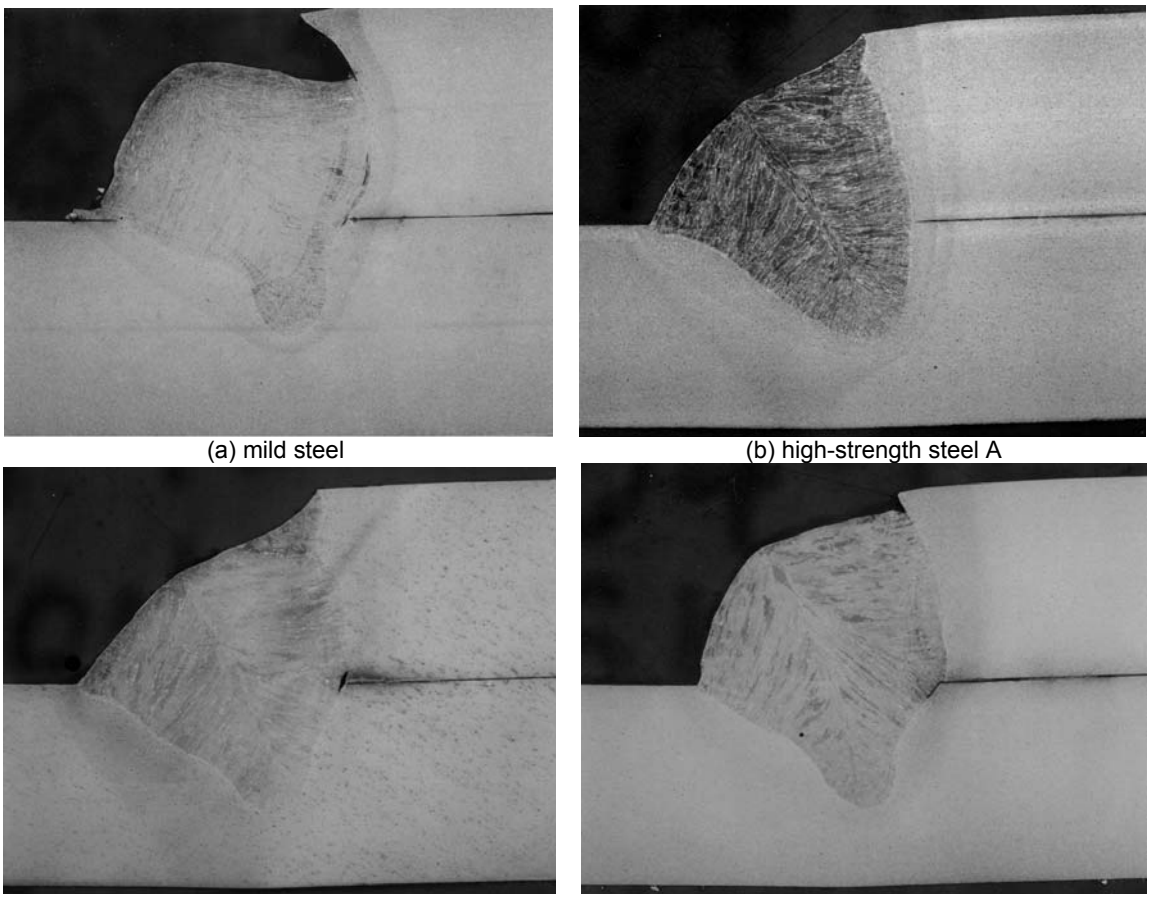

(a) mild steel (b) high-strength steel A

(c) high-strength steel B (d) high-strength steel C

Figure 1: Cross-section view of weld profile. Mild steel weld (a) has the worst weld profile compared to these of high-strength steel welds (b, c, and d).

Different steels formed different microstructure under the same welding conditions. As shown in Fig. 2, the microstructures in the coarse grain region of the heat affected zone of three 100-ksi, grade high-strength steels are quite different. This illustrates that, due to composition differences, the same grade of high-strength steels can have different mechanical properties in the weld region. This will be an important factor that must be fully considered in design and service of high-strength steel welded structures.

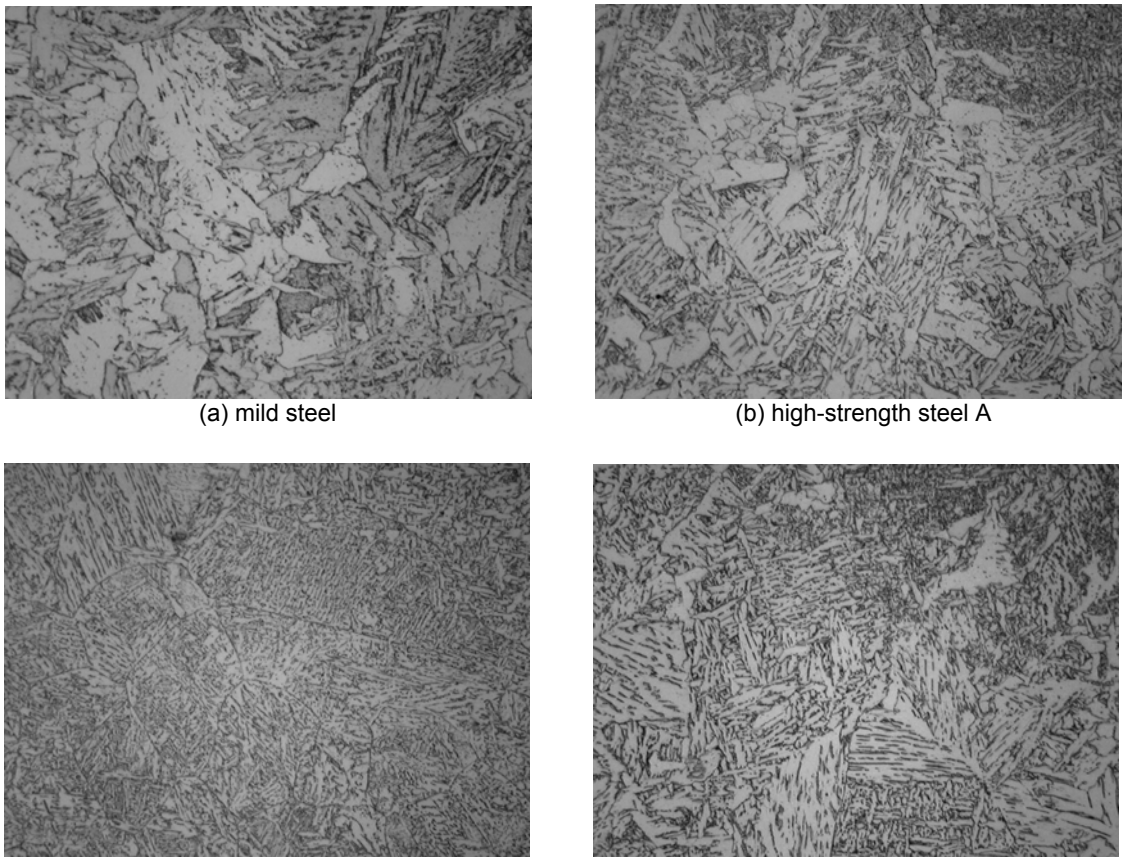

(a) mild steel (b) high-strength steel A

(c) high-strength steel B (d) high-strength steel C

Figure 2: Comparison of microstructures in the coarse grain region of HAZ. Magnification: 450×.

Mechanical testing and micro-hardness measurement will be conducted to further evaluate and differentiate the structural performance of these welds, in a follow-on study.

Reports/Publications/Awards:

J. Chiang,C. Jiang, Z. Feng and J. McNabb, “Weld Pool Dynamics and Its Effects on Weld Profile and Properties of High-Strength Steels,” Final MPLUS report, June 2004.

LIST OF PROJECTS

FY 2003 MPLUS Proposal List

Proposal No.	Organization	Proposal Title	Organization PI	ORNL PI	Relevance
MC-03-001	Lehigh University Bethlehem, PA	Melting of Experimental Alloys for Corrosion Studies	John DuPont 610-758-3942	Vinod K. Sikka 865-574-5112	Chemical Petrochemical Pulp & Paper
MC-03-002	MATTEC, LLC Knoxville, TN	Determination of the Mechanism Leading to the Formation of Surface Irregularities on Nitrided, Hot-Isostatically Pressed Nb-50 wt % Ti-20 wt % W Alloy Compacts	William Snyder 865-966-1194	Vinod K. Sikka 865-574-5112 G. Muralidharan 865-574-4281	Aluminum
MC-03-003	ALLVAC Monroe, NC	Effect of Processing/ Microstructure on the Corrosion Polarization Response of a Corrosion-Resistant Alloy: Phase II	John Pridgeon 704-289-4511	Dane F. Wilson 865-576-4810 Edward A. Kenik 865-574-5066 Steven J. Pawel 865-574-5138 Vinod K. Sikka 865-574-5112	Forest Products Chemical Petrochemical
MC-03-004	F.W. Gartner Thermal Spray Co. Houston, TX	High-Density-Infrared (HDIR) Densification of Thermal Spray Coatings for Spherical Surfaces	Jimmy Walker, Jr. 713-225-0010 John B. Williams 281-449-0291	Craig A. Blue 865-574-4351 Puja Kadolkar 865-574-9956	Steel
MC-03-005	Applied Thin Films Evanston, IL	Cerablak Release Coatings for Aluminum Die Casting	Sankar Sambasivan 847-467-5282 Kimberly Steiner 847-431-8026	Gail M. Ludtka 865-576-4652	Aluminum Metal Casting
MC-03-006	Lawrence Berkeley National Laboratory Berkeley, CA	Thermal Conductivity vs. Temperature Measurement of Nanostructured Insulating Materials	Arlon J. Hunt 510-486-5370	Hsin Wang 865-576-5074	Heat Treating
MC-03-007	Ametek Wallingford, CT	High-Energy Wire Annealing Method	Jack Easley 202-265-6731 Clive Scorey 203-949-8828	Vinod K. Sikka 865-574-5112 Yogesh Bhambri 865-576-6031	Heat Treating
MC-03-008	IPSCO Axis, AL	Causes of Damage of Steckel Mill Drums during Hot Rolling of Steel Slab	Steven S. Hansen 251-662-4450 Kevin Marsden 412-390-2715	Vinod K. Sikka 865-574-5112 Yogesh Bhambri 865-576-6031	Steel
MC-03-009	Cancelled				

MPLUS Proposal List (continued)

Proposal No.	Organization	Proposal Title	Organization PI	ORNL PI	Relevance
MC-03-010	Metamic L.L.C. Lakeland, FL	Development of Hot Rolling Fabrication Parameters for Aluminum Boron Carbide Metal Matrix Composite Materials	Thomas Haynes 863-709-9448 Donald Wiggins 804-233-6201 Patrick Colgate 863-709-9448	Craig A. Blue 865-574-4351 Puja Kadolkar 865-574-9956	Aluminum
MC-03-011	Cancelled				
MC-03-012	Metal Casting Technology, Inc. Milford, NH	Quantifying Correlating Lost Foam Pattern Properties with Metals Fill Casting Performance: Under-standing the Process	Qi Zhao 603-673-9720, ext. 2307	R. B. Dinwiddie 865-574-7599	Metal Processing Metal Casting
MC-03-013	Inductoheat Madison Heights, MI	Optimizing Induction Heating to Obtain Profile Hardening of Gears	Madhu Chatterjee 248-629-5004	R. B. Dinwiddie 865-574-7599	Steel Heat Treating
MC-03-014	Foseco-Morval Bessemer, AL	Optimization of IR Imaging of the Lost Foam Metal Casting Process	Dennis Nolan 519-763-7177	R. B. Dinwiddie 865-574-7599	Metal Casting
MC-03-015	Commonwealth Industries, Inc. Lexington, KY	Development of Welding Process to Join Aluminum Alloy Sheets Coil to Coil	Zhong Li 859-514-4951 John Moore 252-212-3102	Robert W. Reed 865-574-4843 Jeff McNabb 865-574-4811 Stan A. David 865-574-4804	Aluminum
MC-03-016	ACuPowder TN LLC Greenback, TN	Process Improvements for Complete Oxidation of Copper Chops for Ease of Production of Fine, Easily Compactable Cu and Cu Alloy Powders	Krishna Patel 865-856-3021	Vinod K. Sikka 865-574-5112 Yogesh Bhambri 865-576-6031	Powder Metallurgy
MC-03-017	HK Casting, Inc. Weston, WV	Utilizing Graphite Expansion to Compensate Solidification Shrinkage in High-Strength Gray Cast Iron	Patricia Minehardt 304-269-7809 Roy Burkhammer 304-269-7809	Qingyou Han 865-574-4352	Steel Metal Casting
MC-03-018	Pyromation Fort Wayne, IN	Coating of Temperature Sensors for Solder Resistance	Richard Wilson 231-386-5094 Mark Everhart 260-484-2580 Peter C. Wilson 260-484-2580	Craig A. Blue 865-574-4351 Puja Kadolkar 865-574-9956	Die Casting Aluminum Extrusion Forging Cross-Cutting

MPLUS Proposal List (continued)

Proposal No.	Organization	Proposal Title	Organization PI	ORNL PI	Relevance
MC-03-019	Commonwealth Aluminum Lewisport, KY	Characterization of Dross form a Sidewall Melter Producing 3004 and 3105 Aluminum from Undercoated Scrap	Joe Tessandori 270-295-5431	Karren More 865-574-7788	Aluminum
MC-03-020	University of Kentucky Lexington, KY	Characterization of Precipitation in In-Line Annealed Aluminum Alloys	Tony Zhai 859-257-4958	E. A. Kenik 865-574-5066	Aluminum
MC-03-021	MET Group Dayton, OH	Effect of Processing Parameters on Fabrication of Mo Sheet High Powder Metallurgy	Howard Sanderow 937-832-1583 Sunil Jha 520-878-9596	G. Muralidharan 865-574-4281 Vinod K. Sikka 865-574-5112	Steel Aluminum Heat Treating Metal Forming
MC-03-022	Tennessee Technological University Cookeville, TN	Study of Pyrolysis Product Generation and Behavior in the Lost Foam Casting Process	Fred Vondra 931-372-3527 Graham Walford 865-482-4995	R. B. Dinwiddie 865-574-7599	Metal Forming Metal Casting Metal Processing
MC-03-023	DELTM M Corporation Oak Ridge, TN	Development of a Process to Hermetically Seal a Thermal Sensor using a Vitreous Sealing Glass	Reg McCulloch 865-483-1569	Craig A. Blue 865-574-4351 Puja B. Kadolkar 865-574-9956	Petrochemical Pulp & Paper
MC-03-024	Century Aluminum of West Virginia, Inc. Ravenswood, WV	Methods to Improve Aluminum Smelter Hardware Materials	Richard O. Love 304-273-6562	Vinod K. Sikka 865-574-5112 Yogesh Bhambri 865-576-6031	Aluminum
MC-03-025	Ford Motor Company Dearborn, MI	Weld Pool Dynamics and Its Effects on Weld Profile and Properties of High-Strength Steels	John Chiang 313-323-1063 Cindy Jiang 248-813-0130	Zhili Feng 865-576-3797 Jeff McNabb 865-576-3797	Cross-Cutting
MC-03-026	Energy Industries of Ohio Independence, OH	Characterization of Aluminum Foam Prepared by Casting Process	Robert Purgert 216-643-2952	Vinod K. Sikka 865-574-5112 Yogest Bhambri 865-576-6031	Aluminum
MC-03-027	Commonwealth Aluminum Concast, Inc. Uhrichsville, OH	Heat Transfer Modeling of Continuously Cast Aluminum Slab	Zhong Li 859-514-4951 Paul Platek 740-922-8329	B. Radhakrishnan 865-241-3861	Aluminum
MC-03-028	University of Alabama Birmingham, AL	Metal Filling of Lost Foam Castings	Wanliang Sun 205-975-8839 Harry Littleton 205-975-3890	R. B. Dinwiddie 865-574-7599	Aluminum
MC-03-029	IMCO Recycling Inc. Rockwood, TN	The Mechanisms of Oxide Formation Found in Solidified Aluminum 5182 Alloy RSI	Ray D. Peterson 865-354-6375	Qingyou Han 865-574-4352	Aluminum

MPLUS Proposal List (continued)

Proposal No.	Organization	Proposal Title	Organization PI	ORNL PI	Relevance
MC-03-030	Century Aluminum of West Virginia, Inc. Ravenswood, WV	Methods to Improve Anode Rod Preheat Energy Requirements	Richard O. Love 304-273-6562	Craig A. Blue 865-574-4351 Puja B. Kadolkar 865-574-9956	Aluminum
MC-03-031	Haynes International Inc. Kokomo, IN	The Mechanism by which Boron and Zirconium Improve the Resistance of Haynes 214 Alloy to Strain Age Cracking	Mark D. Rowe 765-456-6228	S. S. Babu 865-574-4806 M. K. Miller 865-574-4179	Glass Steel Aluminum Chemical
MC-03-032	Amcast Automotive Southfield, MI	Optimized Heat Treatment for Cast A356 Aluminum Wheels	Jagan Nath 248-799-2207 Chuck Russo 260-495-5602, ext. 310 Sara Chen 248-799-2219	Qingyou Han 865-574-4352	Metal Casting Heat Treating
MC-03-033	GM Powertrain Saginaw, MI	Qualifying Production Grade Foam and Coatings with Real Time X-Ray, Infrared and Capacitive Methods for the Lost Foam Casting Process	Jerry Barendreght 989-757-0810	R. B. Dinwiddie 865-574-7599	Metal Casting
MC-03-034	Cancelled				
MC-03-035	Cancelled				
MC-03-036	IMCO Recycling Inc. Rockwood, TN	The Measurement of Moisture/Water Content in Recycled Aluminum Scrap and RSI	Ray Peterson 865-354-6375	Qingyou Han 865-574-4352	Aluminum
MC-03-037	Cancelled				
MC-03-038	Citation Corporation Birmingham, AL	Thermodynamic Simulation of Porosity Potential in Ductile Irons	Al Alagarsamy 205-271-7402	Qingyou Han 865-574-4352	Metal Casting
MC-03-039	Stoody Company Bowling Green, KY	The Evaluation of Various Cladding Materials for Down-Hole Drilling Applications using the Pin on Disk Test	Ravi Menon 270-781-9777, ext. 2009	Peter J. Blau 865-574-5377	Petrochemical
MC-03-040	Equistar Chemical Company Cincinnati, OH	Microwave Activation of Catalysts	Emory A. Ford 413-584-0512	Alicia L. Compere 865-574-4970	Petrochemical
MC-03-041	Cancelled				

STAFF CONTACTS AND GENERAL INFORMATION

Staff contacts and sources for general information are listed below.

Program:

Dr. Peter Angelini, Program Manager
Oak Ridge National Laboratory
1 Bethel Valley Rd.
Oak Ridge, TN 37831-6065
Phone: (865) 574-4565, Fax: (865) 576-4963, Email: angelinip@ornl.gov

General information and submittals:

Ms. Millie Atchley
MPLUS Administrative Specialist
Metals Processing Laboratory User (MPLUS) Facility
Oak Ridge National Laboratory
1 Bethel Valley Rd.
Oak Ridge, TN 37831-6083
(865) 574-4358, Fax: (865) 574-4357, Email: atchleyml@ornl.gov

User Center Leaders:

Processing:

Dr. Vinod Sikka, (865) 574-5112, Email: sikkavk@ornl.gov

Joining:

Dr. Stan David, (865)574-4804, Email: davidsa1@ornl.gov

Characterization:

Corrosion: Dr. Peter Tortorelli, (865) 574-5199, Email: tortorellipf@ornl.gov
Mechanical: Dr. Edgar Lara-Curzio, (865) 574-1749, Email: laracurzioe@ornl.gov

Materials/Processing Modeling:

Dr. B. Radhakrishnan, (865) 241-3861, Email: radhakrishnan@ornl.gov

Additional information and proposal applications are available at
http://www.ms.ornl.gov/emfacility/mplus/mplus.htm

ACKNOWLEDGMENTS

Research sponsored by the U.S. Department of Energy, Office of Energy Efficiency and Renewable Energy, Industrial Technologies Program, Industrial Materials for the Future and Aluminum Industry of the Future under contract DE-AC05-00OR22725 with UT-Battelle, LLC.